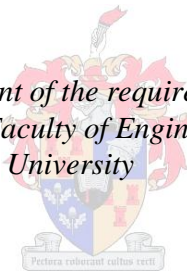


Simulation and control implications of a high-temperature modular reactor HTMR cogeneration plant

by

Mubenga Carl Tshamala

*Thesis presented in fulfilment of the requirements for the degree of
Master of Science in the Faculty of Engineering at Stellenbosch
University*



Supervisor: Mr Robert T. Dobson

April 2014

DECLARATION

By submitting this thesis electronically, I declare that the entirety of the work contained therein is my own, original work, that I am the sole author thereof (save to the extent explicitly otherwise stated), that reproduction and publication thereof by Stellenbosch University will not infringe any third party rights and that I have not previously in its entirety or in part submitted it for obtaining any qualification.

Signature:

Mubenga Carl Tshamala

Date:

ABSTRACT

Simulation and control implications of a high-temperature modular reactor (HTMR) cogeneration plant

M.C. (Carl) Tshamala

Traditionally nuclear reactor power plants have been optimised for electrical power generation only. In the light of the ever-rising cost of dwindling fossil fuel resources as well the global polluting effects and consequences of their usage, the use of nuclear energy for process heating is becoming increasingly attractive. In this study the use of a so-called cogeneration plant in which a nuclear reactor energy source is optimised for the simultaneous production of superheated steam for electrical power generation and process heat is considered and analysed. The process heat superheated steam is generated in a once-through steam generator of heat pipe heat exchanger with intermediate fluid while steam for power generation is generated separately in a once-through helical coil steam generator. A 750 °C, 7 MPa helium cooled HTMR has been conceptually designed to simultaneously provide steam at 540 °C, 13.5 MPa for the power unit and steam at 430 °C, 4 MPa for a coal-to-liquid fuel process. The simulation and dynamic control of such a typical cogeneration plant is considered. In particular, a theoretical model of a typical plant will be simulated with the aim of predicting the transient and dynamic behaviour of the HTMR in order to provide guideline for the control of the plant under various operating conditions. It was found that the simulation model captured the behaviour of the plant reasonably well and it is recommended that it could be used in the detailed design of plant control strategies. It was also found that using a 1500 MW-thermal HTMR the South African contribution to global pollution can be reduced by 1.58%.

Keywords: Nuclear energy, power generation, coal-to-liquid, dynamic simulation

OPSOMMING

Simulasie en beheer-implikasies van 'n Hoëtemperatuur Modulêre Reactor (HTMR) mede-opwekkingsaanleg

M.C. (Carl) Tshamala

Tradisioneel is kernkragaanlegte vir slegs elektriese kragopwekking geoptimeer. In die lig van die immer stygende koste van uitputbare fossielbrandstohulpbronne asook die besoedelingsimpak daarvan wêreldwyd, word die gebruik van kernkrag vir prosesverhitting al hoe meer aanlokliker. In hierdie studie word die gebruik van 'n sogenaamde mede-opwekkingsaanleg waarin 'n kernkragreaktor-energiebron vir die gelyktydige produksie van oorverhitte stoom vir elektriese kragopwekking en proseshitte oorweeg ontleed word. Die oorverhitte stoom word in 'n enkeldeurvloei-stoomopwekking van die hittepyl-hitteruiler met tussenvloeistof opgewek en stoom vir kragopwekking word apart in 'n enkeldeurvloei-spiraalspoel-stoomopwekker opgewek. 'n 750 °C, 7 MPa heliumverkoelde HTMR is konseptueel ontwerp vir die gelyktydige veskaffing van stoom by 540 °C, 13.5 MPa, vir die kragopwekkings eenheid, en stoom by 430 °C, 4 MPa, vir 'n steenkool-tot-vloeibare (CTL) brandstoff proses. Die simulasie en dinamiese beheer van 'n tipiese HTMR mede-opwekkingsaanleg word beskou. 'n die besonder word 'n teoretiese model van die transiënte en dinamiese gedrag van die aanleg gesimuleer om sodoene riglyne te identifiseer vir die ontwikkeling van dinamiese beheer strategieë vir verskillende werkstoestande van die aanleg. Daar was ook gevind dat die simulasie model van die aanleg se gedrag goed nageboots word en dat dit dus gebruik kan word vir beheer strategie doeleindes. Indien so 'n 1500 MW-termies HTMR gebruik word sal dit die Suid Afrikaanse besoedling met 1.58% sal kan verminder.

Slutelwoorde: kernkrag, kragopwekking, steenkool-na-vloeistof, dinamiese simulie

DEDICATION

Dedicated to him who is my Lord most high and Almighty, Christ Jesus, for his grace upon me strengthens, inspires and brightens up my knowledge; my parents Francois Mubenga and Rachel Musau for their support, love and guidance. Let this be received as a reflection of your efforts.

ACKNOWLEDGEMENTS

I would like to thank the following people:

My supervisor, Mr Robert Dobson, for his patience, tutelage, endless encouragement, guidance and enthusiasm that made this research a meaningful project and enjoyable journey;

All the Mechanical and Mechatronics staff members for their spontaneity, reliability and availability smoothing the research path;

My sister, Francine Mubenga, for the unconditional financial support during the weak and fragile beginnings of this project that only Heaven could successfully reward;

My colleagues, brothers and sisters for their moral support and positive criticism regarding this project;

In this, find the expression of my deepest appreciation.

TABLE OF CONTENTS

DECLARATION	I
ABSTRACT.....	II
OPSOMMING	III
DEDICATION	IV
ACKNOWLEDGEMENTS	V
TABLE OF CONTENTS.....	VI
LIST OF FIGURES.....	X
LIST OF TABLES.....	XII
NOMENCLATURE.....	XIII
1 INTRODUCTION.....	1
1.1 Background.....	1
1.2 Previous studies	1
1.3 Thesis objective.....	2
2 LITERATURE SURVEY	4
2.1 Current world-wide energy consumption.....	4
2.2 Coal-to-liquid fuel.....	7
2.3 Hydrogen carrier	8
2.3.1 <i>Hydrogen production</i>	9
2.3.2 <i>Hydrogen using nuclear power</i>	12
2.4 Power generation.....	12
2.4.1 <i>Gas turbine unit</i>	12
2.4.2 <i>Steam Turbine unit</i>	13

2.5	Nuclear reactors	13
2.5.1	<i>Generation IV nuclear reactors</i>	13
2.5.2	<i>HTR-PM</i>	14
2.6	Heat pipe heat exchangers (HPHE)	15
3	APPLICABLE THEORIES	16
3.1	Generation IV nuclear reactors	16
3.1.1	<i>Nuclear fission process</i>	17
3.1.2	<i>Nuclear power generation</i>	19
3.1.3	<i>Nuclear reactor heat balances</i>	21
3.2	Steam generation process.....	25
3.2.1	<i>Heat exchanger and steam generator types</i>	25
3.2.2	<i>Steam generator energy balance</i>	27
3.2.3	<i>Overall heat transfer coefficient and concept of effectiveness</i>	30
3.2.4	<i>Moving boundaries assumptions</i>	32
3.3	Control aspects of steam generated by nuclear reactor.....	32
4	MATHEMATICAL MODELLING	35
4.1	Nuclear reactor	35
4.1.1	<i>Overall plant description</i>	35
4.1.2	<i>Modelling philosophy</i>	38
4.1.3	<i>Dynamic modelling formulation of the HTMR</i>	42
4.2	Steam generator.....	46
4.2.1	<i>Once-through steam generator design</i>	46
4.2.2	<i>Mathematical modelling of the once-through steam generator</i>	48

4.3	Special heat pipe heat exchanger	53
4.3.1	<i>Special heat pipe heat exchanger design</i>	54
4.3.2	<i>Mathematical modelling of the special heat exchanger</i>	55
4.4	Primary side and metal tube equations	56
5	HTMR – THEORETICAL SIMULATION RESULTS	58
5.1	Nuclear reactor simulation results	58
5.1.1	<i>Reactor power</i>	58
5.1.2	<i>Helium outlet and reactor core temperature</i>	59
5.2	Power unit steam generator results	61
5.2.1	<i>Outlet steam temperature</i>	61
5.2.2	<i>Economizer, Evaporator and Superheater lengths dynamics</i>	62
5.3	Heat pipe heat exchanger steam generator results	64
5.3.1	<i>Superheated steam outlet temperature</i>	64
5.3.2	<i>Helium outlet temperature</i>	66
6	CONTROL MODEL VALIDATION	68
6.1	Theory, programme and results of the HTR-PM	68
6.1.1	<i>HTR-PM power curve</i>	68
6.1.2	<i>HTR-PM reactor core temperature</i>	69
6.1.3	<i>HTR-PM steam temperature</i>	70
6.2	Comparison of published HTR-PM results and HTMR results	71
6.2.1	<i>Reactor power</i>	71
6.2.2	<i>HTR-PM and HTMR Temperatures comparison</i>	71
7	DISCUSSION, CONCLUSION AND RECOMMENDATIONS	76

8 REFERENCES	78
APPENDIX A: STEADY-STATE CALCULATION OF THE HTMR	82
A.1 HELICAL COIL STEAM GENERATOR	82
<i>A.1.1 Once-through helical coil steam generator design specifications</i>	82
<i>A.1.2 Overall heat transfer coefficient of the HTMR (Steady state)</i>	83
<i>A.1.3 Superheater, economiser and evaporator lengths</i>	84
A.2 Heat pipe heat exchanger	96
<i>A.2.1 Heat pipe design specifications</i>	96
<i>A.2.2 Heat pipe overall heat transfer coefficient</i>	96
<i>A.2.3 Heat pipe economiser, evaporator and superheater lengths</i>	103
A.3 Nuclear reactor steady-state calculations	104
APPENDIX B: HTMR SIMULATION M-FILE IN MATLAB FOR STEADY STATE	109

LIST OF FIGURES

Figure 2.1 World primary energy predictions to 2100 (Elder, et al., 2009) 5

Figure 2.2 Global primary energy mix: history and outlook projected to 2100 (Jess, 2010)6

Figure 2.3 South African energy supply map in percentage (Statistics South Africa, 2005)6

Figure 2.4 Simplified CTL process (Mantripragada, et al., 2011) 8

Figure 2.5 The sulphur iodine cycle (Elder, et al., 2009) 10

Figure 2.6 Single module hybrid sulphur block diagram (Greyvenstein, 2008)..... 11

Figure 2.7 Thermodynamics of high-temperature electrolysis (Elder, et al., 2009) 12

Figure 3.1 Conceptual flow diagram of a PBMR power conversion unit (Slabber, et al., 2006) 17

Figure 3.2 Once-through steam generator sections (Hoffer, *et al.*, 2011) 27

Figure 3.3 Temperature distributions between helium and water/steam 30

Figure 3.4 Pump head as a function of mass flow rate (McAllister, 2009) 33

Figure 4.1 Electrical power unit and process heat for solid-coal to liquid fuel production, cogeneration plant for 6 (3x2) reactors 36

Figure 4.2 Cross section of helium loop of the HTR-PM (Zeng, Shi & Dong, 2009) 38

Figure 4.3 Heat flow diagram of unit 1 of the HTMR plant..... 40

Figure 4.4 Cogeneration heat flux diagram (nuclear reactor connected to special heat exchanger for heat process and steam generator for power generation) 41

Figure 4.5 Reactor heat flux and coolant gas flow path 49

Figure 4.6 Helical coil once-through steam generator pre conceptual design (Hoffer, *et al.*, 2011) 48

Figure 4.7 Schematic view of the sections of the once-through steam generator..... 49

Figure 4.8 Heat pipe heat exchanger for process heat steam generation..... 54

Figure 4.9 PBMR coupled to combined power and CTL process (Greyvenstein, 2008).... 55

Figure 4.10 Schematic view of the sections of the heat pipe heat exchanger (HPHE) 55

Figure 5.1 HTMR reactor power as function of time 59

Figure 5.2 Reactor outlet temperature as function of time	60
Figure 5.3 Reactor core temperature as function of time	60
Figure 5.4 Steam outlet temperature as function of time	61
Figure 5.5 Economiser length l_{13} as function of time.....	62
Figure 5.6 Evaporator length l_{35} as function of time.....	63
Figure 5.7 Superheater length l_{57} as function of time.....	63
Figure 5.8 Heat pipe heat exchanger outlet steam temperature	64
Figure 5.9 Heat pipe heat exchanger outlet steam specific enthalpy	65
Figure 5.10 Heat pipe heat exchanger outlet steam quality.....	65
Figure 5.11 Heat pipe heat exchanger helium outlet temperature as a function of time	66
Figure 5.12 Cogeneration loop reactor power as a function of time	67
Figure 6.1 HTR-PM reactor power as function of time (Li, et al., 2008b)	69
Figure 6.2 HTR-PM reactor core temperature as function of time (Li, et al., 2008b).....	70
Figure 6.3 HTR-PM outlet steam temperature as a function of time (Li, et al., 2008b) ...	71
Figure 6.4 HTMR outlet steam temperature, reactor core temperature and reactor outlet helium temperature as function of time	74
Figure 6.5 Variation of helium mass flow rate of the HTR-PM from a compensator feedback (Li, et al., 2008b).....	75

LIST OF TABLES

Table 2.1 Potential of Generation IV nuclear energy systems to meet prescribed goals (Abram, <i>et al.</i> , 2008)	14
Table 3.1 Fission energy distribution (King, 1964)	18
Table 3.2 Criterion for better moderator (King, 1964)	19
Table 3.3 Relevant parameters used in the HTR-10 (Li, et al., 2008a).....	23
Table 3.4 Thermodynamic properties of helium in the region situated between 30 °C and 1000 °C and 3 MPa and 10 MPa (Barron, 1985).	25
Table 3.5 Nusselt number applicable constants for circular tube cross-section (Wong, 1977)	31
Table 4.1 Main design data of the HTMR (based on HTR-PM and Sasol requirements) (Li, <i>et al.</i> , 2008b)	37
Table 6.1 Simulation input variables of the HTR-PM (Li, et al., 2008b)	68
Table 6.2 Input variables of the HTMR power unit.....	73
Table 6.3 Input variables of the HTMR cogeneration unit.....	73
Table 6.4 Timing of power unit input variables	75
Table 6.5 Timing of the cogeneration unit input variables	75

NOMENCLATURE

A	Area of heat transfer; Area of the flow cross section, m^2
C	Concentration; carbon
c	Specific heat, $kJ/kg\ K$
d	Diameter, m
G	Volumetric flow rate, m^3/s
g	Gravitational acceleration, m/s^2
F	Friction factor of pressure
H	Head, m; hydrogen
h	Specific enthalpy, J/kg ;
k	Pressure loss coefficient, fluid thermal conductivity, $W/m^\circ C$
l	Length, m; lifetime, s
\dot{m}	Mass flow rate $\dot{m} = \rho G$, kg/s
\dot{m}''	Mass flux $\dot{m}'' = G/A$, $kg/s/m^2$
m	Mass of control volume, kg
n	Neutron density; rotational speed, rpm; number
P	Pressure, Pa; Power, W
O	Oxygen
Q	Thermal energy, J
\dot{Q}	Heat flow rate, W
\dot{Q}''	Heat flux, W/m^2
T	Temperature, $^\circ C$; Reactor period
t	Time, s
V	Volume, m^3
W	Work, J
1	Very high
2	High
3	Medium
4	Medium/Low
5	Low
6	Very low

Greeks symbols

α	Temperature reactivity feedback coefficient
β	Delayed neutron fraction; Leakage ratio; Average delayed neutron fraction
ω_f	Power conversion factor
ϵ	Porosity
θ	Angle of the steam generator tube

λ	Decay constant
Λ	Neutron generation time
ρ	Density, kg/m^3 ; Reactivity
Σ_f	Macroscopic fission cross section, m^2
τ	Time constant, s

Subscripts

ave	Average
b	Boiling
c	Reactor core; condensation
cr	From core to reflector
e	Electrical
f	Fuel
fw	Feedwater
HP	Heat pipe
h	Helium; hydraulic
i	i-th delayed neutron
in	Input
l	liquid
m	Moderator
Na	Sodium
out	Output
p	Primary; Pipe; Fuel element
r	Reflector; Relative value
s	Steam
th	Thermal
v	Vapour
w	Wall
0	Steady-state; initial state at time $t=0$
1	Lower plenum of the reactor; Feedwater entry point of steam generator; Very high
2	Lower header of the reactor; Average point of evaporator; High
3	Riser of the reactor; Saturate water point of steam generator; Medium
4	Upper header of reactor; Average point of evaporator; Medium/Low
5	Downcomer of the reactor; Saturate steam point of steam; Low
6	Outlet header of the reactor; Average point of superheater; Very low
7	Outlet point of the superheater
100	Full power

Acronyms

CTL	Coal-to-liquid
GFR	Gas-cooled Fast Reactor
GIF	Generation-IV International Forum
HTMR	High Temperature gas cooled Modular Reactor
HTR-10	10 MW High Temperature Modular Reactor
HTR-PM	High Temperature Reactor – Pebble-bed Modular
LFR	Lead-cooled Fast Reactor
MSR	Molten Salt Reactor
NGNP	Next Generation Nuclear Plant
PBMR	Pebble Bed Modular Reactor
PH	Process Heat
PMW	Pulse Width Modulation
R&D	Research and Development
SCWR	Super-Critical Water-cooled Reactor
SFR	Sodium-cooled Fast Reactor
TOE	Tonnes oil equivalent
VHTR	Very High-Temperature gas-cooled Reactor

1 INTRODUCTION

1.1 Background

Arguments of security of energy supply and climate change in the upcoming years have been raised as major concerns to justify the use of nuclear energy as an important clean contributor for power generation (Teravainen *et al.*, 2011).

In South Africa, with its coal-driven economy, fossil fuels contribute more than 80% of its energy, resulting in more than 435 million of tonnes of carbon dioxide per annum in emissions; power generation is the main contributor to carbon dioxide emission. Coal conversion to hydrocarbons is also identified as a huge contributor to the South African carbon dioxide emission, as it contributes about 11% of emissions (FOEI, 2011). In light of the reason stated, the use of nuclear seems to be a viable option in terms of carbon footprint reduction (Greyvenstein, 2008).

In the wake of the legacy of the pebble-bed modular reactor (PBMR) project, which is closed at this stage, there is renewed interest in developing more effective and clean systems. Using nuclear energy for power generation and process heat for a coal-to-liquid (CTL) process in cogeneration would significantly contribute to improving the overall plant efficiency while reducing the carbon footprint.

The next sections of this chapter will be highlighted the findings of previous researches on world energy demand, the arguments of importance of use of nuclear energy as contributor the world energy supply plan. A description of the context of this study is discussed and the objective of this research closes the chapter.

1.2 Previous studies

Global population is expected to increase from 6.8 billion in 2009 to about 9 billion by 2050. In the light of the world's increasing energy demand, meeting the world's future energy needs poses a serious challenge (Jess, 2010). According to Lewis's (2008) predictions, the world's primary energy demand is expected to increase by about 17 TW to meet the 2050 needs. Failing to supply enough energy in a sustainable way would probably weaken the gross domestic product (GDP) growth and result in a further increase of oil and gas prices. To ensure that energy supply matches the growth in energy demand, it is important to consider an energy mix that will include all types of energy resources. The energy mix projected, considered as a more reliable way of energy generation, would be expected to provide enough energy for the world's population without compromising the environmental aspect. Nuclear energy resources have been identified as a principal contender that has great potential to provide carbon-free energy for the grid (Lewis, 2008).

In 2008, it was established that nuclear energy was the lowest cost option for electricity generation in the fast expanding world energy demand and its contribution to the world electricity supply was evaluated to be about 16% of the world's electricity generation (Greyvenstein, 2008). It is also important to consider nuclear energy for process heat

supply for industrial application such as hydrogen production and CTL processes, where fossil fuels are still used to provide the required heat. In this way, the use of fossil fuel could be reduced, extending their lifetime. Another more efficient configuration suggests that be combined electricity generation and process heat on a single system that would use the same primary energy, nuclear for the matter, to provide energy for both processes. This configuration is called cogeneration.

A typical plant layout using nuclear energy for power generation and process heat for coal conversion to liquid fuel was suggested for the South African context where coal is used to produce hydrocarbons (Botha, 2011). For this type of process, Greyvenstein et al. (2008) recommends that the nuclear reactor supplies heat to both processes via an intermediate heat exchanger due to the temperature ranges between the nuclear reactor outlet temperature and the operating temperature of the heat process, reducing the contamination risk from nuclear radiations. It was suggested that the intermediate heat exchanger be replaced by a heat pipe heat exchanger operating at intermediate temperature between the heat supply source and the process. This type of heat pipe was developed by Laubscher (2012) and proved effective.

1.3 Thesis objective

In China, developments in nuclear energy piqued interest in a new generation of nuclear reactors and led to a design of a high-temperature gas-cooled nuclear reactor (HTR-PM) using a pebble-bed that was expected to be operational for power generation by 2013. This design has successfully produced valuable results that have increased interest in the use of nuclear as heat source for power generation and other industrial applications.

In South African, coal is used to provide heat for power generation (ESKOM) and for the CTL fuel process (Sasol) on one hand; on the other hand, coal is also used as primary resource in the CTL process. Thus the idea of combining power generation and the conversion to liquid fuel CTL on a single plant emerged. This combined plant would use nuclear energy as primary energy resource for heat supply. This design would provide a solution that allows extending the lifetime of coal reserves while significantly contributing to reducing the carbon footprint, since shifting the heat supply from coal combustion to nuclear energy will, considerably reduce the direct emissions.

In the current study, a high temperature nuclear gas cooled reactor of similar performances as the Chinese HTR-PM operating in cogeneration is conceptually designed and simulated. This nuclear reactor is called a high-temperature modular reactor (HTMR) and is expected to provide about 1500 MW_{th} in a 3 x 2 x 250 MW_{th} configuration to the cogeneration plant. The HTMR is supposed to operate at more-or-less constant temperatures as required by the power generation unit and the coal conversion to liquid process. Therefore, the HTMR is simulated for a very high level of power variation in order to predict its response to sudden power demands fluctuations. The HTMR simulation behaviour will be used to describe the control implications and strategies applicable to keep the system running more effectively for all operation conditions. Failure to meet a thermally steady operation would cause either an overheating of the overall system or considering the opposite scenario, the system would fail to supply enough heat as required by the power generating system and the heat process.

The simulation of the conceptually designed HTMR will address the following thesis objectives:

- Propose an alternative means of producing power and providing heat with a low carbon footprint reducing the emissions;
- Generate a mathematical model that would effectively describe the all system for simulations purposes;
- Produce simulation results for a transient operation of the overall plant;
- Use the results produced to provide a guideline and recommend the control strategies that should be applied to secure the safety and reliability of the plant.

A conclusion discussing the study findings is provided at the end to summarize and recommendations ensuring a more reliable operation of the HTMR are made.

2 LITERATURE SURVEY

The world's primary energy consumption at the end of the 20th century was evaluated to be about 8380 million TOE (Elder & Allen, 2009). An expected 1.6% increase per year should be applied to this figure due to population growth and industrialisation. Since economic prosperity, quality of life and political stability are highly dependent on available energy, it is predicted that an additional 17 TW primary energy will be needed to meet the world's energy demand by 2050 (Lewis, 2008). To fill this gap, all renewable and non-renewable energy sources should be considered. This consideration should include not only the engineering challenges of safety, reliability and efficiency, but also public-tolerance towards sustainable development elements, economics and environmental issues (Lewis, 2008).

In this literature survey, we will attempt to review the applicable published information regarding these considerations as well as the design of the high-temperature reactor (HTR).

2.1 Current world-wide energy consumption

In recent years, energy operators have given particular attention to the issues relating to energy conservation and the implementation of high-efficiency energy systems from both a regulatory and a technical point of view. As worldwide energy consumption increases, challenges regarding the reduction of energy dependence on fossil fuel as primary resource and the emergence of environmental constraints on the emission of greenhouse gases have attracted particular attention in the energy sector. Furthermore, new interests in electricity production in more profitable and possible ways exploiting equipment analysis, has developed in many countries (Lewis, 2008).

As the world works toward meeting the increasing demands for energy, due to economic expansion, world population growth and urbanisation, the environmental pollutants from coal, oil, and natural gas combustion continue to build in the atmosphere. According to the International Energy Agency (2006), about 80% of the global energy was supplied from fossil resources by 2004 (Greyvenstein, 2008); and 67% of the world's electricity generation (Elder, et al., 2009).

The world's primary energy consumption at the end of 20th century was evaluated to be 8380 million TOE. The International Atomic Energy Agency predicts a 1.6% annual increase from the beginning of the new century which is expected to double by 2050 (IAEA, 1999).

According to the United Nations Intergovernmental Panel on Climate Change (IPCC), to address the issue of maintaining the concentration of carbon dioxide at present levels, a reduction that range from 50 to 80% in all emissions should be considered (Greyvenstein, 2008). Failure to meet future energy demands in a sustainable way would result in a further increase of oil and gas prices with a possibility of deteriorating overall GDP growth. Despite the fact that fossil fuel reserves are being depleted and their emissions are raising issues around the globe, they are unevenly distributed

throughout the world, causing political and security issues since affordable and abundant energy remains essential for the economic growth of a country.

As fossil fuel reserves are being depleted due to its significant contribution to the global energy supply, greenhouse gases and pollution continue to build in the atmosphere. The need to decrease the contribution of fossil fuel to greenhouse gas emissions in line with the Kyoto Protocol, means that alternative sources of energy and carriers should be developed, while improvement in overall power generation efficiency should be investigated as main contributor to the process.

In discussing the world energy roadmap, let us consider the actual and predicted future energy mix presented in Figures 2.1 and 2.2 below:

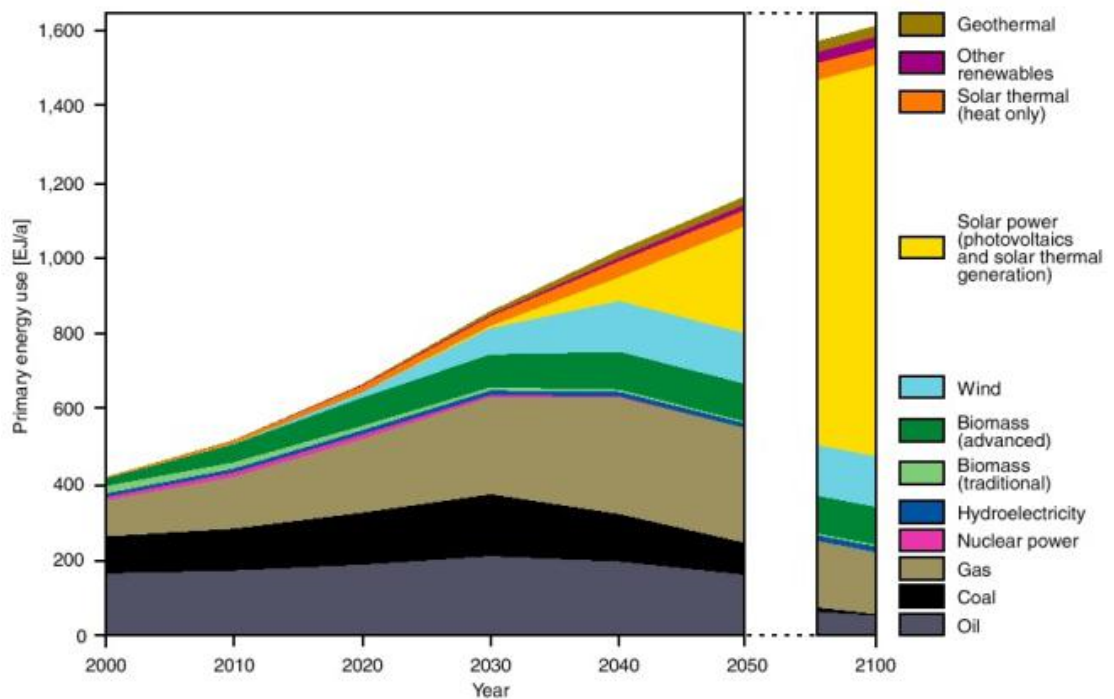


Figure 2.1 World primary energy predictions to 2100 (German Advisory Council on Global Change, 2003)

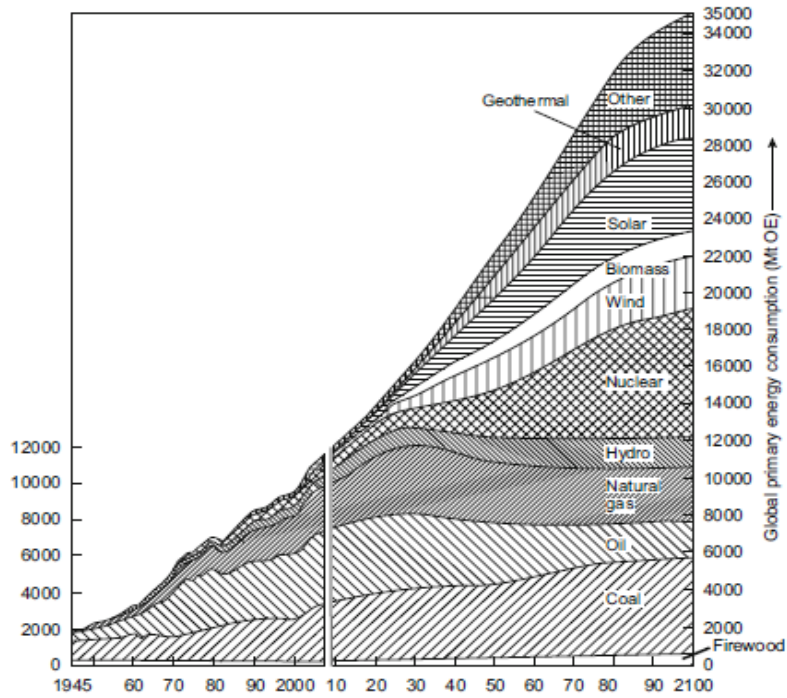


Figure 2.2 Global primary energy mix: history and outlook projected to 2100 (Jess, 2010)

In the South African context, the primary energy supply is dominated by coal, oil, gas, nuclear power and renewable sources such as wind, solar, biomass. Figure 2.3 gives an overview of the South African primary energy supply around at the beginning of this century.

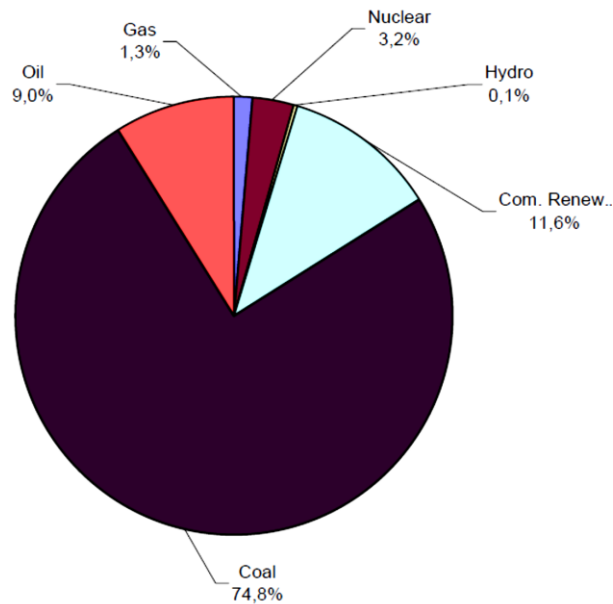


Figure 2.3 South African energy supply map in percentage (Statistics South Africa, 2005)

2.2 Coal-to-liquid fuel

CTL processes use coal to produce synthetic liquid fuels such as gasoline and diesel. Depletion of oil reserves and the associated increase in prices have stimulated interest in synthetic fuels for transportation, to replace and/or supplement conventional gasoline and diesel. In the CTL process, coal is firstly gasified to produce syngas which, in turn, is catalytically treated in a Fisher-Tropsch (F-T) process to produce different liquid fuels such as gasoline and diesel (Mantripragada & Edward, 2009). The high-temperature Fisher-Tropsch process generates liquid products that are mainly constituted of straight-chain α -olefins and paraffins in addition to gaseous products. Two general configurations of CTL plants are possible, as shown in Figure 2.4

- In the typical commercial CTL plant (see Figure 2.4a and 2.4b), the unconverted syngas from the reactor is re-injected in the reactor to improve the productivity of the generated liquid fuel. This kind of plant is also referred to as a 'liquids-only plant';
- The second configuration, also called 'poly-generation' plant, is not yet commercialised but, uses the unconverted syngas from the F-T reactor in a combined gas and steam turbine power plant to generate electricity that can be sold to the grid (Mantripragada & Edward, 2011).

The F-T process is currently used by Sasol to produce about 40% of diesel fuels and gasoline for South Africa. The indirect process first gasifies coal with steam in excess and oxygen to produce syngas. Syngas is a mixture of carbon monoxide, hydrogen, carbon dioxide, hydrogen sulphide and other volatile materials deriving from coal. The major concern of CTL plants is the carbon dioxide emissions produced as part of the process. The gasification process is responsible for a significant fraction of carbon dioxide produced. The amount of carbon dioxide generated in the gasifier depends on the thermodynamic operating conditions such as temperature, pressure and the coal feeding method. The following equations assume input coal with a 0.8 to 1 ratio of hydrogen to carbon:

Partial oxidation:



Steam reforming:

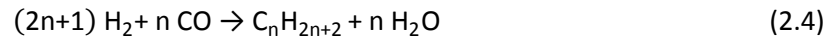


After the volatile materials have been removed from the gas stream, the hydrogen-to-carbon monoxide ratio will be increased by "shifting". The water molecule releases its oxygen, which is transferred to the CO molecule, producing carbon dioxide and more hydrogen provided by steam and carbon monoxide.

Water gas shift:



The carbon dioxide and sulphur are separated from the solution using standard acid gas removal techniques. In the presence of a catalyst, the syngas is reacted in the FT reactor to produce high-quality and clean fuels. This reaction generally occurs in accordance with the formula in equation 2.4 below:



In the CTL conversion process, the carbon dioxide emissions result from hydrogen production using coal as feedstock in the water gas shifting, as well as energy sources needed for process heat, steam and electricity. Therefore, the carbon dioxide emissions could be significantly reduced if an alternative source for hydrogen, replacing the water gas shifting, or an alternative carbon-free source of energy were available (Greyvenstein, 2008).

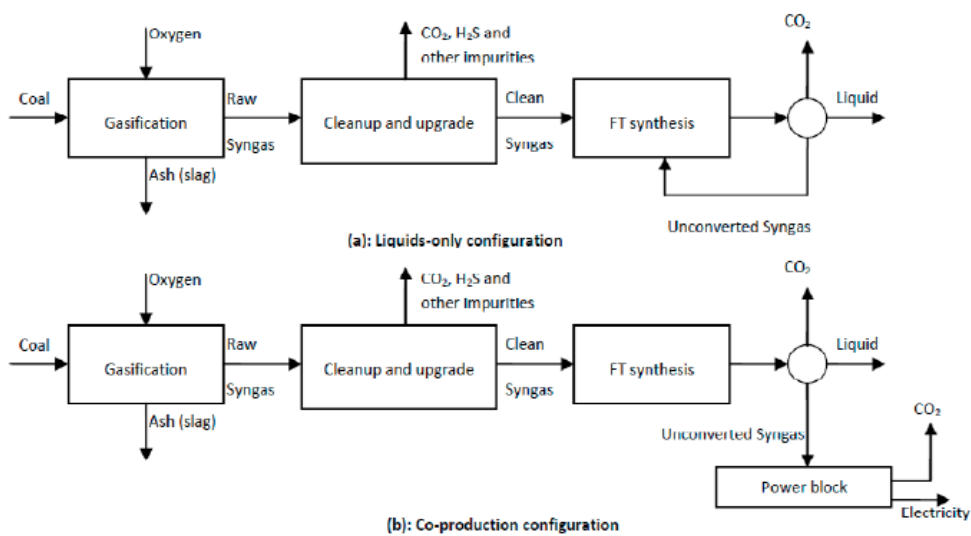


Figure 2.4 Simplified CTL process (Mantripragada, et al., 2011)

2.3 Hydrogen carrier

As greenhouse gas emissions are being decreased in accordance with the Kyoto Protocol and fossil fuel reserves are being depleted, alternative vectors and energy sources need to be developed. Therefore, specific attention has been paid to hydrogen, “the fuel of the future” (Elder, et al., 2009).

The actual annual hydrogen production is about 50 million tons, of which about 90% is used in industrial applications. The modern hydrogen industry employs hydrogen to produce chemicals and refine petroleum during methanol production, and for the production of ammonia, rocket fuel, fertilisers and many other products (Greyvenstein, 2008). Future perspectives consider the use of hydrogen to power vehicles with hydrogen fuel cells, fuel internal combustion engine vehicles, substitute natural gas for heating and cooling homes, fuel stationary power generating plants and reduce the use of coal for liquid fuel products only replacing gasoline or diesel fuels derived from crude oil. Although it is the most abundant element on earth, hydrogen is chemically bound,

mostly in the form of water, carbohydrates, hydrocarbons or other combinations. In fact, hydrogen is regarded more of an energy carrier than an energy source because another form of energy is required to separate it from its chemical bonds.

2.3.1 Hydrogen production

Fossil fuels and water are considered to be the two main sources of hydrogen. As much as hydrogen can be considered a clean fuel, it is essential to recognise the level of environmental impact that its method of production has (Elder, et al., 2009).

a. Hydrogen from fossil fuels

About 96% of the current hydrogen production originates from fossil fuels, of which a massive 48% originates from natural gas with steam reforming (Ewan & Allen, 2005). With nickel as catalyst, methane gas is mixed with high-temperature steam at about 700 to 1100 °C. Firstly, methane reacts stoichiometrically with water to form hydrogen and carbon monoxide. Secondly, the excess water reacts with the carbon monoxide to form carbon dioxide and hydrogen. More often, in order to produce the carbon dioxide, a 300% excess steam is used, shifting the steadiness in the water-gas shift reaction and thus, realising a higher hydrogen yield, therefore preventing carbon deposition due to a Boudouard reaction, also catalysed in the presence of nickel (Elder, et al., 2009).

Thermal cracking process of natural gas, coal gasification with steam and thermal cracking process of heavy oils are also used to produce hydrogen. In the integrated gasification combined cycle, the integration of a steam-coal gasification process in a combined heat and power facility is currently regarded as the cleanest and one of the most efficient coal-fuelled techniques. Hydrogen can also be produced from conversion of fuel gas generated during the pyrolysis and gasification of biomass (Elder, et al., 2009).

b. Hydrogen from water

There is increasing interest in developing large-scale hydrogen production technologies from non-fossil sources. In the transportation sector, the concern is caused by the demand for hydrogen for the refining of increasing low-quality petroleum resources, the projected intermediate-term call for carbon-neutral synthetic fuels, and the prospective long-term demand for clean and environmentally friendly fuel for transportation (O'Brien, et al., 2010). The direct water-splitting process used to produce hydrogen and oxygen requires a very high temperature of around 4400 °C, which is a very large heat input (Elder, et al., 2009). Therefore, the process becomes very expensive since it consumes a lot of energy compared to other water-splitting technologies.

Indirect water-splitting technologies, like electrolysis and thermochemical processes, have the potential to produce hydrogen on a large scale and work at much lower temperatures.

Thermochemical processes

In this process, water is converted into oxygen and hydrogen through a series of chemical reactions. The process is organised in such a way that water is the only raw material and oxygen and hydrogen are the only products while all the intermediate chemicals are internally recycled. The two thermodynamic cycles that are considered to be closest to commercialisation are:

- The Sulphur Iodine (SI) cycle; and
- The Hybrid Sulphur (HyS) cycle.

The sulphur iodine cycle, also known as GA process, entails three distinct sections, as shown in Figure 2.5. In this process, water is reacted at around 120 °C with sulphur dioxide to form sulphuric and hydriodic acids in an exothermic reaction. At specific concentration of reactants, involving an excess of iodine, a phase separation occurs between the two acid products. In the first section sulphuric acid H_2SO_4 and hydriodic acid HI are formed. In the second section, sulphuric acid is decomposed in a two-stage endothermic reaction, first producing SO_3 at a temperature about 400-500 °C and then producing while the second stage produces SO_2 , occurring at 800°C in the presence of a solid catalyst. The third section involves the decomposition of hydriodic acid to form hydrogen and iodine in a slightly endothermic reaction which can be conducted in either a liquid or a gase phase (Elder, et al., 2009).

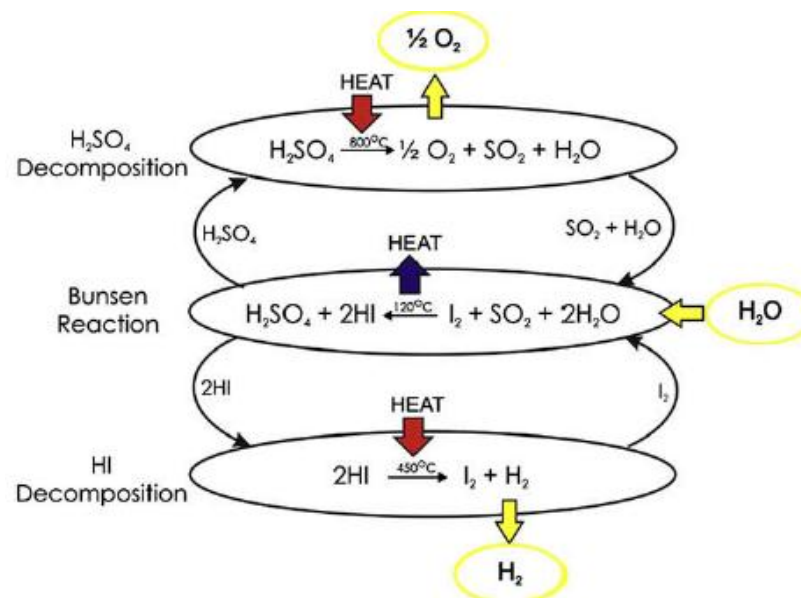


Figure 2.5 The sulphur iodine cycle (Elder, et al., 2009)

The Hybrid Sulphur cycle, also known as the Westinghouse cycle, combines electrolysis and thermochemical processes. The hybrid process principally consists of two stages.

- The electrolysis of water and sulphur dioxide at around 87°C generating sulphuric acid and hydrogen (H_2);
- The decomposition of sulphuric acid to sulphur trioxide (SO_3) and steam and further to sulphur dioxide (SO_2) and oxygen (O_2).

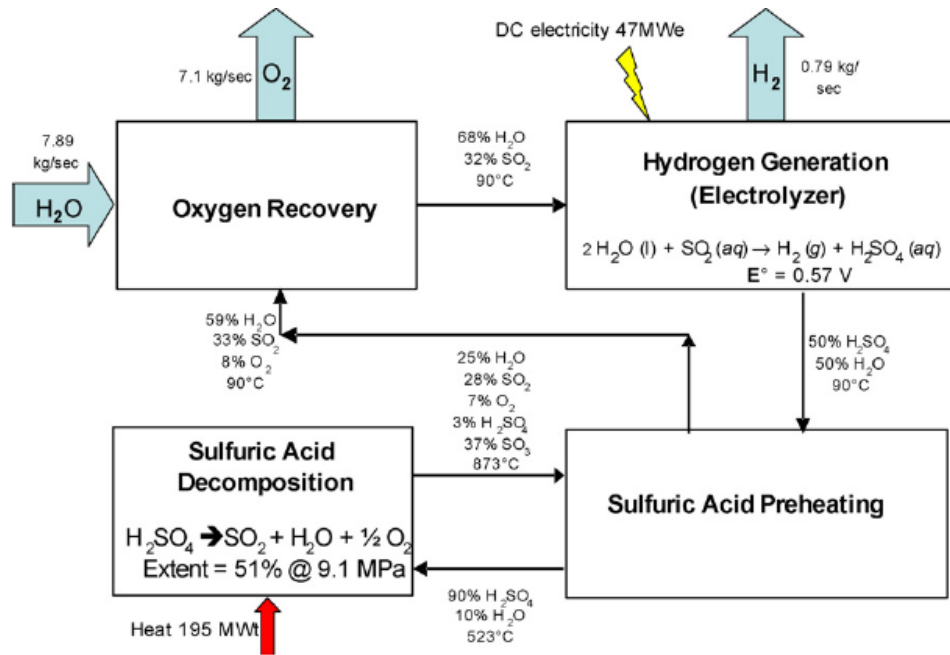


Figure 2.6 Single module hybrid sulphur block diagram (Greyvenstein, 2008)

High-temperature electrolysis

About 4% of the world's hydrogen production is generated by conventional, low-temperature water electrolysis. Water is dissociated into oxygen and hydrogen by an electric current that passes through it. An efficiency of about 80% can be achieved in the process of converting electricity to hydrogen in an electrolyser; however, since converting heat to electricity can only achieve around 40% efficiency, the process yields an overall efficiency of less than 35%. As can be seen in the Figure 2.7, the overall efficiency can be improved by using a higher temperature water-splitting process. However, major challenges exist in constructing long lifetime stacks that meet the requirements of such sophisticated catalysts (Elder, et al., 2009).

To achieve competitive efficiencies, hydrogen production processes require high-temperature operation ($\pm 850^\circ\text{C}$). High-temperature nuclear reactors and concentrated solar radiation are therefore regarded as solutions that can substantially increase the efficiency of hydrogen production technologies, providing a heat process with no fossil fuel consumption, no greenhouse gas production or any other form of air pollution (O'Brien, et al., 2010). The main handicap of solar energy is its varied concentration and availability across the world, which makes room for nuclear energy.

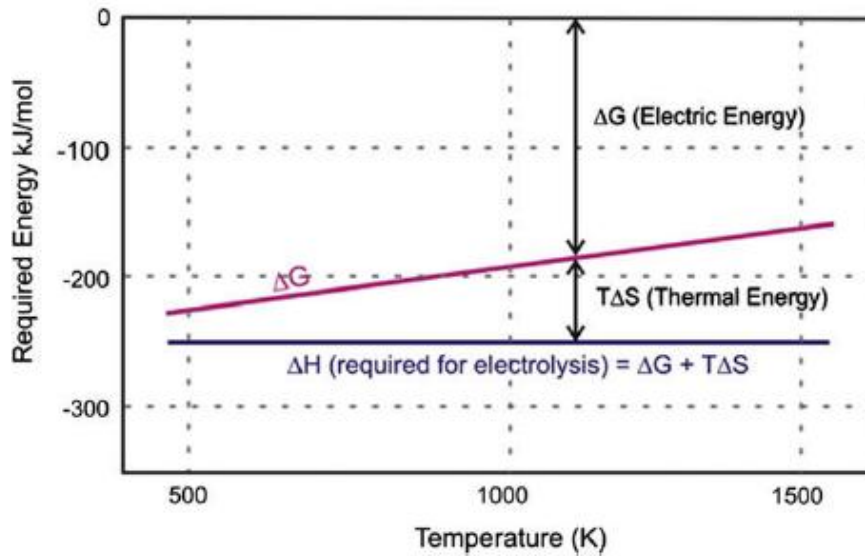


Figure 2.7 Thermodynamics of high-temperature electrolysis (Elder, et al., 2009)

2.3.2 Hydrogen using nuclear power

As main contender for the security of energy supply, nuclear power can provide carbon-free electricity for the grid, but it does not directly provide a transportation fuel as flexible as gasoline. As can be seen in Figure 2.7, hydrogen production from water-splitting requires 250 kJ/kmol (Elder, et al., 2009). An analysis of Figure 2.7 reveals that this process can be made more efficient by realising the electrolysis at much higher temperature since the use of electricity only might be more cost effective (Lewis, 2008). The required thermal energy should ideally be provided by a clean primary energy source such as nuclear power. Using nuclear power for hydrogen production seems to be an optimal option, since it should contribute to extending the lifetime of fossil fuels currently used in most processes requiring heat supply, and it is a non-pollutant and a clean energy source.

2.4 Power generation

A single energy source or fuel can be used in different types of generating systems. These systems include steam cycles, gas cycles and combined steam and gas turbines. In any of these systems, hot gases are delivered to a heat-recovery system, either to produce steam that is used to drive a steam turbine or directly to drive a gas turbine. An improvement on these systems has been found to be the cogeneration, a system that combines both. Each combination of energy source and power-generating system has its specific challenges regarding technical, economic and environmental aspects. In this section, both steam and gas turbine units will be discussed in order to guide the choice made in this study.

2.4.1 Gas turbine unit

The most basic gas turbine unit operates on a Brayton cycle (open cycle) and consists of a compressor, a combustion chamber and a turbine. The compressor is mounted on the

same shaft with the turbine. In general, air is drawn into the compressor, where its pressure is increased and then sent to a combustion chamber, where fuel is burnt to increase the temperature of the working fluid. The high pressure and high temperature gas of combustion is then expanded in the turbine where its energy is transformed to mechanical energy of the turbine. The energy required for the compressor process is withdrawn from the turbine; the remaining energy is called the net output work of the cycle.

A gas turbine unit can be used for turbojet propulsion as well as for power generation. In power generation, the combustion chamber is, depending on the case, sometimes replaced by a heat source such as a nuclear reactor providing heat to the gas (Eastop & McConkey, 1986).

2.4.2 Steam Turbine unit

A steam turbine unit is a power generation unit that produces power from a permanent steam supply to a turbine. Ideally steam need to be supplied to the turbine at high pressure and at high temperature. During the expansion process, the energy of the steam is converted to mechanical energy (work) that can be collected at the turbine shaft. The turbine unit uses a Rankine cycle. A steam turbine unit consists of a pump that increases the pressure of the feedwater, a boiler or steam generator, a turbine and a condenser. The high-pressure water from the pump is sent to a boiler or steam generator, depending on the case, to generate superheated steam that will be supplied to the turbine. After the turbine, the expanded steam is sent to a condenser (Eastop, et al., 1986).

2.5 Nuclear reactors

Through the years, nuclear energy has improved considerably. The very first types, also known as Generation I nuclear reactors, materialised in the early 1950-s, and, the latest nuclear reactor type, the “Generation IV reactors”, expected to be operational from 2030 onward (Abram & Ion, 2008). This evolutionary classification is based on the advancement in technology applied on the nuclear system. In this section the context of the current study will be discussed.

2.5.1 Generation IV nuclear reactors

To meet the future energy needs of the world, the energy mix presented in Figure 2.2 suggests a significant contribution from nuclear energy. In light of this, 10 countries have agreed on a framework for international collaboration in research for a future generation of nuclear energy systems, Generation IV, based on the following goals;

- Economic competitiveness: The level of financial risk should be comparable to other energy projects and its life-cycle cost advantageous over other energy sources,
- Safety and reliability: The probability and extent of reactor damage should be very low while performing under high accountability and safety,

- Sustainability: This new generation of nuclear energy systems should meet clean air objectives, promote long-term availability of the system and fuel utilisation, and minimise and manage their nuclear waste for the improvement of public health protection and the environment,
- Proliferation resistance: These systems should provide increased in protection against terrorism acts and be less attractive or desirable for diversion as weapons-usable materials (GIF & US DOE, 2002).

The Generation IV International Forum (GIF), created in 2000, whose aim is to foster the research and development necessary to promote the development of a new generation of nuclear reactors, has identified six types of reactors that can meet the Generation IV goals. These reactors systems are (Abram, et al., 2008):

- Very high-temperature gas-cooled reactor (VHTR);
- Gas-cooled fast reactor (GFR);
- Sodium-cooled fast reactor (SFR);
- Lead-cooled fast reactor (LFR);
- Molten salt reactor (MSR); and
- Super-critical water-cooled reactor (SCWR).

Generation IV nuclear power plants are expected to play an important role as source of base load power in many countries in the middle-long term (2030 to 2050) (Locatelli, Mancini & Todeschini, 2013). However, even the reactor type that has met the most extensive development criteria does not necessarily meet all the Generation IV goals. The potential of each system to meet the goals for Generation IV nuclear energy systems is presented in Table 2.1 with

Table 2.1 Potential of Generation IV nuclear energy systems to meet prescribed goals (Abram, et al., 2008) (1: very high, 2: high, 3: medium, 4: medium/low, 5: low and 6 very low)

Generation IV goal	VHTR	GFR	SFR	LFR	SCWR	MSR
Electricity efficiency	1	2	2	2	2	2
Process heat temperature	1	2	5	5	5	5
Creation of fissile material	4	2	2	2	5	4
Transmutation of waste	3	1	1	1	5	2
Passive safety	2	6	4	3	6	3
Technical feasibility	2	4	2	3	4	5

2.5.2 HTR-PM

The high-temperature gas-cooled reactor – pebble-bed module (HTR-PM) and the next generation nuclear plant (NGNP) are of the VHTR type, designed to operate at a very temperature for this technology, reaching 750 °C (Locatelli, et al., 2013). The HTR-PM has adopted an indirect Rankine cycle with intermediate steam generator for power generation. The HTR-PM is a 2 x 250 MW_{th} reactor modules feeding a single about 210 MW_e steam turbine generator (Zhang et al., 2009). As it is of VHTR type, with very high potential to high temperature, very high flexibility to high temperature process heat,

high potential for passive safety, high technical feasibility and medium potential for transmutation of waste and creation of fissile material, the HTR-PM could be developed for power generation and process heat such as CTL fuel conversion over medium term. The same consideration could also be studied for the PBMR, which could extensively be used in the hydrogen carrier and has a 900 °C outlet gas temperature (Locatelli, et al., 2013).

2.6 Heat pipe heat exchangers (HPHE)

A heat pipe is by definition a high thermal conductivity device operating without moving parts transporting efficiently to relatively long distances large amounts of heat at constant temperature without any external electricity input (Chaudhry, Hughes & Ghani, 2012). The transport of heat between hot section of the heat pipe, known as the evaporator, and the cold side, known as the condenser, is done by the heat pipe working fluid which is fundamentally at thermal saturation conditions. The heat transfer process is achieved using the latent heat properties of the working fluid. For these reasons, the working fluid for a specific heat pipe heat exchanger is selected depending of the desired operating temperature of the heat pipe while the working fluid pressure should be kept relatively as low as 0.1 – 20 bar (Laubscher and Dobson, 2013). The heat pipe technology is becoming the more and more attractive in heat transfer applications for its passive two-phase heat transfer, high heat transfer capability and operational reliability (Joung, Kim, Yang & Gam, 2013).

3 APPLICABLE THEORIES

As mentioned earlier, nuclear energy's contribution toward power generation and other heat processes could play a significant direct role in terms of the reduction of greenhouse gas emissions, and will indirectly extend the lifetime of the world's fossil fuel reserves (Saito, 2010), since most of the current processes still rely on coal and other types of fossil fuels for power generation and heat supply for most heat processes (Elder, et al., 2009).

In both, power generation and heat processes, fossil fuels are burnt to produce the necessary heat contained in the combustion products which can be directly used in a Brayton cycle to generate power or be supplied to a heat process. Alternatively, the necessary heat produced can be used to first generate steam from water, which will then be used in a Rankine cycle to generate electrical power or be supplied to a heat process such as a CTL process, where high-temperature steam is required for coal gasification (Mantripragada, et al., 2013). Replacing fossil fuels with nuclear materials as energy resources for power generation and heat processes requires further studies for the validation of the safety and feasibility of this technology (Brook, 2012).

In this chapter, a matching of high temperature nuclear reactor with steam generator is analysed based on thermodynamic and heat transfer principals for validation of theoretical feasibility.

3.1 Generation IV nuclear reactors

Worldwide programmes have been launched aimed at the development of safe and reliable nuclear power to contribute to and sustain a carbon dioxide free energy supply, in order to meet the 2030 energy demand and beyond (Bogusch, Carre, Knebel & Aoto, 2008). In line with the above-mentioned target, the GIF has initiated investigation of six types of advanced fission reactors using water, helium, liquid metal and molten salt as coolant. These reactors' design suggests implementation of very-high-temperature and high-temperature reactors, gas-cooled fast reactors and numerous others including liquid metal cooled fission plants (Bogusch, et al., 2008). Countries involved in the programme have independently selected their promising Generation IV reactor system. South Africa has selected, in the PBMR project, a high-temperature reactor consisting of moderated graphite, helium-cooled reactor in which the helium-gas is heated through a process of nuclear fission and is used in a direct Brayton power cycle for electrical power generation. The PBMR project, originally based on the German high-temperature gas-cooled reactor technology, makes use of spherical fuel elements, referred to as pebbles (Slabber, Theron & Matzner, 2006). PBMR technology aimed for a nuclear reactor that would theoretically maintain the inlet-outlet at 500 and 900 °C respectively at 7 MPa, as presented in Figure 3.1. Meanwhile, China has focussed on a relatively lower temperature type of reactor called the HTR-PM. This type differs from the PBMR regarding the following two aspects:

- The HTR-PM used the PBMR nuclear reactor type but maintains the temperature range at 250-750 °C at 7 MPa, as shown in Figure 3.2
- The HTR-PM provides heat for electrical power generation using a Rankine power cycle in which helium, the coolant gas, is recirculated in a closed loop

while exchanging heat in a once-through steam generator with the pressurised feedwater generating superheated steam which is then used in a Rankine cycle for electrical power.

For the current project, suggestions have been made to use a HTR-PM similar design to provide heat for electrical power generation and process heat to a CTL process operating in a cogeneration process.

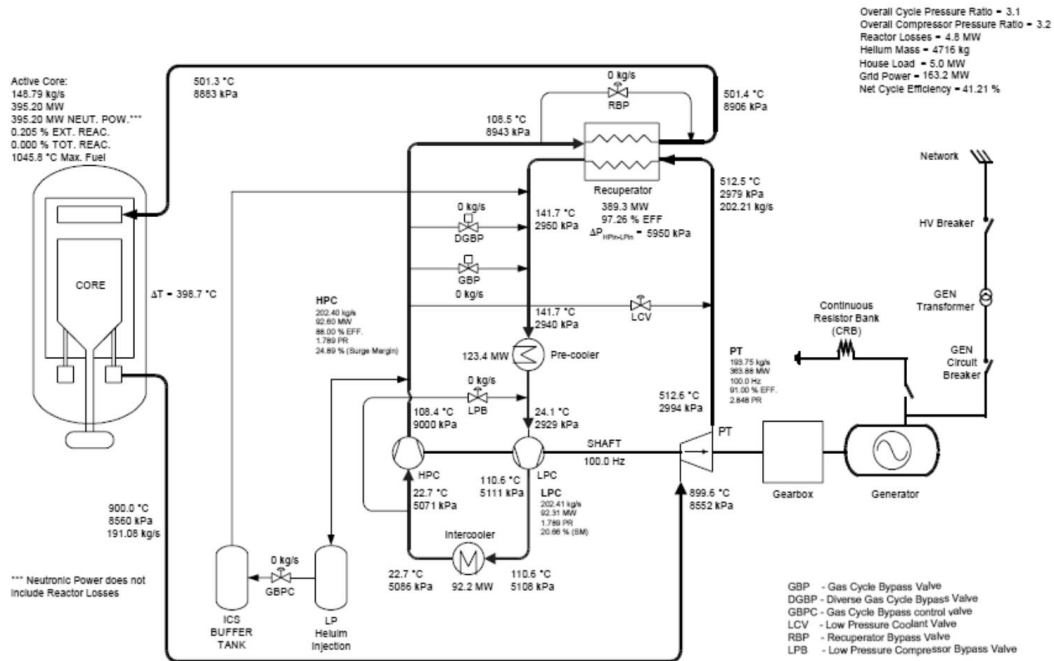
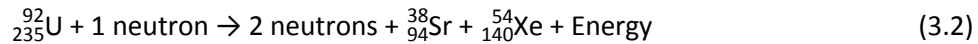
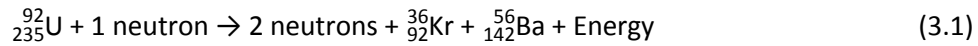


Figure 3.1 Conceptual flow diagram of a PBMR power conversion unit (Slabber, et al., 2006)

3.1.1 Nuclear fission process

Nuclear fission is the process of splitting heavy nuclei such as that of uranium into two or more lighter nuclei with a probable emission of some other radioactive particles. During this process, it might occur that equilibrium between the attractive and repulsive forces acting in heavy nuclei is lost due to the introduction of extra energy in the form of an absorbed neutron. Therefore, the nucleus will oscillate while attempting to regain the equilibrium state until the electrostatic force overcomes, splitting the nucleus apart and at the same time releasing energy in the form of radiation heat (King, 1964). The main fuel or element used in nuclear reactors and certain types of atomic bombs is uranium, in the form of its isotope ^{235}U . When a neutron strikes an isotope ^{235}U , it gets absorbed first, creating a different isotope, ^{236}U , which is naturally unstable, therefore causing the atom to fission. The fissioning of ^{236}U can produce over twenty different products, but in all cases the total mass of 236 should be conserved.

Two main possible reactions can be expected when ^{235}U is shot by a neutron. These two reactions are



where Sr, Kr, Ba and Xe stand for Strontium, Krypton, Barium and Xenon respectively (King, 1964).

From the above two chemical reactions, one can see that for each neutron used on ${}_{235}\text{U}$, two or more neutrons are produced; thereafter, if there is still ${}_{235}\text{U}$ available in the space, each of the two generated neutrons will produce at least two other neutrons, increasing the number of available neutrons in the system. This type of reaction is regarded as a chain-reaction, and will take place until ${}_{235}\text{U}$ fuel is completely spent. The energy released from the fission process, liberated as heat in a reactor, is presented in Table 3.1 below.

Table 3.1 Fission energy distribution (King, 1964)

Type of energy	Energy (Mev)
Kinetic energy of fission fragments	168
Kinetic energy of fission neutrons	5
Instantaneous gamma rays	7
Beta particles from fission products	7
Gamma rays from fission products	6
Neutron capture gamma's	7
Total Mev	~ 200

From Table 3.1, it can be seen that the kinetic energy of fission fragments contributes to about 80 per cent of the total energy released from the fission process. The high kinetic energy in the fission fragments causes a rise in temperature due to the transfer of energy to the material in which they are contained. This internal rise of temperature is then transferred out of the material in the form of heat. In the same way, the dissipated kinetic energy of the fission neutrons through elastic collision between fission neutrons and the struck nuclei, which increases its kinetic energy, is manifested as heat (King, 1964).

When fission neutrons collide with heavy nuclei, the kinetic energy reduces. This process of slowing down neutrons from fission energies to thermal energies is referred to as moderation. Moderation is generally accomplished by elastic collisions of neutrons with nuclei within the nuclear reactor. Depending on the type of nuclei, moderating substance or moderator, it might take more or fewer collisions to reduce the neutron's kinetic energy from its most probable energy, 1 Mev, to its thermal energy range, about 0.025 Mev, which is the required energy for a future fission process. Therefore, the choice of moderator should result from a balance between its slowing down power (SDP) and its moderating ratio (MR) which takes into account the rate of neutron absorption in the moderator, as can be seen in Table 3.2 (King, 1964).

Table 3.2 Criterion for better moderator (King, 1964)

Moderator type	Slowing down power (SDP)	Moderating ratio (MR)
Light water (H ₂ O)	1.36	65
Heavy water (D ₂ O)	0.18	4860 (pure), 2085 (0.25% H ₂ O)
Beryllium (Be)	0.160	150
Carbon (C)	0.063	170

A better moderator should be the one that offers a higher value for the product of slowing down power (SDP) by the moderating ratio (MR) (King, 1964).

3.1.2 Nuclear power generation

As per the South African PBMR fuel description presented in Chapter 2, uranium is contained in the pebbles (Slabber, et al., 2006). The fission process occurring within the fuel element will increase its overall temperature to a very high range; however, this temperature should not exceed a safety limit value of 1620 °C for any operating or accident condition (Zhang, et al., 2009).

Equations 3.1 and 3.2 show that for every fission occurring, a certain amount of energy will be released in the reactor; this energy level has been approximated to 200 Mev as shown in Table 3.1. Therefore, by analogy one would assume that the power level of the overall nuclear reactor is dependent on the number of fission processes occurring within the contained fuel elements.

The power produced within a nuclear reactor can be expressed by the following equation (King, 1964):

$$\text{Power produced} = \sum_{i=1}^n (\phi_i \Sigma_{fi}) V_f Q \quad (3.3)$$

In equation 3.3, the neutron density ϕ gives the number of particles causing the reaction per unit per unit time; Σ_f is the effective target area per cm³ for the fission process. Therefore, the product $(\phi \Sigma_f)$ will represent the number of fissions occurring within a unit time period per unit volume. Multiplying this by the volume of the fuel V_f , we obtain the total number of fissions occurring in the reactor per unit time. This total number of fissions is then multiplied by the constant conversion factor Q , which is the energy released in a single fission, and the total power output of the reactor is obtained. Recall that during nuclear fission process neutrons of all energy groups exist within the reactor in the range of fission energy varying between 18 Mev to 0.025 Mev. Therefore, $i=1,2, \dots, n$ will represent the energy group of the neutron into which the spectrum of neutron's energy in the reactor is divided (King, 1964). In some cases this division has been done up to 30 neutron groups, allowing more accurate calculation of the power output of the reactor by a single term that uses an average flux and an average cross-section for the entire energy spectrum.

a. Multiplication factor k and criticality

The multiplication factor is defined as the ratio of the number of neutrons in one generation to the number of neutrons generated in the previous generation.

$$k = \frac{\text{number of neutrons in one generation}}{\text{number of neutrons in previous generation}} \quad (3.4)$$

This ratio can be greater than, equal to or less than one; therefore the reactor will be qualified as supercritical, critical or subcritical respectively (King, 1964).

b. Variation of the reactor power output

Considering a nuclear reactor operating at a certain power level P_0 at a specific time, in some cases it can require less or even more power from the reactor due to the demand fluctuation with regard to time and need. Therefore one would like to have control over the power level that a nuclear reactor can deliver. Investigating equation 3.3, it can be seen that power level control can be achieved by changing the neutron population from a time step to the next.

Re-writing equation 3.4 from $(i-1)^{\text{th}}$ to i^{th} generation, the following is obtained

$$k = \frac{n_i}{n_{i-1}} \quad (3.5)$$

Further developing equation 3.5 and adding the same quantity on both sides, the following is yielded

$$k n_{i-1} - n_{i-1} = n_i - n_{i-1} = \Delta n \quad (3.6)$$

Written in a differential form,

$$dn = (k-1)n \quad (3.7)$$

Assuming that the average neutron lifetime l is in seconds to realise one generation, then the rate of change of neutrons per unit of time in differential form will be given by the following expression:

$$\frac{dn}{dt} = \frac{n(k-1)}{l} \quad (3.8)$$

For a nuclear reactor initially operating at power level P_0 , the solution of the differential equation provides the following result:

$$n = n_0 e^{\frac{(k-1)t}{l}} = n_0 e^{\frac{\Delta k}{l}t} \quad (3.9)$$

Equation 3.3 has shown that the power output of the reactor is directly proportional to the neutron flux ϕ , as Q , V_f and \sum_f are considered constant. The neutron flux, by definition could be as well expressed in terms of neutron density by the following:

$$\phi = nV \quad (3.10)$$

where n is the neutron density and V is the constant average velocity of the neutrons in the spectrum (King, 1964). Thus, the proportionality between the reactor output power and the neutron flux could be extended to neutron density. Therefore, applying the equation of variation of neutron density (equation 3.9) to the reactor power output, initially operating at P_0 , yields the following result (Coban, 2009):

$$P = P_0 e^{\frac{(k-1)t}{\Lambda}} = P_0 e^{\frac{\Delta k}{\Lambda} t} \quad (3.11)$$

Equation 3.11 shows that to keep constant the power output of the nuclear reactor, the Δk should be kept constant. Therefore, any increase in the value of k will increase the reactor power output; this is referred to as excess multiplication factor k_{ex} , which can experimentally be approximated to the reactor's reactivity ρ as

$$\rho = \frac{k-1}{k} \approx k_{ex} = k-1 \quad (3.12)$$

c. Reactor power control

As described in Section 3.1.2a, the critical condition is obtained if equation 3.4 yields 1, or in other words, by keeping the excess multiplication constant or the reactivity equal to zero. Inserting a negative or positive value of reactivity will respectively reduce or increase the power output of the reactor, as can be seen from equation 3.11; therefore it would be necessary to make use of techniques that allow control of the number of neutrons produced from one generation to the next (King, 1964).

In practice, to achieve such operation, materials such as boron (B) should be used on control rods, since they absorb neutrons without fissioning themselves. A high thermal cross section would be desirable for the control rod material since the purpose is then to absorb neutrons, unlike the other materials of the reactor. In such a way, it would be possible to control the reactor power by inserting the control rods inside the reactor to reduce or even completely shut down the reactor, therefore creating the subcritical conditions within the reactor; pulling out the control rods will result in a rapid increase of power output, creating the supercritical conditions. Once the desired power is achieved, the control rod position should be maintained in the same position to bring the multiplication factor to a strict constant value of 1 to achieve the critical conditions in the reactor (King, 1964).

3.1.3 Nuclear reactor heat balances

Based on HTR-PM similar design, the heat balances within the nuclear reactor could be simulated by applying the conversion of mass, energy and momentum principles and heat transfer occurring between the block graphite of the reactor and the coolant gas for the cooling of the reflector sides, and between the coolant gas and the fuel elements inside the reactor core.

a. *Pebble bed model*

The pebble bed is a type of heat exchanger that uses one single stream flowing through a packed bed of solid particles that can be heated up from a separate process (Mills, 1995). The pebble bed can be used as a heat storage system when hot fluid is circulated through it first, heating up the solid spherical blocks; then the cold fluid is passed through the bed and it is heated up in turn. A pebble bed is characterised by the following:

- The *void fraction* ε which is the ratio of the unoccupied volume over the total volume of the bed. This ratio is generally between 0.3 and 0.5 (Mills, 1995).

$$\varepsilon = \frac{\text{Unoccupied volume}}{\text{Bed volume}} = \frac{\text{Bed volume} - \text{Packing volume}}{\text{Bed volume}} \quad (3.13)$$

The HTR-10 and HTR-PM have used a void fraction of 0.39 for the reactor core (Li, et al., 2008a) which is 39% of the total reactor core volume as presented in Table 3.3.

- The specific surface area a , which is the wetted or heat transfer area per unit volume of the packed bed expressed in m^{-1} .

$$a = \frac{A_p}{V_p} (1-\varepsilon) = \frac{6}{d_p} (1-\varepsilon) \quad (3.14)$$

where A_p , V_p and d_p stand for surface area, volume and diameter of the fuel element respectively.

- The hydraulic diameter d_h which is the ratio of the unoccupied volume or the volume of bed available for flow over the wetted surface in the packed bed (Mills, 1995).

$$d_h = \frac{\text{Volume of bed available for flow}}{\text{Wetted surface in bed}} = \frac{\varepsilon}{a} = \frac{\varepsilon}{1-\varepsilon} \frac{d_p}{6} \quad (3.15)$$

- The *characteristic length* L_c is defined to be six times the hydraulic diameter.
- The *superficial velocity* V_c , which is the velocity of the flow through the packed bed. This velocity can be calculated from the mass flow rate by the following equation (Mills, 1995), where A_c is the cross-section of the bed and ρ is the density of the fluid.

$$V_c = \frac{\dot{m}}{\rho \varepsilon A_c} \quad (3.16)$$

From the above, correlations of pressure drop and heat transfer based on the characteristic length and hydraulic diameter could be expected. The pressure drop across the pebble bed is obtained from the Ergun equation below (Li, et al., 2008a)

$$\frac{dP}{dx} = \frac{150\mu V}{L} + \frac{1.75\rho V^2}{L} \quad (3.17)$$

and the Nusselt number expressing the heat transfer for gases flowing in the bed can be written as (Mills, 1995)

$$Nu = (0.5 Re^{1/2} + 0.2 Re^{2/3}) Pr^{1/3} \quad (3.18)$$

In equation 3.18 Nu, Re and Pr are the Nusselt, Reynold and Prandtl number respectively (Mills, 1995).

Table 3.3 Relevant parameters used in the HTR-10 (Li, et al., 2008a)

Parameters	Description
Void fraction of pebble bed ϵ	0.39
Leakage ratio of helium β	0.1
Average specific heat of helium c_p , (kJ/kg.K)	5195
Number of fuel elements	420000

b. Block reflector cooling

The thermal energy produced during the nuclear fission process in the reactor core is mainly transferred to the cooling gas, therefore keeping the average temperature at about 841 °C (Li, et al., 2008b). Nevertheless, this thermal energy is partly transferred to the reflector side. Therefore, the HTR-PM model assumes that the cooling gas, helium, flows upward in 30 channels, situated in the annulus reflector, while cooling the reflector side before entering the reactor core. This organisation allows maintaining the reflector at a steady-state temperature value of 271 °C, resulting in a pre-heat of the cooling helium (Li, et al., 2008b).

Quantifying the heat removal from the reflector requires the estimation of the convective heat transfer coefficient. This is determined by the flow characteristics and the size of the channels. The assumption made on the annulus reflector to determine the channels individual diameters considers the conservation of the inlet flow characteristics of the gas through the channels. This can be achieved when the mean velocity is approximately maintained at the same steady-state value as in the inlet pipe. Therefore, the current project suggests keeping the overall flow cross-section of all the channels the same as the annulus's inlet cross-section. Once the diameter of a channel is known, other flow characteristics such as the Reynold number, Prandtl number and Nusselt number can be determined, since the steady-state mass flow rate and the density are known, in order to approximate the heat transfer coefficient. The steady-state heat rate transferred from the solid graphite to the moving fluid can be determined by the following equation (Wong, 1977):

$$\dot{Q} = \alpha A (T_{\text{wall}} - T_{\text{fluid}}) \quad (3.19)$$

The heat transfer coefficient in equation 3.19 is obtained using the Nusselt number and can be defined as in equation 3.20 (Wong, 1977), where the characteristic length equals the diameter of the channel. These channels are assumed smooth since they are located in the graphite material

$$\alpha = \frac{k \text{ Nu}}{L} \quad (3.20)$$

c. Helium properties

In recent years another approach to system analysis used by engineers has been the determination of balance points by running simulation. These simulations are performed by mathematical equations rather than graphical procedures (Stoecker & Jones, 1982).

As suggested by Generation IV nuclear reactors, helium is used as coolant in the reactor. Therefore, to determine its thermodynamic properties for various thermodynamic conditions, one would need mathematical equations between the thermodynamic parameters rather than reading the chart provided in Figure A.3. Stoecker and Jones (1982), in the field of refrigeration and air conditioning, suggest that a chart can be converted into mathematical form by applying the binomial equation 3.21 for one unknown desired parameter using two other that are clearly defined (Stoecker, et al., 1982).

$$h(p,T) = C_1 + C_2 p + C_3 p^2 + C_4 T + C_5 T^2 + C_6 pT + C_7 p^2 T + C_8 pT^2 + C_9 p^2 T^2 \quad (3.21)$$

where C_1, C_2, \dots, C_9 are the applicable constants calculated from solving simultaneously the set of nine equations built from data read from the graph in Figure 3.3 (Stoecker, et al., 1982). Samples of the data used to compute the applicable constants are presented in Table 3.4; these data has been selected in the relevant expected region of operation of helium on a typical Generation IV nuclear reactor.

The working region has been assumed between 1 and 9 MPa for pressure range and 30 to 1000 °C for temperature. To build the set of nine equations, nine points have selected to mathematically model the gas thermodynamic properties at any conditions within the assumed region. Each condition, temperature and pressure have been applied to equation 3.21 to make nine equations linking the pressure and temperature to the relevant enthalpy.

Using any two thermodynamic parameters, equation 3.21 can also be re-written for any other thermodynamic parameter that one would like to define. For the purpose of this study, attention has been focussed on only five thermodynamic properties, namely enthalpy h , entropy s , specific volume v , temperature T and pressure p .

Table 3.4 Thermodynamic properties of helium in the region situated between 30 °C and 1000 °C and 3 MPa and 10 MPa (Barron, 1985).

	Temperature, T (°C)	Pressure, P (MPa)	Enthalpy, h (kJ/kg)	Entropy, s (kJ/kgK)	Specific volume v (m ³ /kg)
1	29.31	3.063	32.3	-7.003	0.208
2	30.99	9.114	60.5	-9.231	0.07218
3	30.59	1.006	32.3	-4.67	0.6301
4	548.6	3.063	2727.8	-1.814	0.5597
5	556.2	9.114	2784.3	-4.029	0.1915
6	549.7	1.006	2727.8	0.5049	1.702
7	954.7	1.006	4830.6	2.583	2.538
8	953.6	3.063	4830.6	0.266	0.8343
9	953.3	9.114	4844.8	-1.999	0.2818

Using values from Table 3.4 for temperature and pressure, the enthalpy can be obtained with the following equation

$$h(p,T) = -129.8490 + 5.1944 T + 0.0000 T^2 + 3.2846 p - 0.0030 p^2 - 0.0017 pT + 0.0000 T^2 p + 0.0001 T p^2 + 0.0000 p^2 T^2 \quad (3.22)$$

Using the enthalpy and the pressure, the temperature can be obtained relatively with the following equation:

$$T(p,h) = 24.9981 - 0.6247 p + 0.0002 p^2 + 0.1925 h - 0.0000 h^2 - 0.0001 ph + 0.0000 p^2 h + 0.0000 ph^2 + 0.0000 p^2 h^2 \quad (3.23)$$

For the high-temperature gas-cooled nuclear reactor, since the pressure and desired temperature for inlet and outlet of the coolant gas to the reactor are known, enthalpies for the inlet and the outlet can be calculated with equation 3.22. The change in enthalpy between the inlet and the outlet points will determine the amount of energy removed from the nuclear reactor per kilogram of helium (Mills, 1995).

3.2 Steam generation process

The NGNP design intends to produce high-pressure steam for both process heat and/or the generation of electricity instead of direct processes such as the Brayton cycle for power generation as suggested in the original PBMR project (Wright, Wright & Petti, 2010). This steam generation process is achieved by exchanging heat from hot flowing gas, helium in this case, to the high-pressure feedwater in a cross-counter flow once-through heat exchanger.

3.2.1 Heat exchanger and steam generator types

Steam can be generated in several types of heat exchangers. Heat exchangers can be classified according to the flow configuration and the heat transfer area (Mills, 1995).

According to the geometric flow configuration, a heat exchanger can be classified as one of the following:

Single-stream

In this configuration, only one stream temperature changes in the heat exchanger while the other remains constant. Therefore, the flow direction is immaterial.

Parallel-flow two-stream

In this configuration, two fluids flow in the same and parallel direction. This heat exchanger can simply consist of two coaxial tubes. In practice, however, a large number of tubes is located in a shell to form a shell-and-tube exchanger. The shell-and-tube is generally used for liquids and high-pressure fluids. The plate type consists of multiple plates separated by gaskets and is more suitable for gases at low pressures. This heat exchanger configuration is also known as concurrent configuration.

Counterflow two-stream

Still parallel, the two fluids flow in opposite directions in this case. The counterflow heat exchanger is also known as countercurrent heat exchanger. In practice, for a given number of transfer units, a counterflow heat exchanger offers higher effectiveness and therefore the counterflow will be preferred to a parallel-flow.

Cross-flow two-stream

In a cross-flow configuration, the two streams are at a right angle to each other. One fluid flows inside tubes arranged in a bank or bundle while the second stream is flowing through the bank in a direction at a right angle to the tubes. One or even both of the streams may be unmixed. In terms of effectiveness, this configuration is intermediate between the parallel-flow and the counterflow (Mills, 1995).

Multipass two-stream

In a multipass two-stream heat exchanger tubes of a shell-and-tube exchanger double back one or more times inside the shell. Some passes may be parallel flow and others may be counterflow. The two-pass type of heat exchanger is popular since only one side of the heat exchanger requires perforation to lead in and out the tubes.

Cross-counterflow two-stream

In practice, heat exchanger flow configurations often approximate the idealisation of multipass. As the number of passes increases, the effectiveness is improved and therefore approaches that of an ideal counterflow heat exchanger. A commonly encountered type consists of a coil in which one stream flows while the second flows in the shell.

Regenerators

Traditionally known as recuperators, the two streams alternatively flow through a matrix of substantial heat storage capacity. The matrix rises its temperature when the hot fluid passes through it. Alternatively when the cold fluid passes through the matrix, the stored heat is transferred to the cold fluid, cooling down the matrix. All the above flow configurations can be applied to a regenerator (Mills, 1995).

3.2.2 Steam generator energy balance

In a steam generator, as in any heat exchanger, heat transfer occurs between the cold and hot streams. The role of the steam generator in this project will be to extract heat from the hot helium and utilise it in generating superheated steam for power generation and heat process for coal conversion to liquid fuel. To be considered, a heat-load balance was performed as basis for the steady-state performance of the steam generator.

Since phase change is involved in the steam generation process, the steam generator has been split in three parts, as can be seen in Figure 3.2 (Hoffer, Sabharwall & Anderson, 2011). The section starting from the inlet consisting of feedwater to the point where vaporisation starts is called the “economizer”. The next section, where the vaporisation process basically occurs is called the “evaporator”, in this section a two-phase flow coexists. The last section is called the “superheater”, and is the section in which dry steam is heated to reach the required range at the exit.

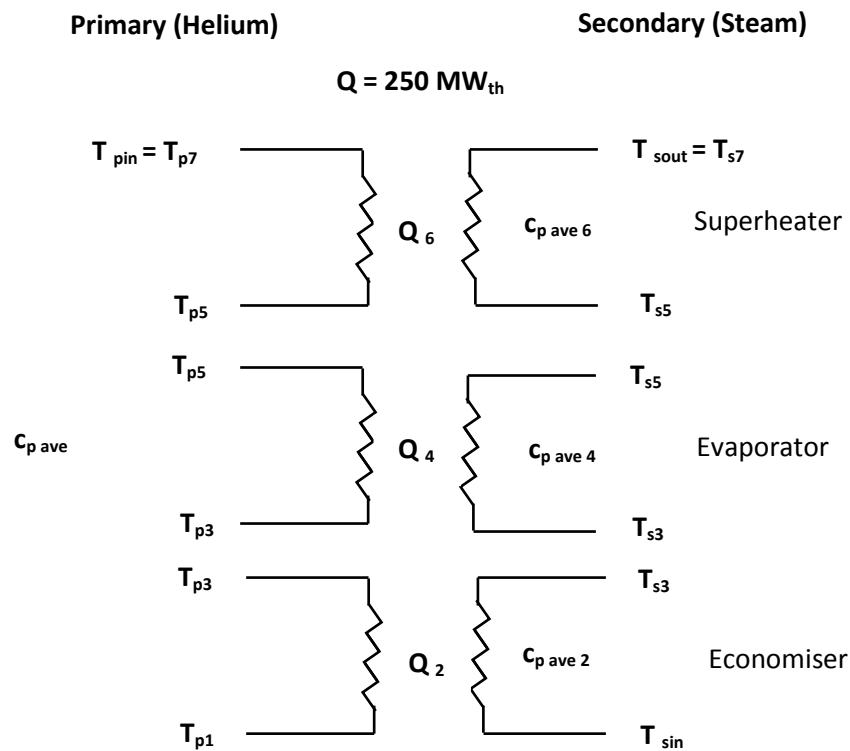


Figure 3.2 Once-through steam generator sections (Hoffer, et al., 2011)

The principal of conservation of energy applied to a heat exchanger yields the following equation (Abuadala & Dincer, 2010):

$$\dot{Q}_{\text{hot}} = \dot{Q}_{\text{cold}} \quad (3.24)$$

which can be re-written as

$$\dot{m}_{\text{hot}}(h_{\text{inlet}} - h_{\text{outlet}})_{\text{hot}} = \dot{m}_{\text{cold}}(h_{\text{outlet}} - h_{\text{inlet}})_{\text{cold}} \quad (3.25)$$

Equation 3.24 is individually applied to the three sections of the steam generator yielding equations 3.25 for the economizer, equation 3.26 for the evaporator and equation 3.27 for the superheater.

$$\dot{m}_{\text{helium}} c_{p \text{ ave}} (T_{\text{inlet}} - T_{\text{outlet}})_{\text{eco}} = \dot{m}_{\text{feedwater}} c_{p \text{ ave } 2} (T_{\text{outlet}} - T_{\text{inlet}})_{\text{eco}} = \dot{Q}_2 \quad (3.26)$$

$$\dot{m}_{\text{helium}} c_{p \text{ ave}} (T_{\text{inlet}} - T_{\text{outlet}})_{\text{eva}} = \dot{m}_{\text{feedwater}} (h_{\text{outlet}} - h_{\text{inlet}})_{\text{eva}} = \dot{Q}_4 \quad (3.27)$$

$$\dot{m}_{\text{helium}} c_{p \text{ ave}} (T_{\text{inlet}} - T_{\text{outlet}})_{\text{sup}} = \dot{m}_{\text{feedwater}} (h_{\text{outlet}} - h_{\text{inlet}})_{\text{sup}} = \dot{Q}_6 \quad (3.28)$$

In the above equations, \dot{m} , eco, eva and sup stand for the mass flow rate, the economiser, the evaporator and the superheater respectively. Note that ideally the evaporation occurs at constant pressure and temperature, therefore, the inlet and the outlet temperatures to the evaporator on the secondary side will be assumed to be equal in our simulation for the sake of simplicity.

To run these calculations, XSteam/Matlab has been used to determine the steam properties at specified thermodynamic conditions. Details on pressure drops in the steam generator are found in appendix A.

The overall heat transferred during the steam generation process can be written in terms of the log mean temperature difference ΔT_{LMTD} and the overall heat transfer coefficient of the steam generation process with the following expression (Mills, 1995):

$$\dot{Q}_{1-7} = U A \Delta T_{\text{LMTD}} = \dot{Q}_2 + \dot{Q}_4 + \dot{Q}_6 \quad (3.29)$$

where

$$\Delta T_{\text{LMTD}} = \frac{(T_{\text{pin}} - T_{\text{sout}}) - (T_{\text{p1}} - T_{\text{s1}})}{\ln \left(\frac{T_{\text{pin}} - T_{\text{sout}}}{T_{\text{p1}} - T_{\text{s1}}} \right)} \quad (3.30)$$

Due to the considerable variation of the steam properties during the steam generation process, it has been suggested that the economiser, the evaporator and the superheater be analysed separately for the calculation of the heat transfer coefficient which in turn highly dependent on the density of the fluid via the Reynolds number (Mills, 1995).

Therefore equations 3.29 and 3.30 will be applied to the three sections of the steam generator in the following paragraphs.

Applying equation 3.30 to the economiser requires that both inlet (T_{p3} , T_{s1}) and outlet temperatures (T_{p1} , T_{s3}) are defined fully. Therefore, equation 3.30 can be written as

$$\Delta T_{\text{LMTD } 1-3} = \frac{(T_{p3} - T_{s3}) - (T_{p1} - T_{s1})}{\ln\left(\frac{T_{p3} - T_{s3}}{T_{p1} - T_{s1}}\right)} \quad (3.31)$$

The amount of heat exchanged in the economiser can be obtained by applying 3.29 to the economiser only, yielding

$$\dot{Q}_{1-3} = (U A)_{1-3} \Delta T_{\text{LMTD } 1-3} = \dot{Q}_2 \quad (3.32)$$

For the purpose of this study, using the feedwater mass flow rate and the change in enthalpy from the inlet to the outlet of the economizer, evaluated in Matlab/XSteam, the heat rate required to bring the feedwater to saturation state could be evaluated.

The same approach was applied to quantify the heat rate and mean log temperature difference in the evaporator and the superheater. Referring to Figure 3.3, the heat rates in the evaporator and superheater can be defined by equations 3.33 and 3.34 respectively while the mean log temperature difference are given by equation 3.35 and 3.36.

$$\dot{Q}_{3-5} = (U A)_{3-5} \Delta T_{\text{LMTD } 3-5} = \dot{Q}_4 \quad (3.33)$$

$$\dot{Q}_{5-7} = (U A)_{5-7} \Delta T_{\text{LMTD } 5-7} = \dot{Q}_6 \quad (3.34)$$

$$\Delta T_{\text{LMTD } 3-5} = \frac{(T_{p5} - T_{s5}) - (T_{p3} - T_{s3})}{\ln\left(\frac{T_{p5} - T_{s5}}{T_{p3} - T_{s3}}\right)} \quad (3.35)$$

$$\Delta T_{\text{LMTD } 1-3} = \frac{(T_{p7} - T_{s7}) - (T_{p5} - T_{s5})}{\ln\left(\frac{T_{p7} - T_{s7}}{T_{p5} - T_{s5}}\right)} \quad (3.36)$$

On the other hand, the heat transfer area can be obtained by the following expression:

$$\text{Heat Transfer Area} = \pi \times \text{pipe diameter} \times \text{length} \quad (3.37)$$

Equation 3.37 applied to the three sections of the steam generator yields 3.38, 3.39 and 3.40 for the economiser, the evaporator and the superheater respectively

$$A_{1-3} = \pi d l_{1-3} \quad (3.38)$$

$$A_{3-5} = \pi d l_{3-5} \quad (3.39)$$

$$A_{5-7} = \pi d l_{5-7} \quad (3.40)$$

The energy balance equation 3.26 applied to the steam generator in its three sections reveals that the ratio of helium to feedwater mass flow rates equals the inverse of their respective change in enthalpy since the steam generator is assumed perfectly insulated.

$$\frac{\dot{m}_s}{\dot{m}_h} = \frac{(h_{in} - h_{out})_h}{(h_{out} - h_{in})_s} \quad (3.41)$$

3.2.3 Overall heat transfer coefficient and concept of effectiveness

In the steam generator, the heat transferred from the nuclear reactor coolant gas to water/steam can be modelled by Figure 3.3. It can be seen clearly that heat flows from the hot helium, is first transferred to the pipes outer area by convection, then flows by conduction through the pipe wall thickness and then finally is transferred to the water/steam from the pipe's inner surface by convection. Both convections are forced since the circulation of helium is achieved with a blower while the feedwater is pumped.

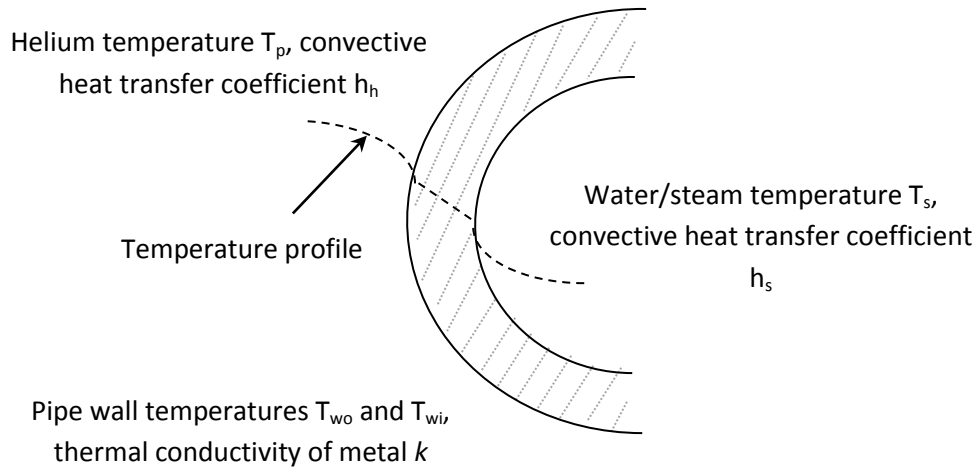


Figure 3.3 Temperature distributions between helium and water/steam

For a system such as depicted in Figure 3.3, the overall heat transfer coefficient can be expressed by the following expression (Mills, 1995)

$$\frac{1}{UA} = \frac{1}{2\pi r l h_h} + \frac{\ln(r_o/r_i)}{2\pi k l} + \frac{1}{2\pi r l h_s} \quad (3.42)$$

Neglecting the conduction term from the above equation and substituting equation 3.42 in 3.43, equation 3.44 is obtained:

$$A = \pi d l = 2\pi r l, \text{ and } r = \frac{r_o + r_i}{2} \quad (3.43)$$

$$\frac{1}{Ul} = \frac{1}{lh_h} + \frac{1}{lh_s} \quad \text{or} \quad \frac{1}{Ul} = \frac{h_h + h_s}{lh_s h_h} \quad (3.44)$$

The water/steam heat transfer coefficient is calculated by the equation below:

$$h_s = \frac{Nu k}{d} \quad (3.45)$$

where

$$Nu = C Re^m Pr^n K \quad (3.46)$$

Equation 3.46 is used to determine the Nusselt number. In this equation the Reynolds (Re) and Prandtl (Pr) numbers are obtained from equation 3.47 while constants C, K, m and n can be read from the Table 3.5 (Wong, 1977). The fluid velocity v in equation 3.47 is obtained from the mass flow rate and the pipe diameter as shown in equation 3.48.

$$Re = \frac{\rho v d}{\mu} \text{ and } Pr = \frac{\mu C_p}{k} \quad (3.47)$$

$$v = \frac{4 \dot{m}}{\rho \pi d^2} \quad (3.48)$$

In this section too the steam properties have been determined using XSteam/Matlab for the relevant thermodynamic conditions. The heat transfer coefficient h_s for the three sections of the steam generator could be determined by repeatedly applying equation 3.42 to 3.48 to the economiser, the evaporator and the superheater to obtain h_{s1-3} , h_{s3-5} and h_{s5-7} .

Table 3.5 Nusselt number applicable constants for circular tube cross-section (Wong, 1977)

Operating conditions	C	m	N	K
Laminar flow short tube, Re < 2000, Gz > 10	1.86	$\frac{1}{3}$	$\frac{1}{3}$	$\left(\frac{d}{l}\right)^{\frac{1}{3}} \left(\frac{\mu}{\mu_w}\right)^{0.14}$
Laminar flow long tube, Re < 2000, Gz < 10	3.66	0	0	1
Turbulent flow of gases Re > 2000	0.023	0.8	0.4	1
Turbulent flow of highly viscous liquids, 0.6 < Pr < 100	0.027	0.8	0.33	$\left(\frac{\mu}{\mu_w}\right)^{0.14}$

In Table 3.5, Gz stands for the Graetz number and is given by the following equation for a circular pipe of diameter d:

$$Gz = \left(\frac{\pi d}{4 l} Re Pr\right) = \frac{\dot{m} C_p}{k l} \quad (3.49)$$

3.2.4 Moving boundaries assumptions

A typical tube of total length l_{17} of a once-through steam generator as modelled in three sections namely the economiser, the evaporator and the superheater, is also split in three sections of three different lengths that respectively correspond to the economiser's length l_{13} , the evaporator's length l_{35} and the superheater's length l_{57} . The moving boundaries assumptions suggest that these lengths can be subject to change due to the mass flow rate and thermodynamic conditions of the fluid since points 3 and 5, representing the liquid saturation state and the vapour saturation state respectively, are allowed to move, while points 1 and 7, representing the inlet and outlet to the tube respectively, are fixed in time.

The steam generator heat rate of equation 3.29 can also be written in terms of the steam mass flow rate and becomes

$$\dot{Q}_{1-7} = U A \Delta T_{LMTD} = \dot{m}_s \Delta h \quad (3.50)$$

Development of equation 3.50 reveals that the steam mass flow rate is directly proportional to the pipe length, as can be seen in 3.51 derived from 3.50. Therefore, the theory assumes that the change in mass flow rate due to fluctuations of the power demand consequently manifested on the pipe length.

$$l = \dot{m}_s \frac{\Delta h}{\pi d U \Delta T_m} \quad (3.51)$$

Equation 3.51 can be applied to the three sections of our steam generator, thus defining their lengths for a finite total length.

3.3 Control aspects of steam generated by nuclear reactor

As in nature, electricity cannot be stored in large quantities; generally, it has to be generated as it is used (Eskom, 2004). Therefore, electricity generation is required to match the supply to the demand.

In the process of matching the supply to the demand, the total energy generated from the HTMR will be subject to fluctuations driven by the demand - the consumer in this case. Reduced to an individual power generating system, it has been found from equation 3.24 that the heat supplied and the heat provided by the system for power generation should be balanced. Written in a different form as equation 3.41, it highlights that, operating within the same thermodynamic conditions, the energy supply and demand could be balanced just by modifying the mass flow rate ratio between feedwater and helium. Due to the continuously fluctuating character of the demand, a perfect match would be achieved by applying a proportional continuous variation of the mass flow rates.

Most pumping applications involving flow variation generally make use of a throttling valve, recirculation line and/or variable motor speed to deliver the desired flow rate. But it has been highlighted that flow control by valve throttling wastes energy while

restricting the pump discharge when diverting the excess flow through a bypass (Al-Khalifah & McMillan, 2012). In addition to the energy lost, valves can in some cases become a source of emissions and experience erosion, corrosion, cavitation, leakage, plugging and sticking.

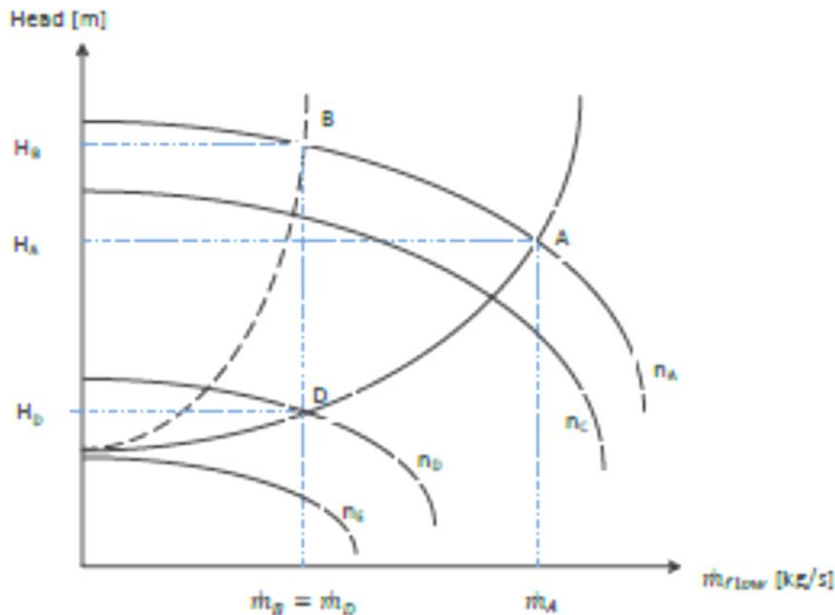


Figure 3.4 Pump head as a function of mass flow rate (McAllister, 2009)

Figure 3.5 illustrate the pump head capacity curves at pump speeds n_A , n_B , n_C , n_D and n_E where $n_A > n_B > n_C > n_D > n_E$ and the system head capacity curves. For a system initially operating in point A, delivering a mass flow rate \dot{m}_A and H_A m head, reducing the mass flow rate can be achieved in possible ways.

- Throttling valve

In this process, additional pressure drops are inserted in the system, transforming the system head capacity curve, moving the operating point from point A to point B, where the mass flow rate and head are respectively \dot{m}_B and H_B . A major implication of the actual process is that the pump still delivers and consumes power that is basically wasted in the throttling process as compared to the shaft power obtained from equation 3.52 (Al-Khalifah, et al., 2012).

- Variable speed drive

Reducing the mass flow rate by variable speed drive proves to be more efficient than using a throttling valve since in the current process reducing the mass flow rate is achieved by reducing the pump driving speed from n_A to n_D , therefore moving the operating point from point A to D, where the mass flow rate \dot{m}_D equals \dot{m}_B and the total head is only H_D , which is much less than in the first case. In this process, power is saved since the pump only delivers what is required by the initial system (McAllister, 2009).

$$\frac{\dot{m}_A}{\dot{m}_D} = \frac{n_A}{n_D} = \left(\frac{H_A}{H_D}\right)^{1/2} = \left(\frac{P_A}{P_D}\right)^{1/3} \quad (3.52)$$

As can also be seen from Figure 3.4 when the pump operates at very low speed n_E the head generated will not be enough to overcome the system head capacity and the static head; therefore no mass flow will be delivered by the pump. In this way, the flow can be stopped while still keeping the pump in low drive speed for the next operation avoiding the peak current demand that generally occurs at the start of electrical motors.

Several types of AC variable speed drives can be found in the market. However, for the purpose of this study, the pulse width modulation (PWM) variable frequency drive was suggested since it is used only to vary the current or voltage frequency before it is supplied to the pump motor. A PWM drive is mainly made up of a rectifier, an inverter and an operator interface. For control purposes, other control and diagnostic microprocessors are added to the three main components. An alternative current (AC) voltage is supplied to the PMW, where it is rectified and filtered to create a direct current (DC) voltage signal. This DC voltage is then inverted to a variable frequency signal where the actual frequency should correspond to the pump's required speed (Al-Khalifah, et al., 2012).

4 MATHEMATICAL MODELLING

4.1 Nuclear reactor

Nuclear power is being recognised as a necessary provider of an economical and “carbon free” source of heat for the generation of electricity. In this fast expanding world energy market, nuclear energy is also expected to play an important role in the industrial sectors by providing process heat for chemicals such as ethylene, fertilisers, ammonia (NH₃) and liquid petroleum fuel production. The HTMR as many other systems will use nuclear energy for power and heat process.

In the following sections, a plant-detailed nuclear plant description and a mathematical simulation model will be presented. The simulation results as well as a steady-state description of the model will be presented and described.

4.1.1 Overall plant description

As shown in Figure 4.1, the HTMR plant has three sets of two nuclear reactors each. One set of reactors is of a double-reactor modular design with identical design features, where each module stands for one nuclear steam supply system (NSSS). Every module consists of principally one 250 MW_{th} reactor, a once-through helical coil steam generator, and one blower connected with suitable pipes. A common steam header connected to a 200 MWe turbo-generator collects the steam generated by both modules. The other sets of reactors, both of identical design, differ from the first set since they successively supply heat for CTL process via a special heat exchanger and generate steam for electrical power generation. Each module of the two sets working in a cogeneration process includes an extra-steam generator of special design connected to the system between the reactor and the helical coil steam generator.

The special heat exchangers under design at Stellenbosch University (Laubscher, 2012) are of the type tube in tube with intermediate fluid (liquid sodium) and will provide 240 MW_{th} to the process heat, which requires superheated steam at 430 °C, 4 MPa to the CTL process, while expecting a 150 MW_e electrical power generation from each cogeneration set.

The HTMR, inspired by HTR-PM, assumes a one-zone pebble-bed core with an augmented 250 MW_{th} power while preserving the inherent safety features. The modular steam generators are helical coil once-through shell-and-tube counter-flow heat exchangers. The steam generators, reactors and special heat exchangers used on the plant are housed in steel pressure vessels which are connected according to the set’s design.

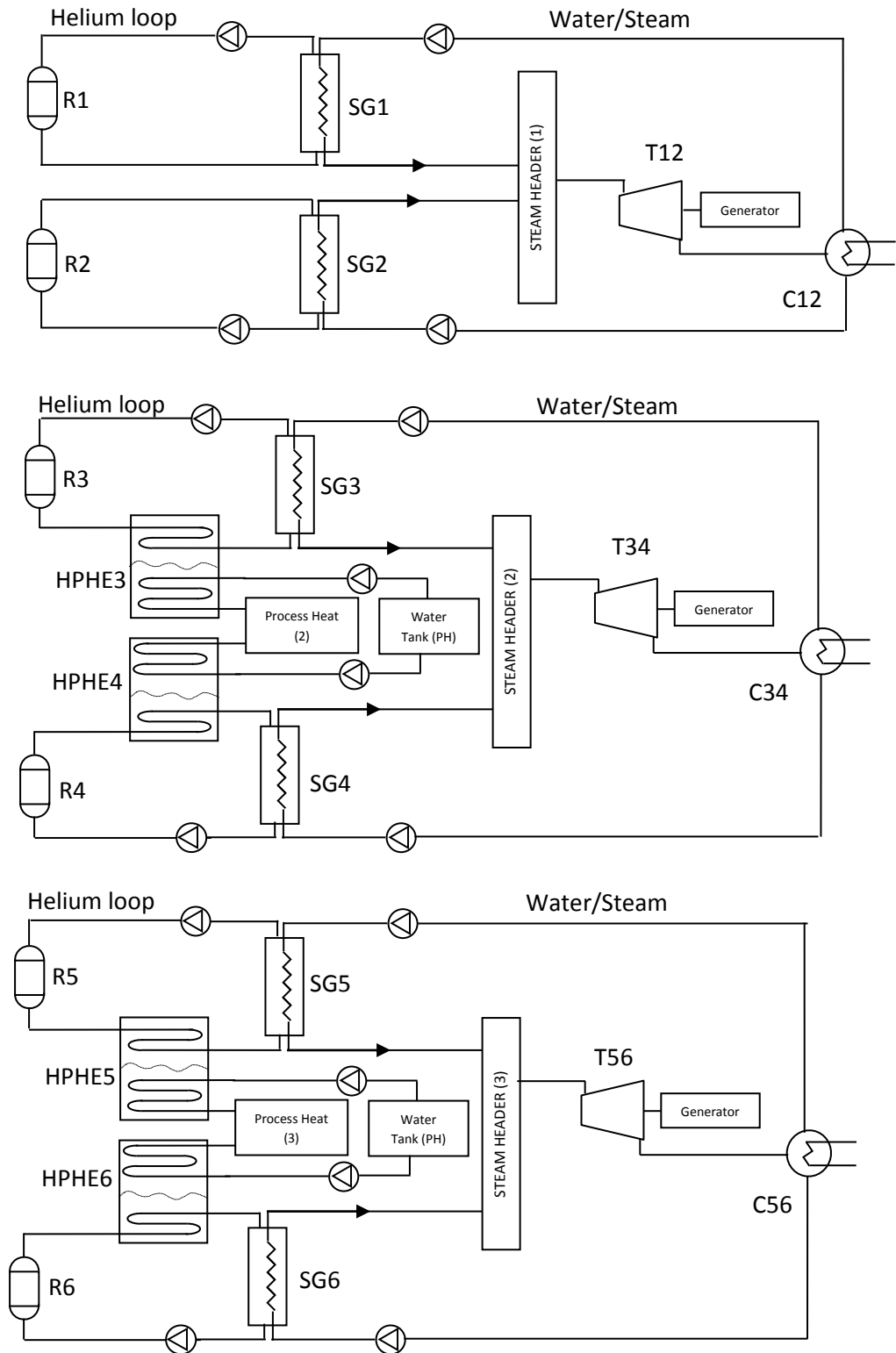


Figure 4.1 Electrical power unit and process heat for solid-coal to liquid fuel production, cogeneration plant for 6 (3x2) reactors. R: reactors, SG: steam generator, T: turbine, C: condenser and HPHE: heat pipe heat exchanger

Helium blowers situated at the top of each steam generator pressurise the gas before flowing into the annulus of a coaxial pipe of a hot gas duct. Cold helium at about 7 MPa and 250 °C from steam generator flows into the annulus connected to the reactor inlet, then enters the reflector channels from the bottom of the reactor while cooling down the reflector, and flows upward to enter the reactor core from the top. Hot helium exits the reactor core, where it flows downward through the pebble bed and heats up to 750 °C (Li, et al., 2008b). After the pebble bed, helium passes through the hot gas chamber situated at the bottom of the reflector and flows through the hot gas pipe to the steam generator or to the special heat exchanger followed by the steam generator, depending on the set's process. In the electrical-power only setup, shown in Figure 4.2, hot helium from the reactor outlet duct goes to the steam generator where heat is transferred to high-pressure water to generate superheated steam in one single process. The generated steam from the two modules is then sent to a common steam header, from where it is delivered to the turbine in order to generate electrical power.

In the cogeneration setup, helium first goes through the heat pipe heat exchanger, where heat is transferred to liquid sodium that evaporates, then exits the special heat exchanger for the steam generator. The evaporated sodium in turn, will transfer heat to the high-pressure feedwater flowing inside another coil to generate steam for the CTL process. The inside temperature of the special heat exchanger is kept at 600 °C and helium exits at about 650 °C on its way to the electrical power steam generator. The main design data are presented in Table 4.1.

Table 4.1 Main design data of the HTMR (based on HTR-PM and Sasol requirements) (Li, et al., 2008b)

Parameters	Value	Unit
Thermal power per set	2x250	MW _{th}
Electrical power unit 1	200	MW _e
Electrical power unit 2 and 3	300	MW _e
Process heat unit 2 and 3	240	MW _{th}
Core outlet temperature	750	°C
Core inlet temperature	250	°C
Active core diameter	3	m
Active core height	11	m
Steam generator outlet steam temperature	540	°C
Steam generator outlet steam pressure	13.5	MPa
Special heat exchanger helium outlet temperature	650	°C
Special heat exchanger outlet steam temperature	430	°C
Special heat exchanger outlet steam pressure	4	MPa
Helium operating pressure	7	MPa

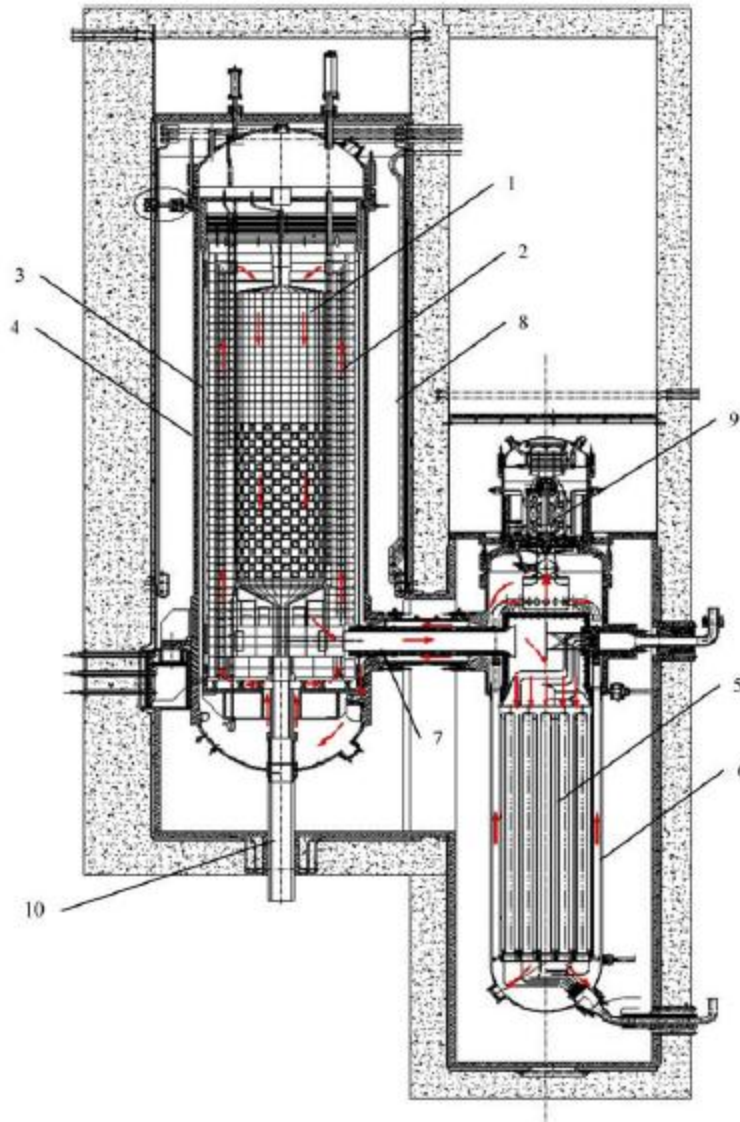


Figure 4.2 Cross section of helium loop of the HTR-PM (Zeng, Shi & Dong, 2009)

In Figure 4.2, note: 1 Core of the reactor; 2 Reflector side and carbon thermal shield; 3 Core barrel; 4 Reactor pressure vessel; 5 Steam generator; 6 Steam generator vessel; 7 Coaxial gas duct; 8 Water-cooling panel; 9 blower; 10 Fuel discharge tube (Zeng, et al., 2009).

4.1.2 Modelling philosophy

The current simulation model was developed from a simplified low order dynamic model that provides clear meaning for the operation research and control system design (Li, et al., 2008a). The lumped parameter technique for the construction of the model based on fundamental conservation of energy, momentum and mass algebraically combined with empirical relationship equations of heat transfer and pressure drop was used. The principle of conservation is based upon the physical axiom that energy, mass and momentum can neither be created from nothing nor vanish into nothing as

expressed by Newton's second law. Any system can be defined and lumped by these laws and can basically be described by the following equations:

Conservation of mass

$$\frac{dm}{dt} = \dot{m}_{in} - \dot{m}_{out} \quad (4.1)$$

Conservation of energy

$$\frac{d(m h)}{dt} = \dot{m}_{in} h_{in} - \dot{m}_{out} h_{out} + Q_{in} - W \quad (4.2)$$

Conservation of momentum

$$P_{out} = P_{in} - k \frac{\dot{m}_{in}^2}{\rho_{in}} \quad (4.3)$$

To simplify the formulation, the following assumptions have been made:

- The module is nodalised into many lumped sections with uniform properties such as flow, temperature and pressure.
- The simplified modular reactor core includes the reactor core and the reflector as two nodes, while the properties of graphite and fuel in the core are averaged as a homogeneous mixture.

According to the above assumptions, the nuclear reactor will include eight sections, namely the core, the reflector, the lower plenum, the lower header, the riser, the upper header, the downcomer and the outlet header. The secondary side of the once-through helical coil steam generator will be nodalised in the direction of the flow as economiser, evaporator and superheater. This nodalisation is based on the current state of water inside the pipes. In radial direction, we observe the heat flux moving from hot fluid to cold. Therefore, the heat transfer in the steam generator will have three stages as well, namely the primary, the metal and the secondary. Figure 4.3 presents the heat flow diagram of the standard set of modules as well as both the primary and secondary fluid flow path, while Figure 4.4 presents the cogeneration set of nuclear reactors.

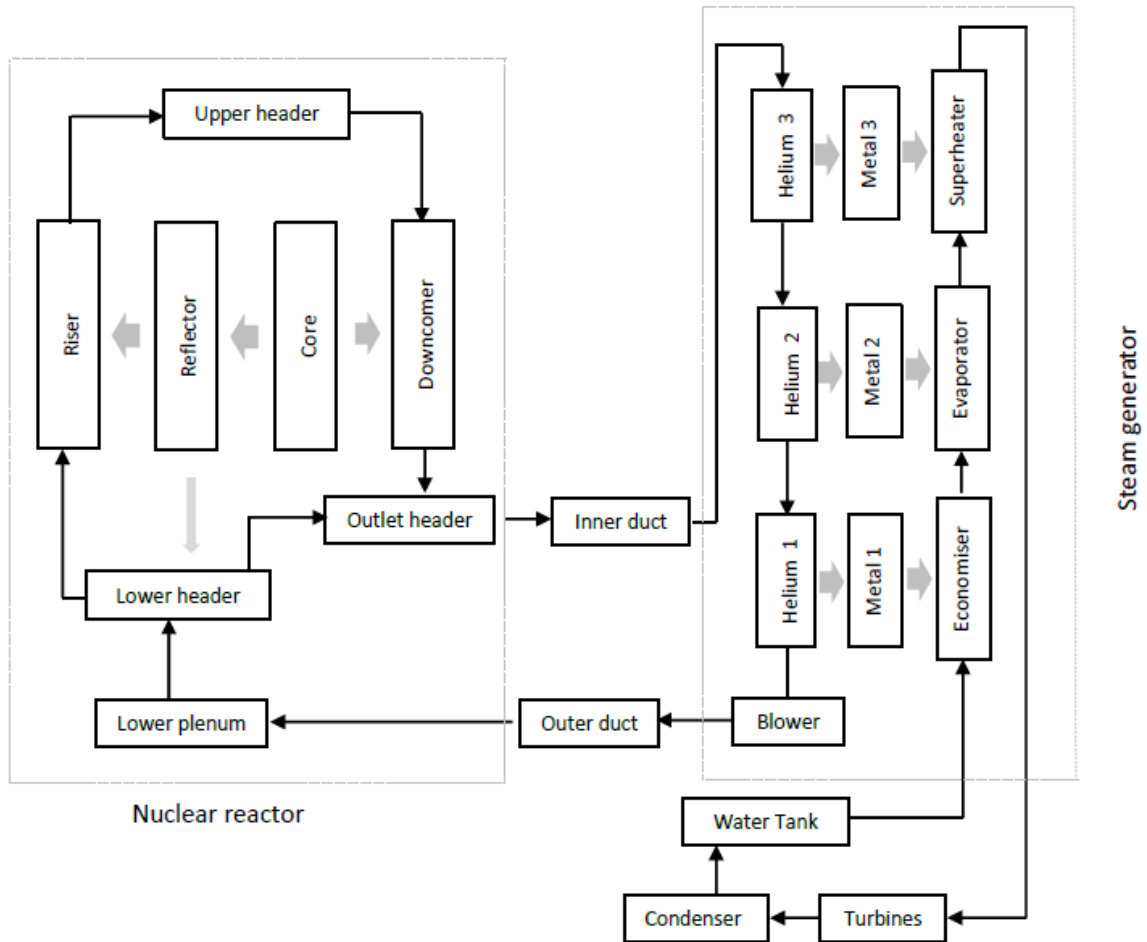


Figure 4.3 Heat flow diagram of unit 1 of the HTMR plant

In Figure 4.3 and 4.4, the lower plenum, the lower header, the riser, the upper header, the downcomer and the outer header will respectively be represented by the following subscript 1, 2, 3, 4, 5 and 6. This will be used in the nuclear reactor equations.

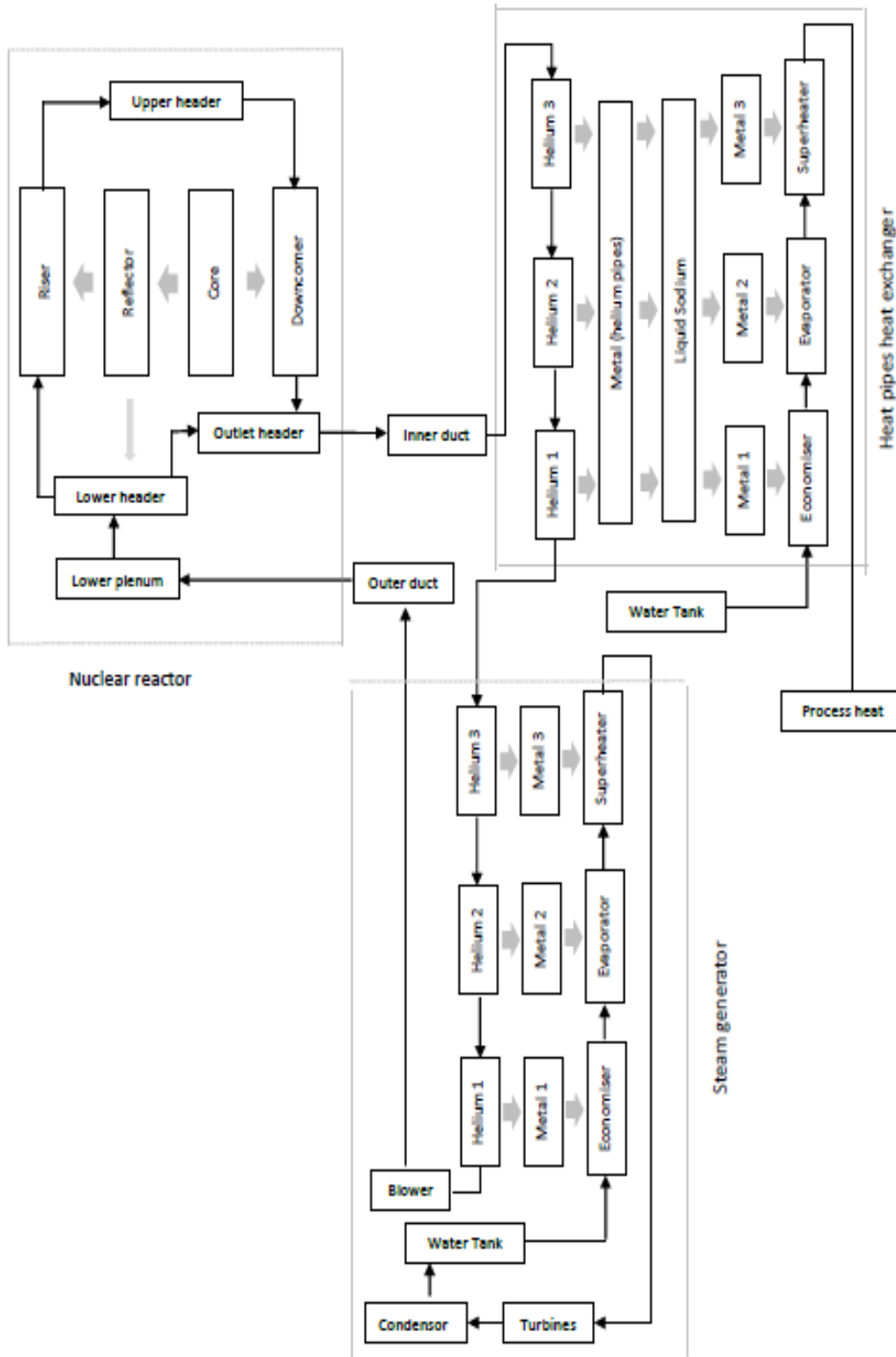


Figure 4.4 Cogeneration heat flux diagram (nuclear reactor connected to special heat exchanger for heat process and steam generator for power generation)

4.1.3 Dynamic modelling formulation of the HTMR

The purpose of this paragraph is to mathematically describe the overall system performance and components interactions with sufficient accuracy, rather than microscopically describe details of the working fluid change during the process. The following sections will separately describe the mathematical formulation of conservation of mass, momentum and energy occurring within different sections of the high temperature modular reactor HTMR.

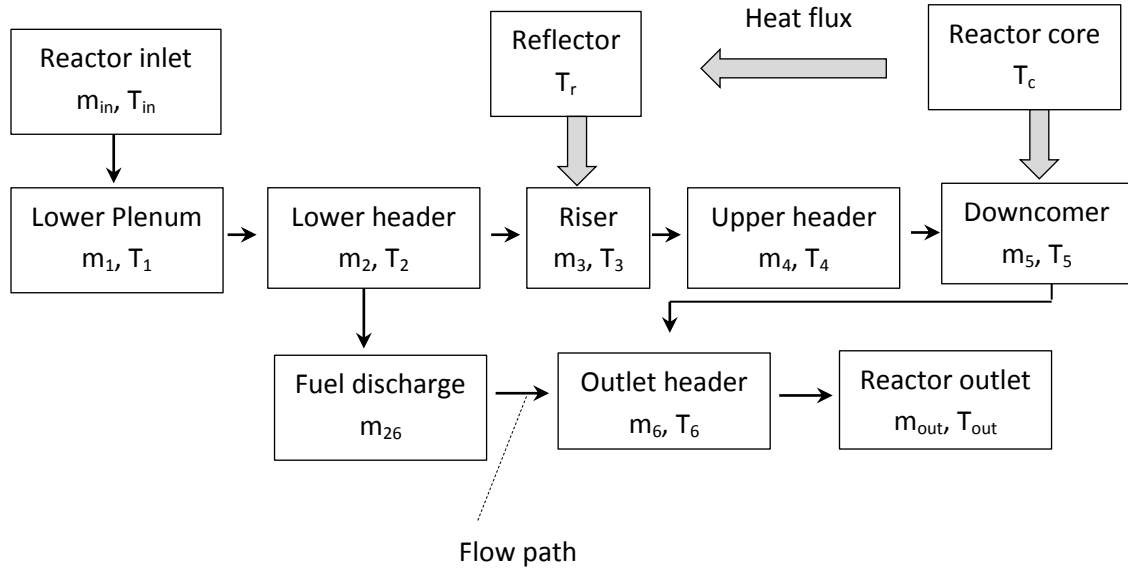


Figure 4.5 Reactor heat flux and coolant gas flow path

a) Reactor core

The HTMR core is of the pebble-bed type. The pebble bed is an open space filled with thousands of spherical fuel elements made of TRISO fuel particles contained in graphite and the bed itself is assumed to be similar to a lumped solid area with a uniform porosity. The fuel elements release fission energy in kinetic energy which forms heat, which is then transferred to the helium flowing between fuel elements in the core represented in Figures 4.3 and 4.4 by the downcomer.

The heat transfer process can be described by

$$(1 - \epsilon_5) V_5 \rho_5 C_c \frac{dT_c}{dt} = P_{100} n_r - h_5 A_5 (T_c - T_5) - h_{cr} A_{cr} (T_c - T_r) \quad (4.4)$$

The above equation can be rearranged as:

$$\frac{dT_c}{dt} = \frac{1}{(1 - \epsilon_5) V_5 \rho_5 C_c} [P_{100} n_r - h_5 A_5 (T_c - T_5) - h_{cr} A_{cr} (T_c - T_r)] \quad (4.5)$$

The fission process in a nuclear reactor known to be responsible for nuclear energy generation can be highlighted by the dynamic equations 4.3 and 4.4, when using a model of six precursor groups of delayed neutrons with one prompt neutron group and two reactivity feedback mechanisms (Li, et al., 2008b). For $i = 1, 2, \dots, 6$;

$$\frac{dn}{dt} = \frac{\rho - \beta}{\Lambda} n + \sum_{i=1}^6 \lambda_i C_i \quad (4.6)$$

$$\frac{dC_i}{dt} = \frac{\beta_i}{\Lambda} n - \lambda_i C_i \quad (4.7)$$

$$\rho = \rho_{rod} + (\alpha_f + \alpha_m)(T_c - T_{c0}) + \alpha_r(T_r - T_{r0}) \quad (4.8)$$

where $\beta = \sum_{i=1}^6 \beta_i$ (King, 1964)

In this study, the model used has been simplified to a lumped model considering one neutron group for neutron density and concentration as shown in the equations below (Ramirez, 2011).

$$\frac{dn}{dt} = \frac{\rho - \beta}{\Lambda} n + \lambda C_L \quad (4.9)$$

$$\frac{dC_L}{dt} = \frac{\beta}{\Lambda} n - \lambda C_L \quad (4.10)$$

Therefore, the reactor power will be calculated from the fission reaction by the following expression:

$$P = \omega_f n V \Sigma_f \quad (4.11)$$

b) Reflector

The reflector is made of graphite bricks arranged to accommodate thermal and radiation provoked distortions throughout the life of the reactor. The heat generated in the reactor core is partly transferred to the reflector, which is in turn cooled by helium flowing through channels situated in the annular reflector. The dynamic equation of heat transfer of the reflector can be expressed by the following expression (Li, et al., 2008a):

$$V_r \rho_r C_r \frac{dT_r}{dt} = h_{cr} A_{cr} (T_c - T_r) - h_3 A_3 (T_r - T_3) \quad (4.12)$$

Rearranged, the above equation can be written as

$$\frac{dT_r}{dt} = \frac{1}{V_r \rho_r C_r} [h_{cr} A_{cr} (T_c - T_r) - h_3 A_3 (T_r - T_3)] \quad (4.13)$$

c) Lower plenum

Situated at the bottom of the reactor and assumed to be a well-mixed chamber with no pressure drop nor energy exchange with the environment, the lower plenum can be modelled by the following energy equation (Li, et al., 2008b);

$$\frac{d T_1}{dt} = \frac{\dot{m}_{in}}{V_1 \rho_1} (T_{in} - T_1) \quad (4.14)$$

d) Lower header

From the lower plenum, a fraction of cold helium is diverted to the reactor fuel elements discharge tube. With this helium leakage ratio β , the mass flow rate distribution can be expressed as (Li, et al., 2008b)

$$\dot{m}_{23} = \dot{m}_1 (1 - \beta_2) \quad (4.15)$$

$$\text{and} \quad \dot{m}_{26} = \dot{m}_1 \beta_2 \quad (4.16)$$

e) Riser

The top view of the reflector is an annulus in which channels have been drawn to make up the riser. Cold helium from the lower header flows upward inside the channels while cooling down the reflector side. The energy balance equation during this process is formulated as

$$V_3 C_p \frac{d(\rho_3 T_3)}{dt} = \dot{m}_{23} C_p T_2 - \dot{m}_{23} C_p T_3 + h_3 A_3 (T_r - T_3) \quad (4.17)$$

The conservation of mass principle applied to the riser yields (Li, et al., 2008a),

$$V_3 \frac{d \rho_3}{dt} = \dot{m}_{23} - \dot{m}_3 \quad (4.18)$$

Substituting equation 4.14 into 4.13 and rearranging the energy equation, the following expression is obtained

$$\frac{d T_3}{dt} = \frac{1}{V_3 \rho_3 C_p} \left[\dot{m}_{23} C_p (T_2 - T_3) + h_3 A_3 (T_r - T_3) \right] \quad (4.19)$$

The conservation of momentum equation applied to the riser yields (Li, et al., 2008b)

$$P_3 = P_2 - k \frac{\dot{m}_{23}^2}{\rho_2} \quad (4.20)$$

f) Upper header

The upper header is a mixing chamber situated in the graphite just above the reactor core that collects the uprising coolant (helium) from all the channels and separates them according to the design ratio so that 1% passes through the reflector control rod tubes and a maximum of 4% passes through between the graphite components. Only 94% of the total mass flow rate passes through the reactor core to cool down the fuel elements (Zeng, et al., 2009).

The conservation of mass principle applied to a mixing chamber entails that the summation of the incoming mass flow rates equal the sum of mass flow rates of the outgoing streams. And since usually considered well insulated and not involving any kind of work, the mixing chamber is assumed to be operating with no pressure variation. Therefore the conservation energy principle applied to the upper header will be analogous to the conservation of mass equation (Cengel & Boles, 2006).

g) Downcomer

The downcomer is basically the core of the reactor. The HTMR core consists of a homogeneous enclosure that contains the hundreds of thousands pebbles, stochastically arranged, with helium gas flowing between them. Therefore, due to the geometry and characteristics of the flow, the pressure drop across the chamber will be considered, and fission energy in the form of heat will be transferred from fuel elements to the flowing fluid and the reflector (Li, et al., 2008b).

Conservation of mass:

$$\epsilon_5 V_5 \frac{d\rho_5}{dt} = \dot{m}_4 - \dot{m}_5 \quad (4.21)$$

Conservation of energy:

$$\epsilon_5 V_5 C_p \frac{d(\rho_5 T_5)}{dt} = \dot{m}_4 C_p T_4 - \dot{m}_5 C_p T_5 + h_5 A_5 (T_c - T_5) \quad (4.22)$$

The energy equation can be rewritten after substitution of equation 4.20 into 4.21 and rearranged to yield the following:

$$\frac{dT_5}{dt} = \frac{1}{\epsilon_5 V_5 C_p \rho_5} \left[\dot{m}_4 C_p (T_4 - T_5) + h_5 A_5 (T_c - T_5) \right] \quad (4.23)$$

The momentum equation applied to the downcomer shows a change in pressure that can be modelled as follows on the dynamic modelling:

$$P_5 = P_4 - k \frac{\dot{m}_4^2}{\rho_4} \quad (4.24)$$

h) Outlet header

The outlet header mixes the down-coming flow, hot helium from the reactor core, the fuel elements exhaust duct cooling stream and the coolant fraction flowing between graphite bricks. It is assumed to operate at constant pressure. Once again neglecting the potential and kinetic energy of the mixture, and considering that there is no heat exchange with the environment and no work done, the energy equation becomes analogous to the mass equation (Cengel, et al., 2006)

$$V_6 \frac{d \rho_6}{dt} = \dot{m}_5 + \dot{m}_{26} - \dot{m}_6 \quad (4.25)$$

$$V_6 C_p \frac{d(\rho_6 T_6)}{dt} = \dot{m}_5 C_p T_5 + \dot{m}_{26} C_p T_2 - C_p \dot{m}_6 T_6 \quad (4.26)$$

The energy equation can be written after substitution of equation 4.25 into 4.26 and rearranged to yield the following (Li, et al., 2008a):

$$\frac{d T_6}{dt} = \frac{1}{V_6 C_p} [\dot{m}_5 (T_5 - T_6) + \dot{m}_{26} (T_2 - T_6)] \quad (4.27)$$

4.2 Steam generator

With the latest improvements in nuclear technologies, the opportunity of bringing into play nuclear plants for process heat supply is closer than ever before (Hoffer, et al., 2011). The next generation nuclear plant (NGNP), which refers to any type of high-temperature gas-cooled reactor design, is aiming to provide process heat to a wide range of high-temperature processes such as generating steam for electrical power generation, CTL process, coal gasification, hydrogen production and other industrial applications.

As described in the thesis objective, nuclear energy is used as energy source in a high temperature modular reactor HTMR to generate steam for a cogeneration process handling electrical power generation and providing process heat for coal to hydrocarbon conversion. For this purpose, steam generators of the once-through helical-coil type have been used. These steam generators are basically heat exchangers of the shell and tube type where the primary fluid (high-temperature helium) flows in a shell and the secondary side is made up of several small tubes taking the working fluid (steam) (Hoffer, et al., 2011). In order to be able to predict and take control of plant performances, a model simulation of a non-linear dynamic model of the steam generator will be described in the following paragraphs.

4.2.1 Once-through steam generator design

Steam generators transfer heat from the shell side coolant to the tube side coolant, to produce steam within the tubes. In some cases such as pressurised water reactors (PWR), lower-pressure steam can be produced on the shell side while the high-pressure reactor coolant flows in tubes. This last configuration minimises the shell wall thickness,

which impacts positively on the heat transfer process but at the same time exposes the shell to corrosion (Ray, 1980).

The helical-coil steam generators used in this study are vertically oriented, once-through, up-boiling, cross-counter-flow, shell and tube heat exchangers as shown in figure 4.5. Tubes are helically wound into bundles. Due to the high temperatures expected from the reactor coolant (≈ 750 °C), adequate material is required. The NGNP design proposes an upper bundle and a lower bundle. The upper bundle, experiencing the high temperature, is made of high-temperature alloys such as Inconel 617 and Incoloy 800H, presenting high resistance to corrosion and structural strength at high temperatures (Hoffer, et al., 2011). The lower bundle, experiencing relatively much lower temperature, is joined to the upper by a bimetallic weld. It is made of alloy 2-1/4Cr-1Mo. The lower bundle has three main parts, namely the economiser, the evaporator and the superheater, whereas the upper bundle is just a finishing superheater (Hoffer, et al., 2011).

The economiser, the first section of the steam generator, preheats the feedwater to saturation conditions. In the evaporator, the second section, the preheated feedwater at saturation condition undergoes a phase change from liquid to vapour. During this process, a two-phase-flow exists inside the pipes. The superheater, the third section, has to initiate the superheating process of the saturated vapour from the evaporator, which will be finalised in the upper bundle to obtain the desired steam outlet conditions.

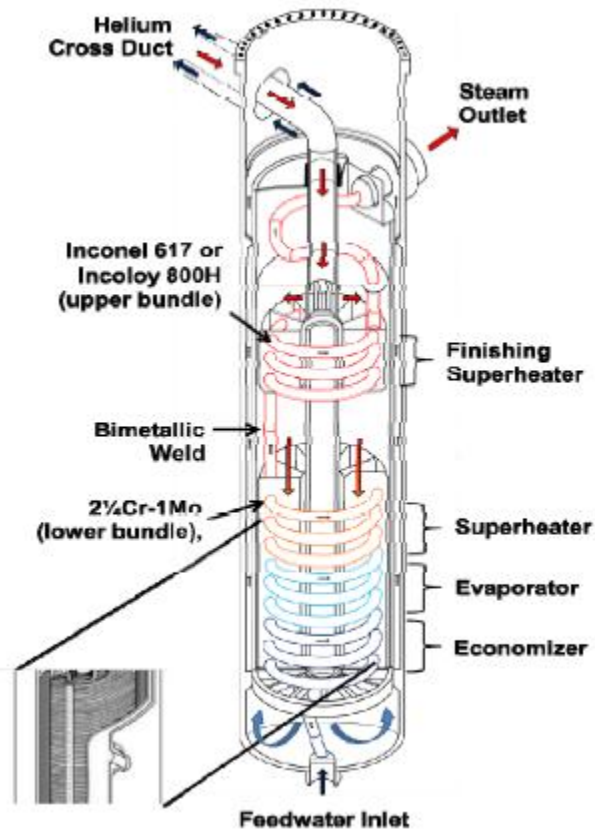


Figure 4.6 Helical coil once-through steam generator pre conceptual design (Hoffer, et al., 2011)

In this type of steam generator, water is fed from the bottom of the steam generator, flows upward in one single pass through the helical coil where it is converted to steam and exits in a superheated state at the top. Meanwhile helium enters at the top and, passes through the shell, transferring heat to the steam, and exits at the bottom. As a result, the heat transfer process is equivalent to a combined cross and counter-flow making for a cross-counter-flow heat exchanger.

4.2.2 Mathematical modelling of the once-through steam generator

In order to describe the dynamic response of the overall system, a mathematical model of the once-through steam generator is required. This model has to describe accurately enough the steam generator with regards to its performance and interaction between its components. Therefore, the physical process of steam generation is mathematically represented by nonlinear partial differential equations with space and time as independent variables (Ray, 1980). These partial differential equations are then simplified and reduced to a set of ordinary differential equations with time as the independent variable.

The once-through steam generator was modelled by a typical tube that has three sections. In the economiser, the first section, numbered 1 to 3 in Figure 4.6, compressed water is heated to saturation temperature. The water then enters the evaporator, the

second section, numbered 3 to 5 in Figure 4.6, where it ideally evaporates at constant pressure and temperature. Saturated vapour from the evaporator enters the superheater, the third section, numbered 5 to 7 in Figure 4.6 where it is heated to the desired temperature. This model assumes moving boundaries between the consecutive sections (Li, et al., 2008b). The secondary wall temperature remains constant in the evaporator and will be linear with respect to the length of the tube for the other sections (Ray, 1980). The above assumptions yield the following:

$$T_{w1} = 2T_{w2} - T_{w4} \quad (4.28)$$

$$T_{w3} = T_{w4} \quad (4.29)$$

$$T_{w5} = T_{w4} \quad (4.30)$$

$$T_{w7} = 2T_{w6} - T_{w4} \quad (4.31)$$

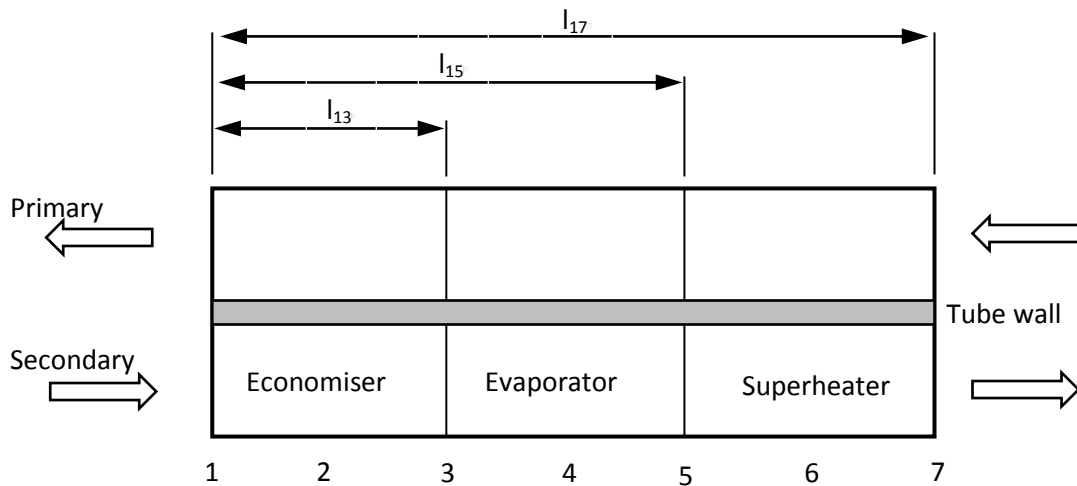


Figure 4.7 Schematic view of the sections of the once-through steam generator

Once again, the model uses the simultaneous application of the principles of conservation mass, energy and momentum on the steam generator's sections separately.

a. Economizer

The economiser, represented in Figure 4.6 by the section numbered 1 to 3, is the section through which feedwater runs and where water is heated by the hot gas, helium in this case. In this section of the steam generator, only compressed water flows inside the pipes. Point 1 in Figure 4.6 represents the inlet of the economiser while point 3 represents the outlet of the economiser. Point 3 also has a significant meaning in terms of fluid properties since it represents a saturation state of water. Therefore, the expected temperature in point 3 should be the saturation temperature at required pressure.

The economiser model can be obtained by applying the principles of mass, energy and momentum conservation.

The conservation of mass applied to the economiser yields:

$$\frac{d(\rho_2 l_{13})}{dt} - \rho_3 \frac{dl_{13}}{dt} + \dot{m}_3 - \dot{m}_1 = 0 \quad (4.32)$$

The conservation of energy applied to the economiser yields:

$$\frac{d}{dt}(\rho_2 h_2 l_{13}) - \rho_3 h_3 \frac{dl_{13}}{dt} + \dot{m}_3 h_3 - \dot{m}_1 h_1 = \frac{\dot{Q}_2}{A_2} + \frac{d(P_2 l_{13})}{dt} - P_3 \frac{dl_{13}}{dt} \quad (4.33)$$

and the conservation of momentum yields:

$$P_3 = P_1 - g\rho_2 l_{13} \sin \theta - F_2 l_{13} \dot{m}_2^2 \quad (4.34)$$

The differentiation of equation 4.34 respective to time gives the following:

$$\frac{dP_3}{dt} = -\left(g\rho_2 \sin \theta + F_2 \dot{m}_2^2\right) \frac{dl_{13}}{dt} - 2F_2 l_{13} \dot{m}_2 \frac{d\dot{m}_2}{dt} \quad (4.35)$$

Using the saturation properties, the following can be written (Chaibakhsh, Ghaffari & Moosavian, 2007)

$$\frac{dh_3}{dt} = \left. \frac{\partial h_3}{\partial P_3} \right|_{P_3} \frac{dP_3}{dt} \quad (4.36)$$

The assumptions made in the formulation of the above equations are:

$$h_2 = \frac{h_1 + h_3}{2} \quad (4.37)$$

$$\dot{m}_2 = \frac{\dot{m}_1 + \dot{m}_3}{2} \quad (4.38)$$

$$P_2 = \frac{P_1 + P_3}{2} \quad (4.39)$$

Considering the transport delay due to water flow at relatively low velocity in the economizer, the feedwater flow rate and inlet enthalpy can be treated as first order lag with τ as a time constant (Li, et al., 2008b).

$$\frac{d\dot{m}_3}{dt} = \frac{\dot{m}_1 - \dot{m}_3}{\tau} \quad (4.40)$$

$$\frac{dh_1}{dt} = \frac{h_{fW} - h_1}{\tau} \quad (4.40a)$$

where τ is given by the following

$$\tau = \frac{A_{13} \rho_2}{2 \dot{m}_1} \quad (4.40b)$$

Combining the economiser equations described above yields (Li, et al., 2008b),

$$\begin{aligned} & \left[\frac{\rho_3(h_1 - h_3)}{2} + (P_3 - P_2) + \frac{(g\rho_2 \sin \theta + F_2 \dot{m}_2^2/A_2^2)}{2} \times \left(1 - \rho_2 \frac{\partial h_3}{\partial P_3} \Big|_{P_3} \right) \right] l_{13} \frac{dl_{13}}{dt} + \frac{\rho_2 l_{13}}{2} \frac{dh_1}{dt} \\ & + \left[\frac{F_2 \dot{m}_2}{2A_2^2} \left(1 - \rho_2 \frac{\partial h_3}{\partial P_3} \Big|_{P_3} \right) \right] l_{13}^2 \frac{d\dot{m}_3}{dt} = \frac{(\dot{m}_1/A_1 + \dot{m}_3/A_3)(h_1 - h_3)}{2} + \frac{\dot{Q}_2}{A_2} \end{aligned} \quad (4.41)$$

b. Evaporator

The evaporator is shown in Figure 4.6 by the section number 3 to 5. It is characterised by water phase change from a liquid saturation state to saturated vapour. During this process a two-phase flow co-exists inside the steam generator's pipes. The heat supplied to the fluid during this process results in the internal energy change and theoretically without changing the molecular temperature of the fluid. Therefore, this change in internal energy is referred to as the "latent heat of evaporation". Based on this, the saturated vapour temperature in point 5 will be considered to be equal to the saturated water in point 3 for simplification purposes of the simulation. The evaporator can also be described mathematically by applying the principles of conservation of mass, conservation of energy and conservation of momentum principles to the section numbered 3 to 5 in Figure 4.6. The continuity equation 4.1 applied to the evaporator yields the following results

$$\frac{d(\rho_4 l_{35})}{dt} - \rho_5 \frac{dl_{15}}{dt} + \rho_3 \frac{dl_{13}}{dt} + \dot{m}_5 - \dot{m}_3 = 0 \quad (4.42)$$

Applying the energy equation to the evaporator gives

$$\begin{aligned} & \frac{d}{dt}(\rho_4 h_4 l_{35}) - \rho_5 h_5 \frac{dl_{15}}{dt} + \rho_3 h_3 \frac{dl_{13}}{dt} + \dot{m}_5 h_5 - \dot{m}_3 h_3 \\ & = \frac{\dot{Q}_4}{A_4} + \frac{d(P_4 l_{35})}{dt} - P_5 \frac{dl_{15}}{dt} + P_5 \frac{dl_{13}}{dt} \end{aligned} \quad (4.43)$$

For this model, only the temperature has been assumed to remain constant during the evaporation process. Therefore, the momentum equation applied to the evaporator, the following is obtain

$$P_5 = P_3 - \rho_4 g l_{35} \sin \theta - F_4 l_{35} \dot{m}_4^2 \quad (4.44)$$

Combining equations 4.42, 4.43 and 4.44, the final dynamic equation for the evaporator is

$$\begin{aligned}
 & \left\{ \rho_3(h_3 - h_4) + (P_4 - P_3) - \frac{\left(\rho_4 g \sin \theta + \frac{F_4 \dot{m}_4^2}{A_4^2}\right)}{2} \times \left(1 - \rho_4 \frac{\partial h_5}{\partial P_5}\bigg|_{P_5}\right) l_{35} - \left(\rho_2 g \sin \theta + \frac{F_4 \dot{m}_2^2}{A_2^2}\right) \right\} \frac{dl_{13}}{dt} \\
 & \quad \times \left[\frac{\rho_4}{2} \left(\frac{\partial h_3}{\partial P_3}\bigg|_{P_3} + \frac{\partial h_5}{\partial P_5}\bigg|_{P_5} \right) - 1 \right] l_{35} \\
 & + \left[\rho_5(h_4 - h_5) + (P_5 - P_4) + \frac{\left(\rho_4 g \sin \theta + \frac{F_4 \dot{m}_4^2}{A_4^2}\right)}{2} \times \left(1 - \rho_4 \frac{\partial h_5}{\partial P_5}\bigg|_{P_5}\right) l_{35} \right] \frac{dl_{15}}{dt} \\
 & + \left\{ \frac{F_4 \dot{m}_4 \left(1 - \rho_4 \frac{\partial h_5}{\partial P_5}\bigg|_{P_5}\right) l_{35}^2}{A_4^2} - \left[\frac{F_2 \dot{m}_2}{2A_2^2} \left(\rho_4 \left(\frac{\partial h_3}{\partial P_3}\bigg|_{P_3} + \frac{\partial h_5}{\partial P_5}\bigg|_{P_5} \right) - 2 \right) \right] l_{13} l_{35} \right\} \frac{d \dot{m}_3}{dt} \\
 & = \dot{m}_5 \frac{(h_4 - h_5)}{A_5} + \dot{m}_3 \frac{(h_3 - h_4)}{A_3} + \frac{\dot{Q}_4}{A_4} \tag{4.45}
 \end{aligned}$$

where the subscript 4 represents for the average value between the conditions in 5, saturated vapour, and the saturated liquid conditions in point 3.

c. Superheater

The saturated steam generated in the evaporator, will be superheated in the last section, numbered 5-7 of the Figure 4.6, which has its first part in the lower bundle part of the steam generator and continues the superheating process in the upper bundle made up with high-temperature material. This section is called the superheater.

Steam is heated up to more or less 540 °C for power generation purposes (Hoffer, et al., 2011). The superheater mathematical model can also be obtained by applying the golden principles of conservation of mass, conservation of energy and conservation of momentum to the section numbered 5 to 7 in Figure 4.6. Point 5 represents a theoretical superheater inlet while point 7 represents the steam generator outlet conditions.

The conservation mass principle applied to the superheater yields

$$\frac{d(\rho_6 l_{57})}{dt} + \rho_5 \frac{dl_{15}}{dt} + \dot{m}''_7 - \dot{m}''_5 = 0 \tag{4.46}$$

The superheater energy equation obtained by applying the conservation of energy principle to section 5 to 7 in Figure 4.6 is

$$\frac{d}{dt}(\rho_6 h_6 l_{57}) + \rho_5 h_5 \frac{dl_{15}}{dt} + \dot{m}''_7 h_7 - \dot{m}''_5 h_5 = \frac{Q_6}{A_6} + \frac{d(P_6 l_{57})}{dt} + P_5 \frac{dl_{15}}{dt} \tag{4.47}$$

And the momentum equation is

$$P_7 = P_5 - \rho_6 g l_{57} \sin \theta - F_6 l_{57} \dot{m}_6^2 \quad (4.48)$$

Combining equations (4.46), (4.47) and (4.48) yields the following:

$$\begin{aligned} & \left(\rho_2 g \sin \theta + \frac{F_2 \dot{m}_2^2}{A_2^2} - \rho_4 g \sin \theta - \frac{F_4 \dot{m}_4^2}{A_4^2} \right) l_{57} \frac{d l_{13}}{dt} + \rho_6 l_{57} \frac{d h_6}{dt} \\ & + \left\{ \rho_5 (h_5 - h_6) + (P_6 - P_5) + \left[\rho_4 g \sin \theta + \frac{F_4 \dot{m}_4^2}{A_4^2} - \frac{1}{2} \left(\rho_6 g \sin \theta + \frac{F_6 \dot{m}_6^2}{A_6^2} \right) \right] l_{57} \right\} \frac{d l_{15}}{dt} \\ & + \left(\frac{F_2 \dot{m}_2 l_{13}}{A_2^2} + \frac{2 F_4 \dot{m}_4 l_{35}}{A_4^2} + \frac{F_6 \dot{m}_6 l_{57}}{A_6^2} \right) l_{57} \frac{d \dot{m}_3}{dt} = \frac{\dot{m}_7 (h_6 - h_7)}{A_7} + \frac{\dot{m}_5 (h_5 - h_6)}{A_5} + \frac{Q_6}{A_6} \quad (4.49) \end{aligned}$$

In equation 4.49, the subscript 6 refers to the average value between the saturation state of vapour 6 and the steam generator outlet conditions 7, while the subscripts 2 and 4 refer to the average values within the economiser and the evaporator respectively.

4.3 Special heat pipe heat exchanger

Over the years, the thermal power generation sector has been subject to low grade efficiencies due to thermal energy conversion challenges. Improvement in this field has led to a type of primary energy saving by successively combining two or more processes on one plant while using only one primary energy source. The aim of this combination is to utilise the thermal energy available in the exhaust gas for another heat process; thus increasing the overall efficiency of the plant. This technique is called “cogeneration”.

Cogeneration has been used in the present study to provide process heat for the conversion of coal to liquid fuel and steam for power generation. 7 MPa and 750 °C helium from the nuclear reactor is circulated in a heat pipe heat exchanger, where it is cooled down to 650 °C, generating steam for process heat before entering the power generation helical coil once-through steam generator.

Due to high-pressure flow in the primary loop, which contains helium, radioactive dust produced by friction between fuel elements and graphite in the reactor can be deposit throughout the primary loop (Stempniewicz, Winters & Caspersson, 2012). This agglomeration of radioactive dust in the primary circuit might be a source of contamination of steam generated in a direct process. For this reason, this study has suggested the utilisation of a special heat exchanger type using an intermediate fluid, reducing chances of contamination. This type of heat exchanger is represented in Figure 4.1 by the process heat of units 2 and 3.

4.3.1 Special heat pipe heat exchanger design

The steam generation process for process heat using the heat pipe heat exchanger designed at Stellenbosch University suggests (Dobson & Laubscher, 2013) that sodium liquid is vaporised by hot helium and the vaporised sodium exchanges heat with the feedwater while condensing. In this process, the heat pipe heat exchanger is meant to be operating at constant temperature; therefore, the quality of sodium should be strictly kept higher than zero and less than one at all time. For this purpose, the operating pressure of the heat pipe heat exchanger should be the saturation pressure of sodium maintaining an average temperature of about 600°C.

The heat pipe heat exchanger generates steam in a once-through process providing superheated steam at 430 °C, 4 MPa to a CTL process involving coal gasification to produce synthesis which will then catalytically be converted to liquid fuel in a Fisher-Tropsch process (Mantripragada, et al., 2011). This steam generator is of the tube-and-tube type. Helium from the nuclear reactor flows through the primary circuit pipes, transferring heat to liquid sodium, which evaporates in the open space of the heat pipe heat exchanger. The evaporated sodium is meant to keep the room at a constant average temperature of 600 °C. Water is fed into the secondary side of the steam generator. Liquid water enters the steam generator at about 205 °C and is converted to superheated steam, meanwhile condensing the vapour sodium. The aim of the use of intermediate fluid is to reduce the chance of steam contamination during the process (Stempniewicz, et al., 2012).

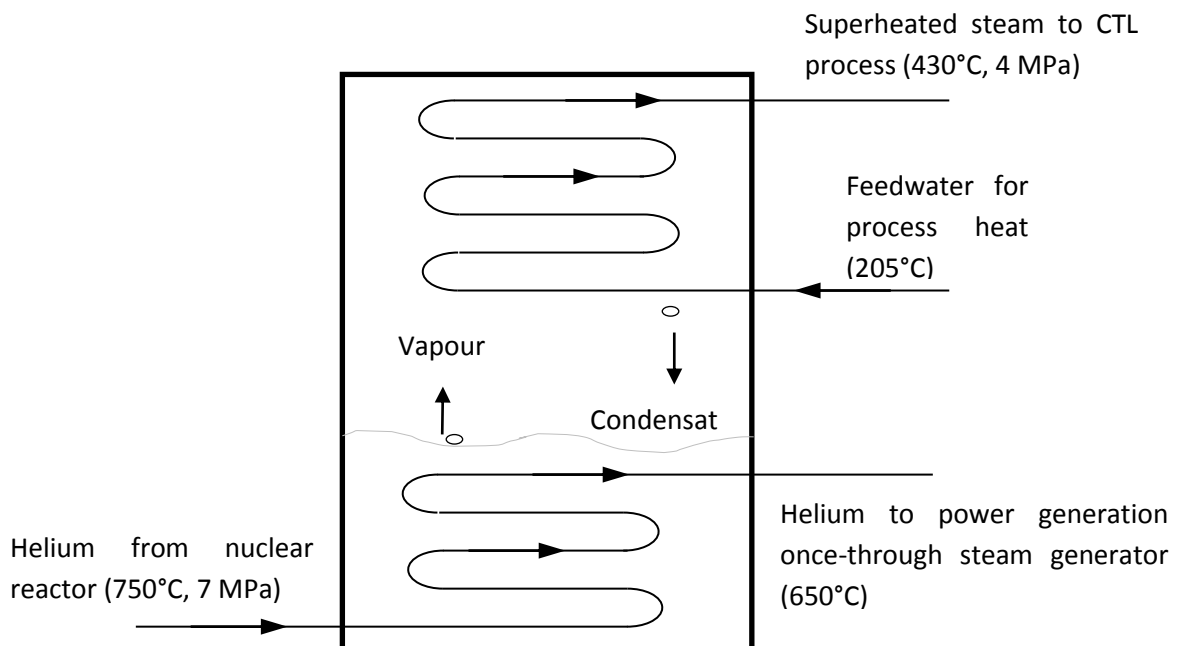


Figure 4.8 Heat pipe heat exchanger for process heat steam generation

The high-temperature helium from the nuclear reactor flows through 320 pipes immersed in the liquid sodium, while steam is generated in pipes of 31.8 mm outer diameter forming helical-coils situated in the upper region of the heat exchanger. These helical-coil pipes are immersed in a 600°C vapour sodium environment. The

configuration shown in Figure 4.7 would be equivalent to a system using an intermediate loop, presented in Figure 4.8, as suggested by Greyvenstein for the PMBR in South Africa (Greyvenstein, 2008).

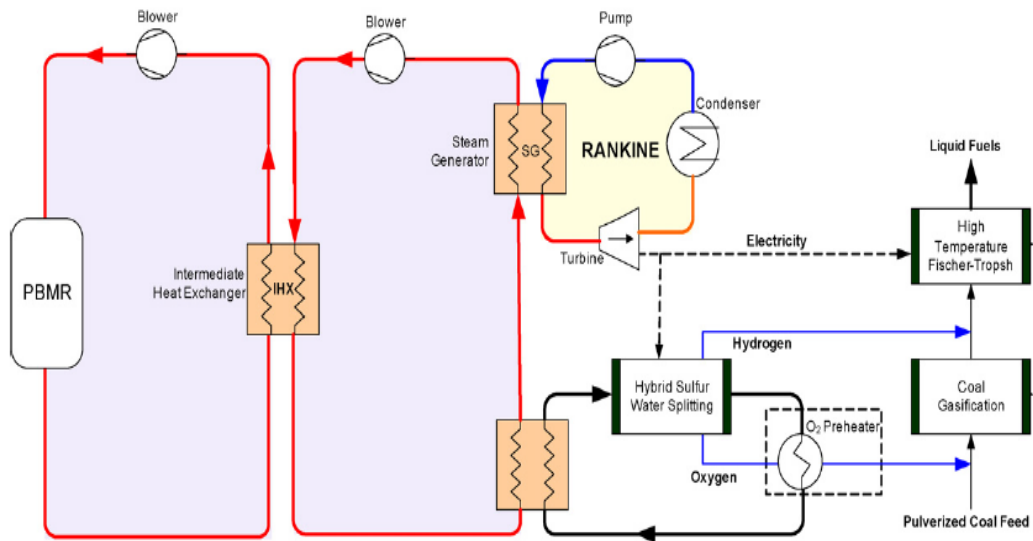


Figure 4.9 PBMR coupled to combined power and CTL process (Greyvenstein, 2008)

4.3.2 Mathematical modelling of the special heat exchanger

Since steam is generated in a once-through process, the mathematical model can be developed using the same approach presented for the once-through steam generator of a simple power generation unit. Therefore, Figure 4.6 can be transformed to Figure 4.9 to validate the intermediate fluid approach.

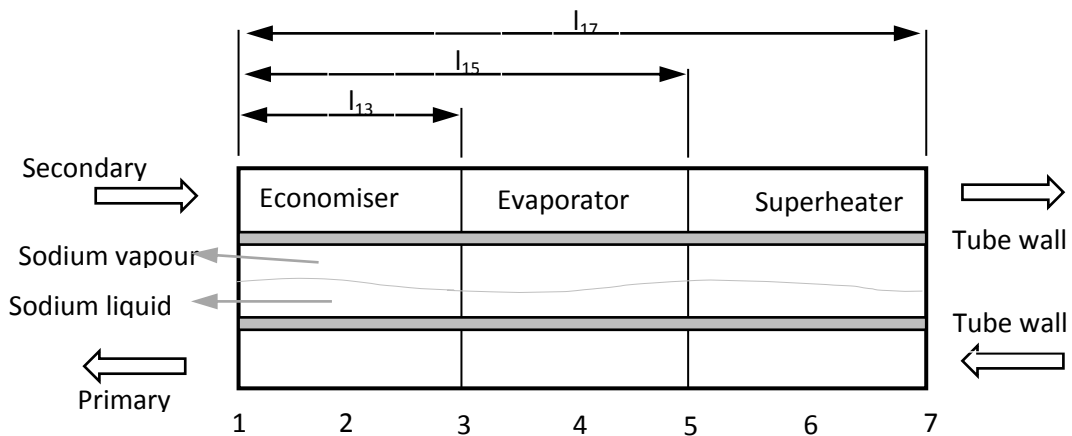


Figure 4.10 Schematic view of the sections of the heat pipe heat exchanger (HPHE)

However, a few changes in the system will be considered due to the implications of using of an intermediate fluid.

As mentioned in Section 4.3.1, helium flowing in the primary side of the heat exchanger transfers heat to liquid sodium that evaporates. This vapour sodium in turn will exchange heat with the feedwater of the secondary side, generating superheated steam. Due to the amount of sodium liquid used in the system, its thermodynamic properties such as its thermal conductivity and latent heat of vaporisation should be considered, causing, rising concerns about the thermal transport delay that could apply to the actual situation.

Ignoring the wall effect on both the primary and secondary sides, the overall heat transfer process is considered to be conducted from helium to liquid sodium and from vapour sodium to feedwater. Considering the two major processes, the thermal transport delay expressed per unit time can be written as

$$\tau = \frac{A l_{13} \rho_2}{2 \dot{m}_1} + \frac{m h_{fg}}{\dot{Q}_{\text{helium}}} \quad (4.50)$$

where h_{fg} is the latent heat required to evaporate the liquid sodium, m its mass and \dot{Q}_{helium} the heat rate supplied to sodium from helium.

This approach assumes a constant overall temperature for sodium. The required operating temperature of the heat exchanger should be equal or slightly greater than the saturation temperature of sodium to achieve the vaporisation. Also, condensation occurs when steam is generated in the secondary side. Due to the above, the sodium should be brought to the required thermodynamic conditions such as pressure to accommodate its evaporation at the operating temperature.

4.4 Primary side and metal tube equations

The steam generator in Section 4.2 and the heat pipe heat exchanger in Section 4.3 were modelled from the secondary side. Section 4.4 will model the primary side for dynamic equations of heat supply. Dividing the primary into three sections and using the same approach of movable boundaries for the economiser, evaporator and superheater of the secondary stream, and keeping in mind that in the primary stream we only have a single phase at all times, the energy and momentum equations shall be identical in all three sections. Therefore, the primary side dynamics could be ignored and the steady-state energy balance equation can be written as

$$\dot{Q}_p = c_p \dot{m}_p (T_{p,in} - T_{p,out}) \quad (4.51)$$

where the p stands for primary, and in and/or out are used to define the inlet and/or outlet of the different sections.

The metal tube equation dynamics can be described by applying the energy equation to the metal in the three sections separately to obtain the following equations

$$C_m \frac{d}{dt} (l_{13} T_{m2}) = Q_{p2} - Q_2 + C_m T_{m3} \frac{d}{dt} l_{13} \quad (4.52)$$

$$C_m \frac{d}{dt} (I_{35} T_{m4}) = Q_{p4} - Q_4 + C_m T_{m5} \frac{d}{dt} I_{15} - C_m T_{m3} \frac{d}{dt} I_{13} \quad (4.53)$$

$$C_m \frac{d}{dt} (I_{57} T_{m6}) = Q_{p6} - Q_6 - C_m T_{m5} \frac{d}{dt} I_{15} \quad (4.54)$$

In this chapter a brief description of the plant was presented. This description covered the different parts or sections of the overall plant for which a layout is shown in Figure 4.1. In this figure, one can see the three units of nuclear reactors providing 1500 MW thermal in total. Two types of units (group of two nuclear reactors) can be observed, one for power generation only and the other for a cogeneration process consecutively providing process heat for a CTL plant and steam for power generation.

The second type of unit contains two nuclear reactors, two steam generators and two heat pipe heat exchangers. In sections 4.1, 4.2 and 4.3 respectively the nuclear reactor, steam generator and heat pipe heat exchanger were mathematically described from a dynamic point of view.

In the next chapter, simulation results of the different systems will be presented and discussed. These simulations were run using Matlab/Simulink for the dynamic responses.

5 HTMR – THEORETICAL SIMULATION RESULTS

As described in Chapter 3 and modelled in Chapter 4, the High-temperature modular reactor (HTMR) is made up of three sets of 2x250 MW_{th} nuclear reactors, similar, to the high-temperature gas cooled reactor pebble-bed module (HTR-PM) demonstration plant. For the control and operating condition predictions, the HTMR has been simulated for various operation conditions assuming fluctuation of the power demand.

The simulation of the HTMR is done to predict its behaviour for a transient operation under various operating conditions. The response is expected to be close enough to the results published for the HTR-PM in order to validate to be validated for a feasibility study of use of a HTR-PM nuclear reactor type in a cogeneration plant. This simulation is run assuming a linear increase of the reactor reactivity, the coolant gas mass flow rate and the feedwater mass flow rate as presented in Tables 6.4 and 6.5.

In this section the following have been simulated:

- The nuclear reactor described in Section 4.1;
- The power unit steam generated as in Section 4.2;
- The heat pipe heat exchanger introduced in Section 4.3

5.1 Nuclear reactor simulation results

The HTR-PM demonstration plant consists of two identical nuclear reactors of 250 MW_{th} each. The nuclear reactor's simulation was implemented in a Matlab/Simulink environment and simulates two main performances, namely; reactor power and coolant gas outlet temperature. This simulation analyses these important parameter characteristics dynamically. This is done by assuming that the modular power demand increases from steady-state operating conditions at 20% to a full-power demand 100%. For smooth operations the actual reactor operator employs a linear increase from 20% to 100% for normal operation. The increase rate used was the same as for the HTR-PM, increasing reactor power from 20 % to 100% in 16 minutes (Li, et al., 2008b). The input variables (helium flow rate, feedwater flow rates and reactivity) will be presented in Table 6.3, which provides information about starting time and rate of increase to get to the results presented in this study.

5.1.1 Reactor power

The HTMR has been suggested to deliver an operating power of 1500 MW_{th}. As per the design considerations, the 1500 MW_{th} (3x2x250) should be provided by six identical and independent nuclear reactors of 250 MW_{th} each. The operating conditions for the current simulation suggest that the reactor thermal power be increased from 20 % to full load in 16 minutes (Li, et al., 2008b). During the current simulation, it has been recorded that from a 20 % load at steady-state, the nuclear power is increased by control rod withdrawal while the control rod reactivity is increased from an initial negative value of -0.0053 to a final zero reactivity within 16 minutes. The available thermal power caused by the nucleic power, theoretically defined by equation 3.11, is presented in Figure 5.1. The simulation result shows that at lower reactivity value, the

available thermal power is slightly below 50 MW_{th}. The smooth increase in control rod reactivity increases the thermal power which overshoots at 2285 seconds from the beginning of the simulation by 9.88% of the full operating load and then stabilizes at the required operating value of 250 MW_{th} after a further 1620 seconds.

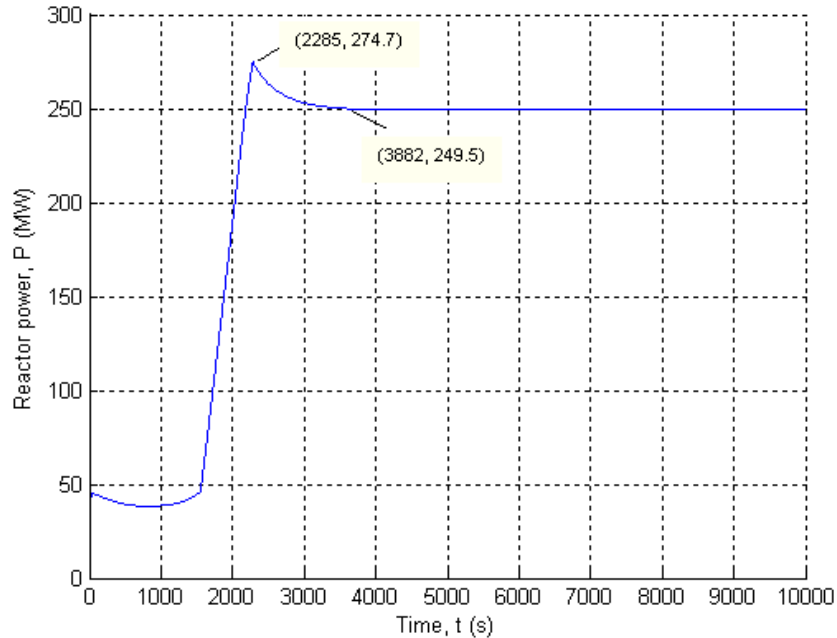


Figure 5.1 HTMR reactor power as function of time

5.1.2 Helium outlet and reactor core temperature

The gas-cooled HTMR design requires a reactor temperature difference of about 500 °C between the inlet coolant helium at 7 MPa and the outlet temperature. As can be seen from Table 4.1, the inlet temperature should be kept at 250 °C while the outlet temperature is at 750 °C. Figures 5.2 and 5.3 present the reactor coolant gas outlet temperature and the reactor core temperature obtained from the simulation. The reactor outlet temperature profile in Figure 5.2 shows that the coolant gas will drop to 680 °C after 850 seconds before rising to overshoot to 830 °C at the 2136th second from the beginning of the simulation. The nuclear reactor coolant gas outlet temperature decreases after about 2100 seconds after which it stabilises at 764.4 °C.

The reactor core temperature profile is kept at a safe (< 1600°C) stable value of 896.5°C during normal operation at full power, as can be seen in Figure 5.3. During the power increase process the simulation has shown that the reactor core temperature increases from 703 °C to overshoot at 958 °C after 2213 seconds, then decays to the operational stable value mentioned above after 3663 seconds.

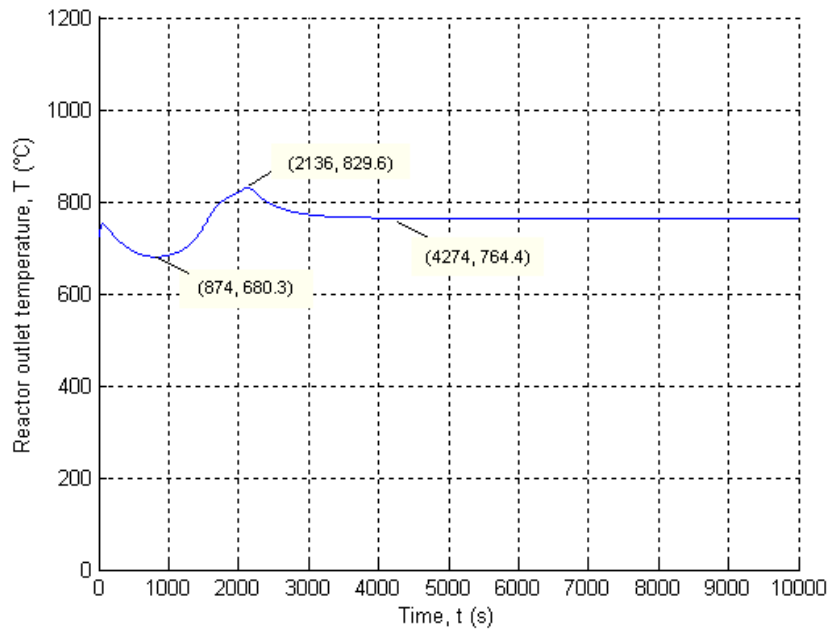


Figure 5.2 Reactor outlet temperature as function of time

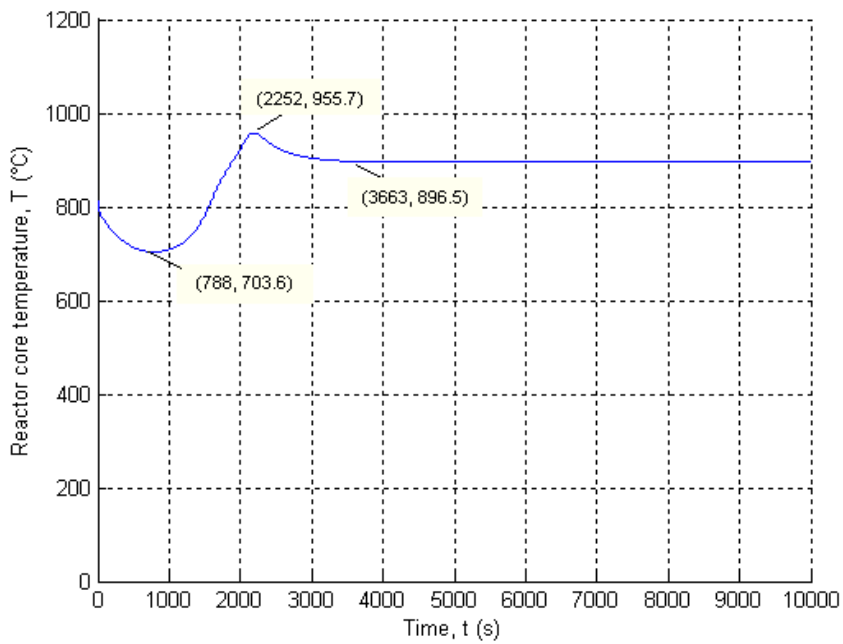


Figure 5.3 Reactor core temperature as function of time

5.2 Power unit steam generator results

The power unit, as described in Section 4.1 and illustrated in Figure 4.3, consists of the nuclear reactor coupled to a once-through helical coil steam generator. In this configuration, helium passes through a closed loop after having supplied heat to generate steam. This closed loop results in feedback to the reactor in the transient simulation according to Hoffer *et al.* (2011). In the following paragraphs the dynamic once-through helical coil steam generator results are presented.

5.2.1 Outlet steam temperature

The once-through helical coil steam generator produces high-temperature steam at 13.5 MPa; high enough to drive the turbine connected to the generators. The simulation of the steam generator of the power unit is shown in Figure 5.4. It can be seen that for the current simulation conditions, the steam temperature increasingly fluctuates before it suddenly drops from 530 °C at 1504 seconds to 414 °C, after which it immediately increases. This drop is due to the increase of the mass flow rate of the feedwater launched at 1500 seconds, while the increase follows due to the increase of the coolant mass flow rate started at 1550 seconds. This temperature will continue to increase before peaking at 637 °C at 2284 seconds from the beginning of feedwater flow rate increase. After the peak, the steam temperature progressively increases and stabilises at an operational 534°C after 4326 seconds.

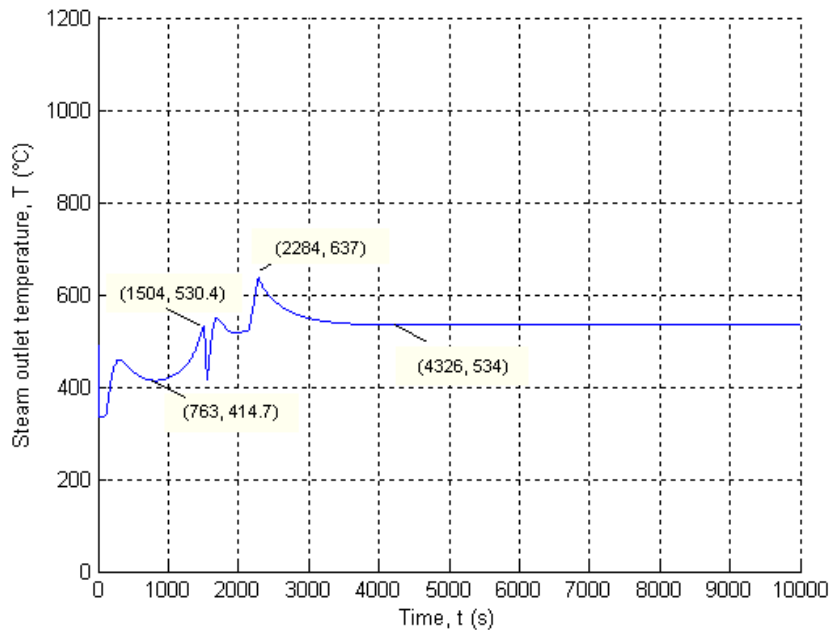


Figure 5.4 Steam outlet temperature as function of time

5.2.2 Economizer, Evaporator and Superheater lengths dynamics

In Section 3.2.4, the moving boundaries assumption was developed and defined by equation 3.5. According to this assumption, the three parts of the steam generator lengths l_{13} , l_{35} and l_{57} are subject to change every time that the energy balance changes, since the length is directly linked to the heat transfer rate. During the current simulation, the economiser, the evaporator and the superheater's lengths have been analysed for the transient model. Figures 5.5, 5.6 and 5.7 below present the relevant lengths of economiser, the evaporator and the superheater. These lengths were found to be highly dependent on the mass flow rate of the fluids. For a fixed total length of pipe, the mass flow rates were found to be the most important factor in determining the outlet temperature of the steam generated.

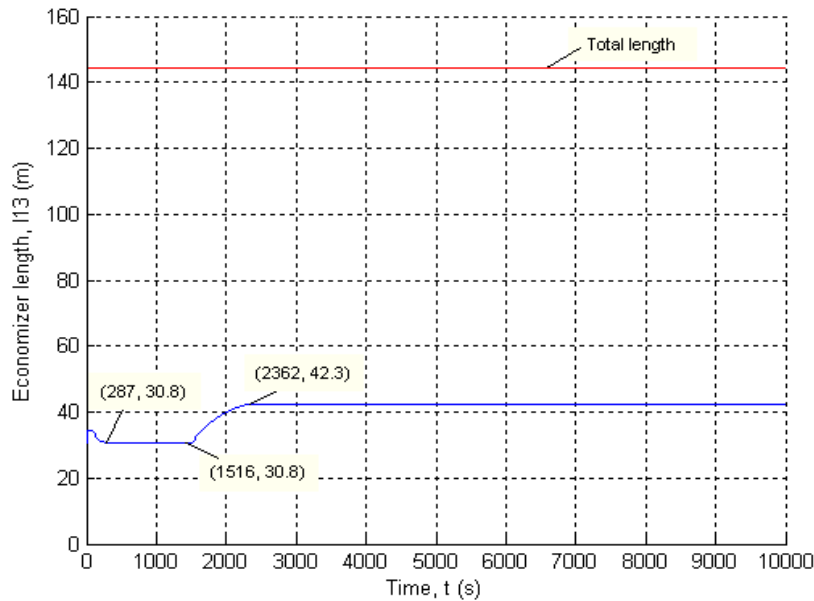


Figure 5.5 Economiser length l_{13} as function of time

In Figure 5.5, it can be seen that the economiser's length stabilises at 31 m for the 20% load operation before length rapidly increase to 42.31 m as the operating conditions change to full power. For this simulation, equations 3.44, 3.45, 3.46, 3.47 and 3.48 applied to the economizer were combined in equation 3.51 in order to determine the economiser's length. This combination shows a significant dependence of the length for varying fluids mass flow rates. This dependence can also be seen in the overall heat transfer coefficients expressed as a function of single fluid mass flow rate. Sample calculations related to the current issue are presented in Appendix A.

The simulation of the evaporator has shown that at 20% load the evaporator needs to be 21 m long. The sudden increase in the reactor coolant gas's mass flow rate produces a significant reduction of the evaporator's length to 14.3 m, after which, it increases from the 1589th second to overshoot at 29 m after 859 seconds before dropping slightly to 28.65 m due to the combined increase in the reactor power, feedwater and coolant gas mass flow rate. The evaporator length is presented in Figure 5.6 below.

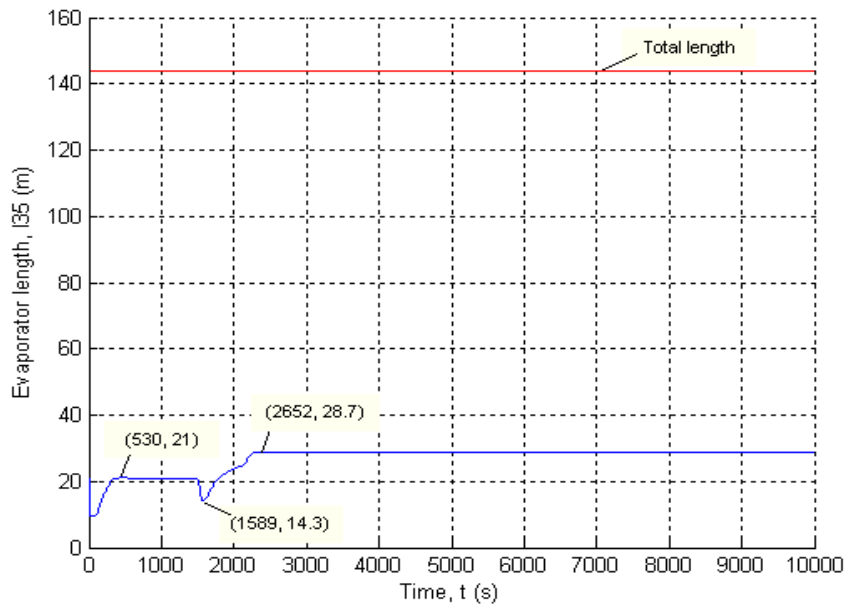


Figure 5.6 Evaporator length I_{35} as function of time

The superheater's length was determined to be the remaining part of the pipe after the economiser and the evaporator. This length is obtained by subtracting the length of the economiser and the evaporator from the total pipe's length. The superheater was found to be 92 m when operating at 20% load. The simulation has shown that at full power, the superheater will stabilise at about 72.62 m.

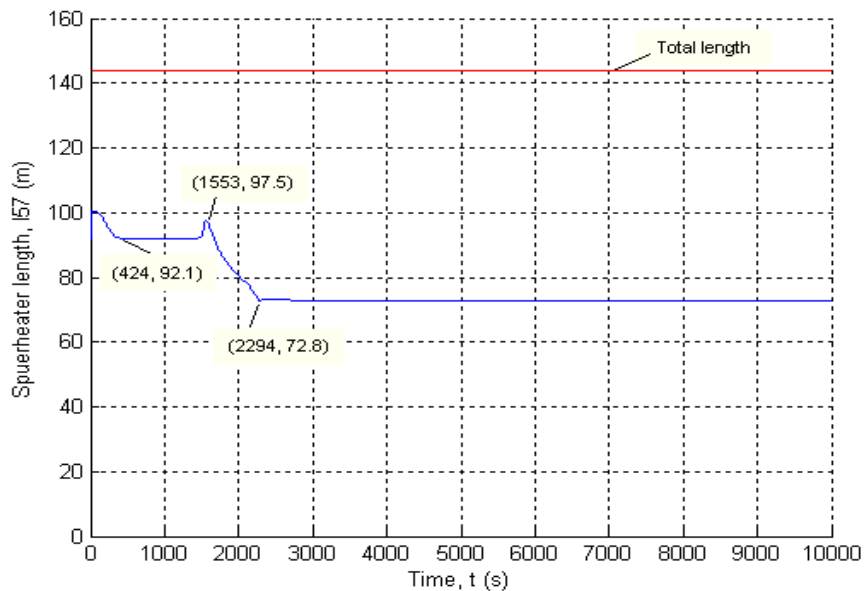


Figure 5.7 Superheater length I_{57} as function of time

5.3 Heat pipe heat exchanger steam generator results

The HTMR is intended to provide 243 MW_{th} of the 1500 MW_{th} to process heat in the form of superheated steam (Botha, 2011). This steam is generated in a heat pipe heat exchanger that uses liquid sodium as intermediate fluid (Laubscher, 2012). This configuration is advised to reduce the probable risk of contamination of the steam by the nuclear radiation carried in the graphite particles conveyed by the high-pressure reactor coolant gas as described in Section 4.3.1 (Stempniewicz, et al., 2012). The next paragraphs will present the simulation results of the block of Figure 4.4. This block consists of a closed loop consecutively connecting a nuclear reactor to a heat pipe steam generator and a helical coil once-through steam generator.

5.3.1 Superheated steam outlet temperature

The results of the outlet temperature simulation of the heat pipe heat exchanger for steam generation in a once-through heat exchanger model are presented in Figure 5.8. It can be seen that for the first 1000 seconds the outlet temperature drops to about 290 °C, where it stabilises. As soon as the increase is applied to the reactor power, this temperature increases as well to about 370 °C before dropping quickly with the increase in the feedwater mass flow rate to about 250 °C. This temperature remains constant for about 1300 seconds, then increases smoothly to the recommended value of 430 °C. In investigating the flat 250 °C zone, it can be seen that this temperature corresponds to the steam saturation temperature at 4 MPa. Therefore, it was found that during this period the reactor did not provide enough energy to generate superheated steam as compared to the required amount to bring the instantaneous feedwater mass flow rate beyond the steam saturation state.

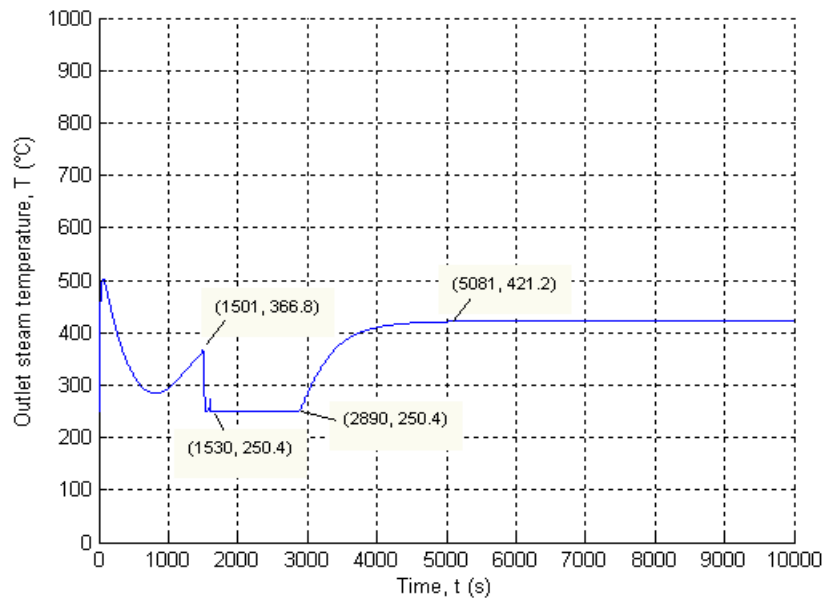


Figure 5.8 Heat pipe heat exchanger outlet steam temperature

To confirm this, a plot of the outlet steam enthalpy and the steam quality is provided in Figures 5.9 and 5.10 respectively, which show that during this period the enthalpy drops from 3100 kJ/kg to 1250 kJ/kg while the quality drops from 100% to 80% at 2375 seconds from the beginning of the simulation.

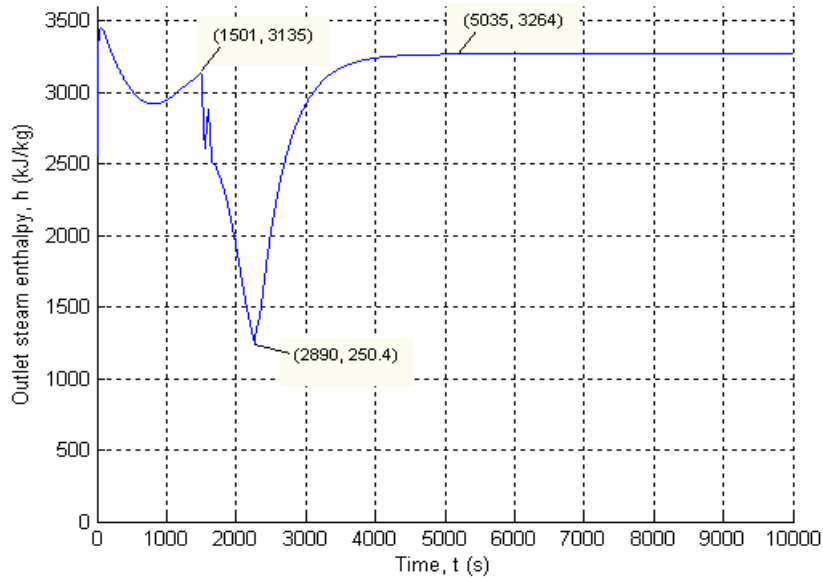


Figure 5.9 Heat pipe heat exchanger outlet steam specific enthalpy

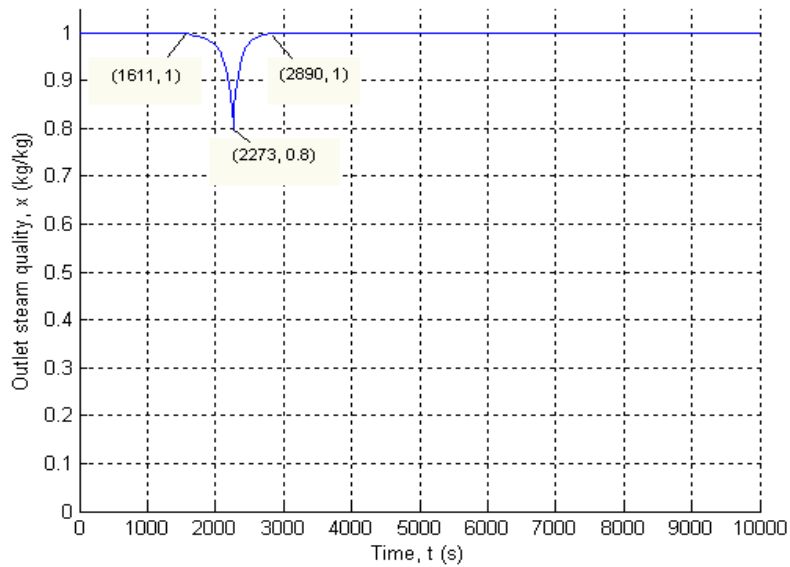


Figure 5.10 Heat pipe heat exchanger outlet steam quality

5.3.2 Helium outlet temperature

The theoretical expectations of the HTMR simulation show that helium from the nuclear reactor passing through the heat pipe heat exchanger generates superheated steam at 4 MPa, and 430 °C for coal conversion to liquid fuel, the process regarded as primary objective, before entering the once-through helical coil steam generator for power generation. Requirements are such that helium should be kept hot enough after the heat pipe heat exchanger to generate superheated steam at 13.5 MPa and 540 °C during the reactor's full power operation. The simulation of the second block in Figure 4.4 has shown that for the current design and simulation conditions, helium would exit the heat pipe heat exchanger at about 400 °C at 20% power operation. During this period the cogeneration block (the second block in Figure 4.4) is not expected to be generating power but the excess thermal energy of helium could be used for other processes such as pre-heating the system's feedwater.

The reactor power increase of the loop presented in Figure 4.4 shows a much smoother power increase with no overshoot. The combined increase in helium, heat pipe heat exchanger feedwater, and helical coil once-through steam generator feedwater mass flow rates results in a sudden drop of the heat pipe heat exchanger's helium outlet temperature to about 380 °C at 1740 seconds from the beginning of the simulation. This temperature immediately increases to stabilise at a desired value of 650 °C after a negligible overshoot.

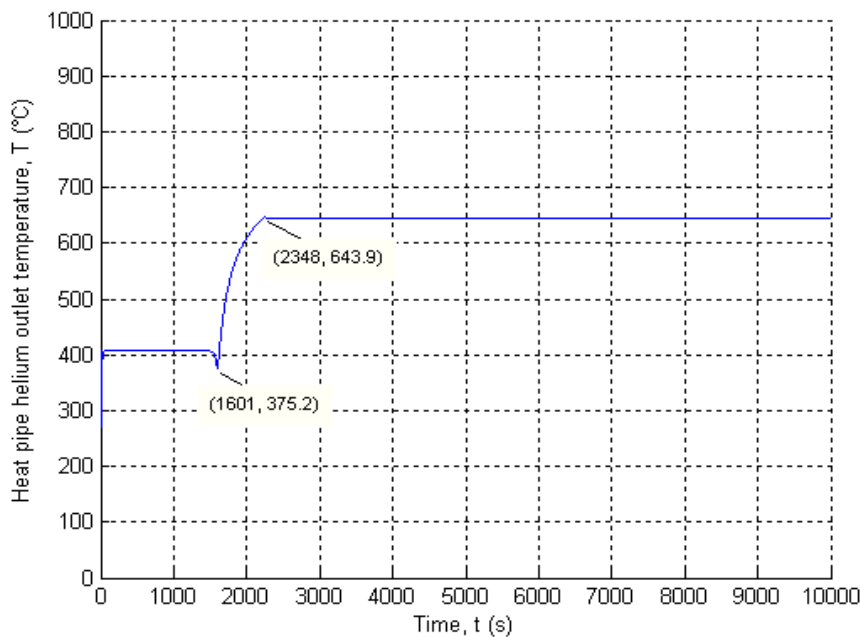


Figure 5.11 Heat pipe heat exchanger helium outlet temperature as a function of time

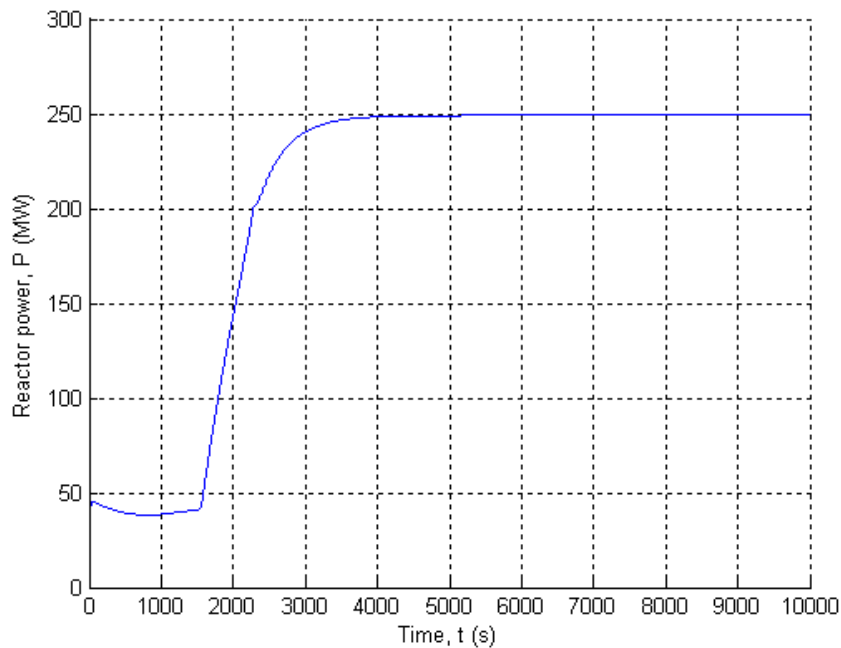


Figure 5.12 Cogeneration loop reactor power as a function of time

With regard to power manoeuvring of nuclear reactor operation, maintaining the plant parameters within a reasonable range is a high priority for safety and performance achieving (Li, et al., 2008a). The HTMR's power manoeuvring for this simulation is from 50 MW to 250 MW. During the simulation an operation ratio of about 10 % was applied to all parameters except for the outlet steam temperature shown in Figure 5.4, where the steam temperature was allowed to extend beyond the operation ratio in order to highlight the effect of the temperature of the feedwater. To prove the relevance of the approach applied to the HTMR, the next chapter will compare the current results to the published HTR-PM simulation results in order to provide explanations for deviations observed in the two reactors' simulation results.

For simplicity of operation, the simulation was run on one module of the power unit and one module of the cogeneration unit. This approach assumes that the six modules are independently controlled using electronic devices such as dispatchers that will distribute the grid demand and the process heat required among the six reactors. Each module's control system will have to apply the control strategies to produce the expected output (Li, et al., 2008b).

6 CONTROL MODEL VALIDATION

To be able to check the accuracy of the simulation results, a comparison between the HTMR simulation results and the published HTR-PM demonstration plant is discussed in this Chapter (Li, et al., 2008b). To validate the results presented in Chapter 5, the developed mathematical model of the HTMR was simulated and will be compared to the HTR-PM open loop results.

6.1 Theory, programme and results of the HTR-PM

It was suggested that the HTR-PM demonstration plant be built with two modules (reactors), operating between 250 and 750 °C, and using high-pressure helium at 7 MPa as coolant gas (Zhang, et al., 2009). The fundamental principles of conservation of mass, momentum and energy were used to develop a dynamic model in order to investigate the operation and control characteristics of the HTR-PM plant. The suggested dynamic model was aimed at describing the plant behaviour at a high level of power demand variation. In this simulation, the main parameters that were observed are the outlet steam temperature and the reactor power level, while maintaining the reactor operating temperature difference (Li, et al., 2008b). The steam temperature was regarded as the most important parameter since it was meant to be able to drive the turbine during the power generation process.

6.1.1 HTR-PM power curve

Initially under steady state for the first 1000 seconds, the reactor power was assumed to linearly increase from 20% to 100%. Then at the 1000th second, simultaneous increase in the input parameters was applied with their maximum allowable increase rate, as follows. The control rod reactivity increased from an initial value of -0.0053 to a final value of 0 within 16 minutes therefore the reactor power increased. The primary (helium) and the secondary (feedwater) flow rates both increased from an initial value of 17.87 kg/s to 97.53 kg/s at 4.8765 kg/s per minute, while the feedwater temperature increased from 147°C to 205°C, at a linear rate of 3.625°C per minute (Li, et al., 2008b). Applying the above, the reactor power prediction was found to be as shown in Figure 6.1, while the reactor power linearly increased to full power. The reactor power overshoot by 5% of its full power at about the 2000th second, then decreased to stabilise at 250 MW at about the 5000th second. The HTR-PM input values are presented in Table 6.1.

Table 6.1 Simulation input variables of the HTR-PM (Li, et al., 2008b)

Parameters	Unit	20% load	100% load
Control rod reactivity		-0.0053	0
Primary helium flow rate	kg/s	17.87	97.53
Primary helium pressure	MPa	7	7
Secondary steam outlet pressure	MPa	13.5	13.5
Secondary steam inlet feedwater flow rate	kg/s	17.87	97.53
Secondary feedwater temperature	°C	147	205

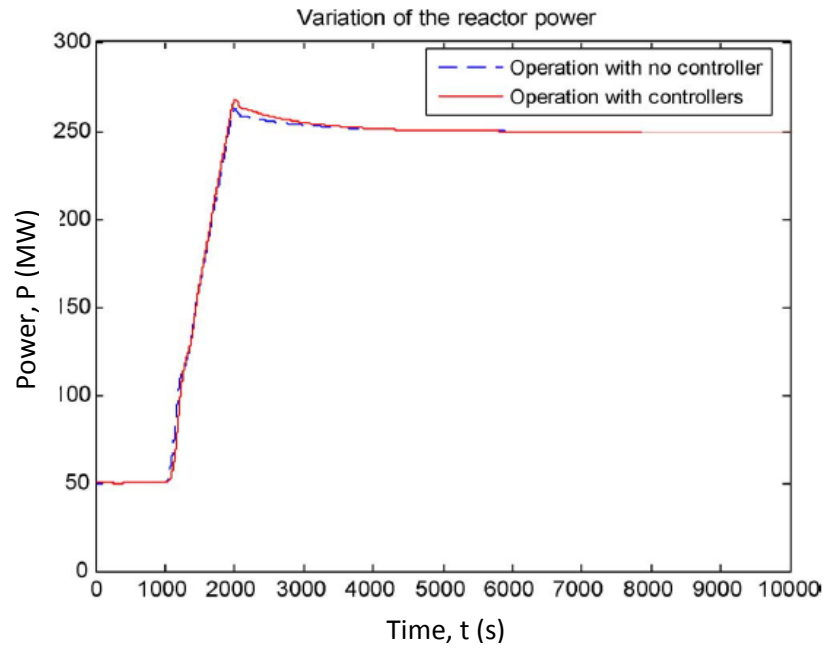


Figure 6.1 HTR-PM reactor power as function of time (Li, et al., 2008b)

6.1.2 HTR-PM reactor core temperature

At 20% steady-state operation, the reactor's core average temperature was found to be 812 °C. Immediately after the simultaneous increase in the input variables described in Table 6.1, the reactor's core temperature dropped to a minimum value of about 806 °C, after which it smoothly increased to reach 841 °C around the 8000th second (Li, et al., 2008b). These reactor core temperature values were found acceptable compared to the reactor safety limit temperature of 1600 °C (Li, et al., 2008a). Figure 6.2 illustrates the simulated reactor core temperature of the HTR-PM.

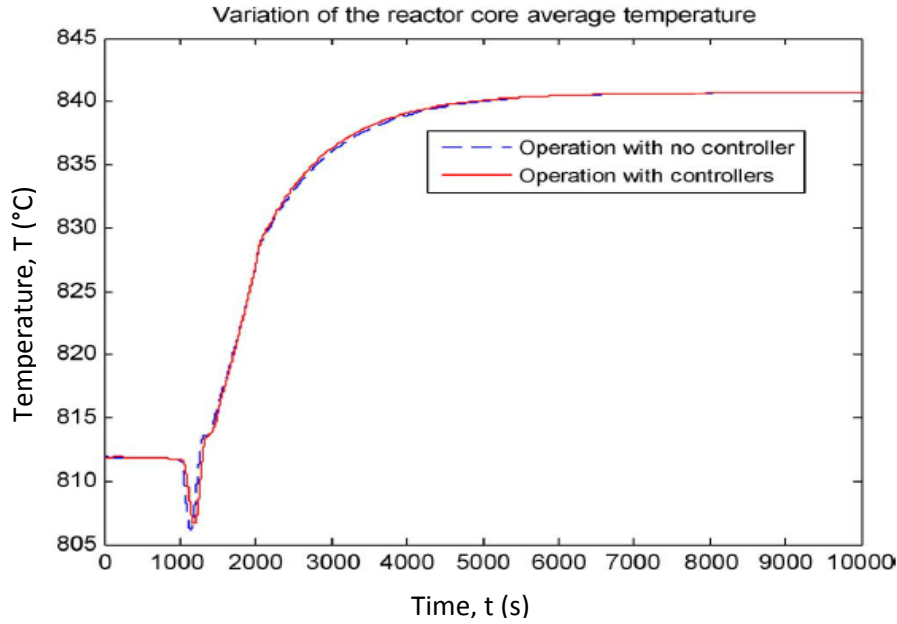


Figure 6.2 HTR-PM reactor core temperature as function of time (Li, et al., 2008b)

6.1.3 HTR-PM steam temperature

The HTR-PM simulation results predicted that the steam generated from the once-through helical coil steam generator for 20% operation would be supplied in superheated steam at 540 °C and 13.5 MPa as required for power generation. The steam generator outlet profile of Figure 6.3 shows that combined effect of the increase in the parameters listed in Table 6.1 is reflected by an instantaneous and sharp overshoot to 655 °C, which gradually decreases to 517 °C at about the 2000th second; after which the steam temperature increases smoothly to become steady to 540 °C at about the 5000th second. This type of fluctuation is not allowable for power plant operations which generally allow an acceptable variation of about ± 10 °C (Li, et al., 2008b). To rectify this aspect, a controller has been added to the system, reducing the overshoot to about 548 °C.

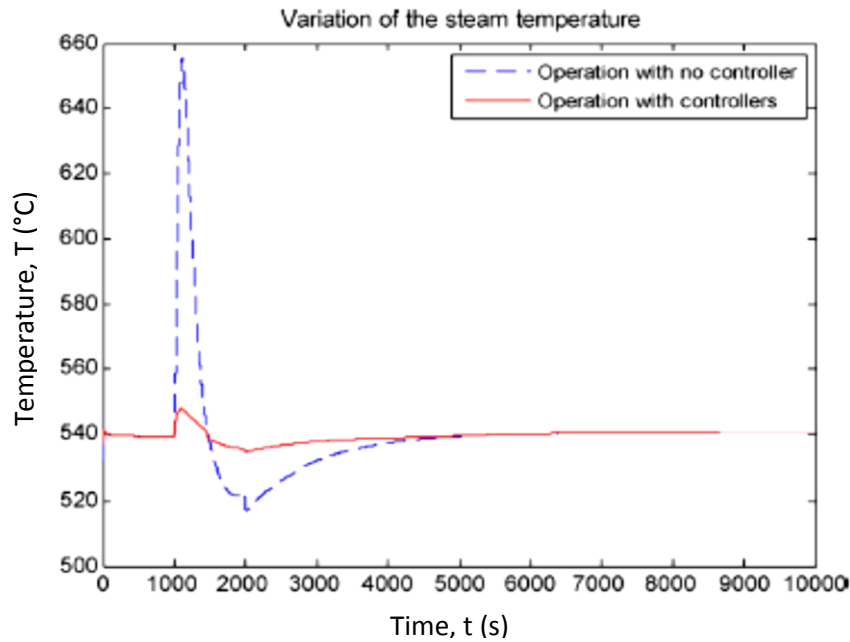


Figure 6.3 HTR-PM outlet steam temperature as a function of time (Li, et al., 2008b)

6.2 Comparison of published HTR-PM results and HTMR results

6.2.1 Reactor power

The simulation of the HTMR has shown appreciable results for reactor power as shown in Figure 5.1, with slight differences that can be observed at two levels. Firstly, at 20% operation, the HTMR generated about 44 MW instead of 50 MW due to the little temperature difference between the reactor coolant inlet and outlet temperatures. The helium leaves the steam generator at a much higher temperature due to the low overall heat transfer coefficient in the steam generator at low mass flow rates, as can be seen in Appendix A.1.3. Since used in a closed loop, helium is supplied to the reactor at about 271 °C, which is strictly higher than the ideal 250 °C, while the outlet temperature is also significantly lower than 750 °C due to the low heat transfer coefficient at low mass flow rate in the reactor bed. Secondly, a difference is seen in the overshoot ranges. The HTMR presents a 9.88% overshoot while the HTR-PM only 5%. This is because the HTMR's helium outlet temperature peaks at 830 °C while the HTR-PM's outlet temperature smoothly increases to 745 °C. Differences of that magnitude could be due to differences in the configuration of the nuclear reactor, such as physical size and design.

6.2.2 HTR-PM and HTMR Temperatures comparison

In this section, three temperatures are considered, namely the reactor core temperature, the reactor coolant gas outlet temperature and the steam outlet temperature. These temperatures, presented in Figure 6.4, have been selected since they provide a general overview of the plant's behaviour during transient operation.

The HTR-PM reactor core has a sharper drop in its temperature (see Figure 6.2) due to the suddenly increasing coolant gas mass flow rate, while the rate of power increase presents a certain delay. It then smoothly increases to reach the full power operating value of 841 °C without overshooting. Meanwhile, the HTMR reactor core temperature first drops during 20% load operation. In the process of power increase, the HTMR reactor core temperature increases too with a considerable overshoot to about 956 °C at the 2252th second. The difference between these two profiles is due to the delay applied to the mass flow rate of the coolant gas of the HTMR, allowing control of the outlet temperature of the coolant gas. To achieve control of the gas temperature it was decided to first allow the available reactor power to increase before increasing the gas mass flow rate.

The simulation has shown that to keep the outlet temperature within an acceptable range, the coolant gas mass flow rate should be increased considering parameters such as the rate of increase and the beginning of the increase process. Increasing the coolant gas too early or too fast results in a significant drop in the gas outlet temperature; starting the increase process of the coolant gas flow rate at a very late stage or at a very low increase rate would expose the reactor core to overheating that might exceed the safety critical reactor temperature of 1600 °C. To keep the outlet temperature of the reactor coolant gas and the reactor core temperature at reasonable values, a 0.10833 kg/s increase rate was applied to the coolant gas mass flow rate, delayed by about 450 seconds relative to control rod reactivity withdrawal. Since the reactor coolant gas inlet temperature depends on the steam generator feedback, the feedwater mass flow rate increase was also delayed by 400 seconds relative to control rod reactivity withdrawal at 0.12583 kg/s.

In addition, the deviations between HTMR and HTR-PM results are also due to fact that the HTMR simulation used a constant feedwater temperature of 205 °C while the HTR-PM used a feedwater temperature of 147 °C for 20% load operation, which was then increased to 205 °C with a linear increase of 58°C within 16 min (Li, et al., 2008b). Increasing the feedwater temperature would theoretically increase the average temperature of the secondary flow of the steam generator for a constant steam outlet temperature of about 540 °C, as can be seen from equation 3.19, when applied to the steam generator between the reactor coolant gas and steam.

The HTMR simulation input variables are displayed in Table 6.2. The simulation was run for a certain number of operating conditions for both the power unit and the cogeneration unit presented in Figure 4.4. The power unit variables are presented in Table 6.2 and the cogeneration unit input variables in Table 6.3.

Table 6.2 Input variables of the HTMR power unit

Parameter	Unit	20% load	100% load
Control rod reactivity		-0.0053	0
Primary helium flow rate	kg/s	17.87	97.53
Primary helium pressure	MPa	7	7
Secondary steam outlet pressure	MPa	13.5	13.5
Secondary steam inlet feedwater flow rate	kg/s	17.87	97.53
Secondary feedwater temperature	°C	205	205

Table 6.3 Input variables of the HTMR cogeneration unit

Parameter	Unit	20% load	100% load
Control rod reactivity		-0.0053	0
Primary helium flow rate	Kg/s	17.87	97.53
Primary helium pressure	MPa	7	7
Steam generator outlet pressure	MPa	13.5	13.5
Steam generator inlet feedwater flow rate	Kg/s	5	74
Steam generator feedwater temperature	°C	205	205
Heat pipe outlet pressure	MPa	4	4
Heat pipe inlet feedwater flow rate	kg/s	12.5	25
Heat pipe feedwater temperature	°C	205	205

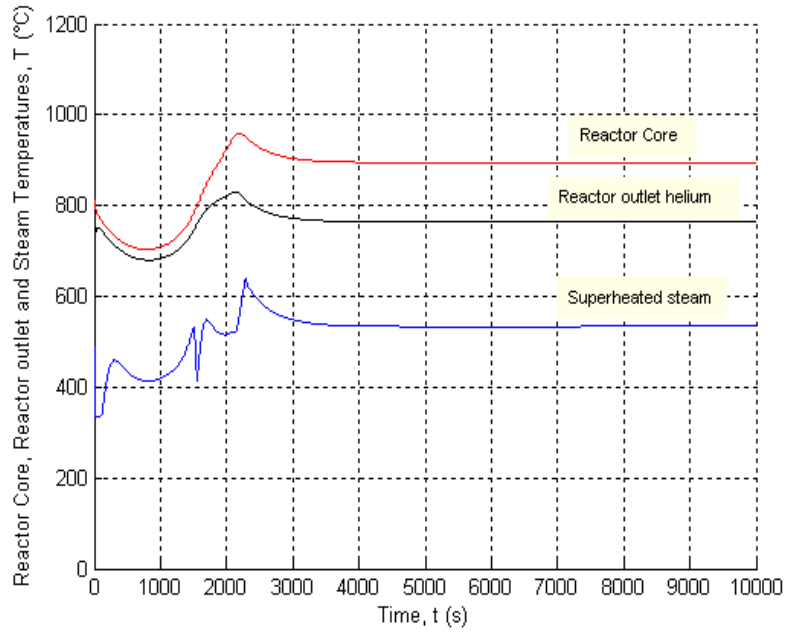


Figure 6.4 HTMR outlet steam temperature, reactor core temperature and reactor outlet helium temperature as function of time

The comparison between the HTR-PM and HTMR results has shown similarities and few deviations in general. Most deviations were due to the simulated operating conditions of the HTMR. The operating conditions of both types of reactor were presented in Table 6.1, Table 6.2 and Table 6.3 for the HTR-PM module, the power unit of the HTMR and the cogeneration unit of the HTMR respectively. However, two more important parameters were identified, on which the concept of the control strategies of the HTMR were based. These parameters are the starting time of each input variable and the rate at which these variables should be increased. The relevance of the concept of control was initiated when it was found that changing the starting time and/or the rate of increase of any of the input variables would result in a much bigger deviation from the desired value of output parameters such as steam temperature, reactor core temperature or reactor outlet helium temperature. The current simulation was run using the data presented in Table 6.4 for the power unit and Table 6.5 for the cogeneration unit. As for the HTR-PM, a compensator was used to insert a certain delay in the increase of the mass flow rate of the reactor coolant gas, as can be seen in Figure 6.5. The control strategies of the HTMR will be discussed in Chapter 7 and the recommendations made for future work.

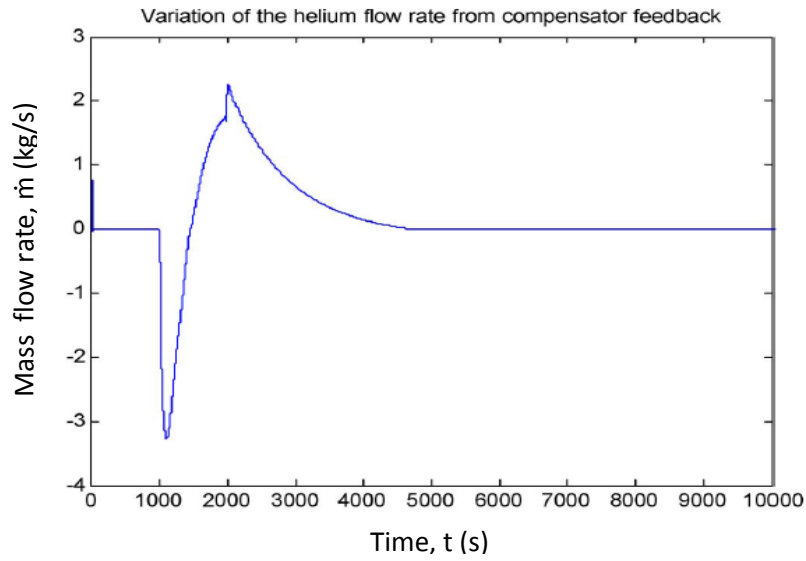


Figure 6.5 Variation of helium mass flow rate of the HTR-PM from a compensator feedback (Li, et al., 2008b)

Table 6.4 Timing of power unit input variables

Parameter observed	20 % load	100 % load	Starting time	Rate of increase per second
Helium mass flow rate (kg/s)	18	97.5	1550	0.108333
Steam generator feedwater mass flow rate (kg/s)	17.5	97.8	1500	0.102583
Control rod Reactivity	-0.0053	0	1100	0.00000552

Table 6.5 Timing of the cogeneration unit input variables

Parameter observed	20 % load	100 % load	Starting time	Rate of increase per second
Helium mass flow rate (kg/s)	18	97.5	1550	0.108333
Heat pipe feedwater mass flow rate (kg/s)	12.5	25	1500	0.082583
Steam generator feedwater mass flow rate (kg/s)	5	74	1600	0.102583
Control rod Reactivity	-0.0053	0	1400	0.00000552

7 DISCUSSION, CONCLUSION AND RECOMMENDATIONS

To stabilise the concentration of carbon dioxide in the atmosphere, the United Nations Intergovernmental Panel on Climate Change (IPCC) recommended that carbon dioxide emissions be reduced by 50 to 80% (Greyvenstein, 2008). Implementation of this measure in some fossil-fuel-driven economies such as South Africa, where about 77% of energy is generated from coal, would be a huge challenge. To overcome this challenge, the development of alternative carbon-free sources of energy, such as renewables, nuclear and hydrogen carrier, would be necessary.

Nuclear energy is currently mostly used for electricity generation; it contributes about 16% of the world's electricity generation (Greyvenstein, 2008). In this study it is suggested that nuclear energy use is extended to also provide process heat for the conversion of coal to liquid fuel using the Fisher-Tropsch process. This way, if the HTMR is built in South Africa, the country's 91% contribution to African emissions could be reduced by about 1.58%. A nuclear assisted combined power generation and CTL plant has been found to be a carbon free and efficient way of primary energy usage, considerably reducing emissions while allowing the extension of the lifetime of the country's fossil fuel reserves.

The HTMR was thermodynamically designed, mathematically modelled and simulated for a high level of power fluctuation in order to predict the transient behaviour of the overall system. The results obtained are used to advise on the control strategies applicable for a safe and more accurate operation. The following steps were followed to produce the current results:

In Chapter 2, an overview of applicable technologies for power generation, hydrogen carrier and coal-to-liquid processes was presented. Topics discussed were the gas and steam turbine for power generation, the hydrogen production using a water-splitting process, the CTL process and the possible role nuclear energy might play as a primary energy substitute for coal, gases and oil.

Chapter 3 investigated the possibility of a combined heat and power plant using nuclear energy. Topics discussed were nuclear reaction design characteristics, as well as the steam generation process for on a once-through steam generator and a heat pipe heat exchanger. The heat pipe heat exchanger is meant to replace the intermediate loop between the reactor coolant gas and the feedwater (Laubscher, 2012). The intermediate loop is advised to reduce the risk of steam contamination from highly radioactive particles carried in the coolant gas. An assumption of power increase from 20% load to full power in about 16 minutes was made and the heat transfer processes in the nuclear reactor and steam generators were described.

In Chapter 4 a mathematical model for transient behaviour of the HTMR was provided. This model was described using the energy conservation equation, the momentum equation and the mass conservation equation. The nuclear reactor is divided into six main sections characterised by the coolant gas flow pattern defined by the physical design and thermal properties depending on the temperature of a specific section of the reactor. The steam generator on the side is analysed by the flow characteristics of its two streams. The gas, a hot stream for which the thermal properties are assumed

constant throughout the steam generator, flows outside the pipes while the feedwater flows inside the pipes. The steam generator is physically and mathematically modelled in three sections defined by the thermodynamic state of the water during the steam generation process. The steam generation process in the heat pipe heat exchanger is approached in the same way as that in the once-through steam generator, for which the time constant takes into account the evaporation and condensation of sodium used as intermediate fluid.

The HTMR mathematical model was simulated for a transient operation using Simulink/Matlab. In this simulation, the steam thermodynamic properties were obtained using the XSteam/Matlab M-file downloaded from the internet. The helium gas thermodynamic properties were calculated as described in Chapter 3, using two of its known properties. The results obtained from the simulation revealed the following:

- The reactor power depends on the control rod reactivity level changing with the control rod position
- The reactor outlet temperature is mainly defined by the reactor power level, the inlet temperature and the mass flow rate of the reactor coolant gas
- Since the coolant gas flows through a closed loop, the reactor inlet temperature depends on the feedwater thermodynamic conditions of the steam and the steam flow characteristics directly linked to its mass flow rate
- The steam generator outlet temperature is defined by the overall heat transfer coefficient of the heat transfer process occurring in the once-through steam generator. The overall heat transfer coefficient is more dependent on the reactor coolant gas's thermo-flow characteristics than the steam's.

From the above findings and the sensitivity analysis operated during the simulations, it is found that the overall plant could be controlled by linearly varying the control rod reactivity, the coolant gas (helium) mass flow rate, and both feedwater mass flow rates of the steam generator and the heat pipe heat exchanger in terms of the rate of increase and the start-time.

These results were compared to the HTR-PM as presented in Chapter 6 and conclusions were drawn. It was found that the HTMR behaviour during transient operation could successfully be controlled by using variable speed drivers for the control of the mass flow rate and the control rod position. This configuration will differ from the HTR-PM since the HTR-PM used controllers that insert negative mass flow rate, as can be seen in Figure 6.5, while in the HTMR a similar result is obtained by delaying to the mass flow rate start-times.

8 REFERENCES

- Abram, T. and Ion, S. 2008. Generation IV nuclear power: A review of the state of the science. *Energy Policy* 36(12): 4323-4330.
- Abuadala, A. and Dincer, I. 2010. Investigation of a multi-generation system using a hybrid steam biomass gasification for hydrogen, power and heat. *International Journal of Hydrogen Energy* 35(24): 13146-13157
- Al-Khalifah, M. and McMillan, G.K. 2012. Control valve versus variable speed drive for flow control. Research Triangle Park, NC: International Society of Automation (ISA).
- Barron, F.R. 1985. *Cryogenic systems (Monographs on Cryogenics 3)*. New York : Oxford University press.
- Bogusch, E., Carré, F., Knebel, J.U. & Aoto, K. 2008. Synergies in the design and development of fusion and generation IV fission reactors. *Fusion Engineering and Design* 83: 936-942
- Botha, F., 2011. Simulation of a cogeneration plant coupled to a high temperature reactor. *Masters thesis*. Stellenbosch University.
- Brook, B.W. 2012. Could nuclear fission energy, etc., solve the greenhouse problem ? The affirmative case. *Energy Policy* 42:4-8.
- Cengel, Y.A. and Boles, M.A. 2006. *Thermodynamics: An Engineering approach*. Singapore : McGraw-Hill.
- Chaibakhsh, A., Ghaffari, A. & Moosavian, S.A.A. 2007. A simulated model for a once-through boiler by parameter adjustment based on genetic algorithms. *Simulation Modelling Practice and Theory* 15:1029-1051.
- Chaudhry, H.N., Hughes, B.R. & Ghani, S.A. 2012. A review of heat pipe systems for heat recovery and renewable energy applications. *Renewable and Sustainable Energy Reviews* 16:2249-2259.
- Coban, R. 2009. Optimal trajectory planning for control of nuclear research reactors using genetic algorithms and artificial neural networks. *Journal of Electrical and Electronics Engineering* 9(2): 1115-1128.
- Dobson, R.T. and Laubscher, R. 2013. Heat pipe heat exchanger for high temperature nuclear reactor technology. Conference paper delivered at the 11th International Heat Pipe Symposium. 9-11 June, Beijing, China.

Eastop, T.D. and McConkey, A. 1986. *Applied thermodynamics for Engineering Technologists*. New York : Longman.

Elder, R. and Allen, R. 2009. Nuclear heat for hydrogen production: Coupling a very high/high temperature reactor to a hydrogen production plant. *Progress in Nuclear Energy* 51(3):500-525.

Eskom. 2004. Overview of electricity demand and supply situation. Public meeting, EIA. Cape Town.

Ewan, B.C.& Allen, R.W.K. 2005. A figure of merit assessment of the routes to hydrogen. *International Journal of Hydrogen Energy* 30(8): 809-819.

FOEI. 2011. How corporations rule, Part 1: Sasol and South Africa's climate policy. Amsterdam, Friends of the Earth International. [Online] Available at www.foei.org/publications. Accessed on November 14, 2013

German Advisory Council on Global Change. 2003. World in Transition: Turning Energy Systems Towards Sustainability. [online] Available at www.wbgu.de

GIF & U.S. DOE. 2002. A technology roadmap for generation IV nuclear energy systems. United States Department of Energy. Nuclear Energy Research Advisory Committee.

Greyvenstein, R., Correia, M. & Kriel, W. 2008. South Africa's opportunity to maximise the role of nuclear power in a global hydrogen economy. *Nuclear Engineering and Design* 238:3031-3040.

Hoffer, N.V., Sabharwall, P. & Anderson, N.A. 2011. Modeling a Helical-coil Steam Generator in RELAP5-3D for the Next Generation Nuclear Plant. Technical Report INL/EXT-10-19621, Idaho National Laboratory.

IAEA. 1999. *Hydrogen as an energy carrier and its production by nuclear power*. IAEA TECDOC-1085. [Online]. http://www-pub.iaea.org/MTCD/publications/PDF/te_1085_prn.pdf. Accessed on November 14, 2013

IEA, International Energy Agency Website, 2006. Key World Energy Statistics, <http://www.iea.org/textbase/nppdf/free/2006/key2006.pdf>.

Jess, A. 2010. What might be the energy demand and energy mix to reconcile the world's pursuit of welfare and happiness with the necessity to preserve the integrity of the biosphere? *Energy Policy* 38(8):4663-4678.

Joung, W., Kim, Y.G., Yang, I. & Gam, K.S. 2013. Operating characteristics of a loop heat pipe-based isothermal region generator. *International Journal of Heat and Mass Transfer* 65:460-470

King, C.D.G. 1964. *Nuclear power systems*. Monterey, California: United States Naval Postgraduate School.

Laubscher, R. 2012. Development aspects of a high temperature heat pipe heat exchanger for high temperature gas-cooled nuclear reactor systems. unpublished masters thesis. Mechanical and Mechatronics Department, Stellenbosch University.

Laubscher, R. and Dobson, R.T. 2013. Theoretical and experimental modelling of a heat pipe heat exchanger for high temperature nuclear reactor technology. *Applied Thermal Engineering* 61:259-267.

Lewis David. 2008. Hydrogen and its relationship with nuclear energy. *Progress in Nuclear Energy* 50:394-401.

Li, H., Huang, X. & Zhang, L. 2008a. A simplified mathematical dynamic model of the HTR-10 high temperature gas-cooled reactor with control system design purposes. *Annals of Nuclear Energy* 35(9):1642-1651.

Li, H., Huang, X. & Zhang, L. 2008b. Operation and control simulation of a modular high temperature gas cooled reactor nuclear power plant. *IEEE Transactions on Nuclear Science* 55(4):2357-2365.

Locatelli, G., Mancini, M., & Todeschini, N. 2013. Generation IV nuclear reactors: Current status and future prospects. *Energy Policy* 61:1503-1520.

Mantripragada, H.C. and Rubin, E.S. 2011. CO₂ reduction potential of coal-to-liquids (CTL) process: Effect of gasification technology. *Energy Procedia* 4:2700-2707

Mantripragada, H.C. and Edward, S.R. 2009. CO₂ reduction potential of coal-to-liquids (CTL) plants. *Energy Procedia* 1(1): 4331-4338.

Mantripragada, H.C. and Rubin, E.S. 2013. Performance, cost and emissions of coal-to-liquids (CTLs) plants using low-quality coals under carbon constraints. *Fuel* 103:805-813.

McAllister E.W. 2009. *Pipeline rules of thumb handbook*. Houston: Professional Publishing.

Mills A.F. 1995. *Heat and mass transfer*. Chicago: Irwin.

O'Brien, J.E., McKellar, M.G., Harvego, E.A. & Stoots, C.M. 2010. High-temperature electrolysis for large-scale hydrogen and syngas production from nuclear energy - Summary of system simulation and economic analyses. *International Journal of Hydrogen Energy* 35(10):4808-4819.

- Ramirez Munoz, P.D. 2011. Dynamic simulation of nuclear hydrogen production systems. Doctoral dissertation. Massachusetts: Department of Chemical Engineering, Massachusetts Institute of Technology.
- Ray, A. 1980. Dynamic modelling of once-through subcritical steam generator for solar applications. *Applied Mathematical Modelling* 4(6):417-423.
- Reay, D.A. and Kew P.A. 2006. *Heat pipes*. 5th edition. Boston: Butterworth-Heinemann.
- Saito, S. 2010. Role of nuclear energy to a future society of shortage of energy resources and global warming. *Journal of Nuclear Materials* 398:1-9.
- Slabber, J., Theron, W. & Matzner, H.D. 2006. Technical description of the PBMR demonstration power plant. Pretoria, PBMR(Pty)Ltd.
- [Online] Available at <http://pbadupws.nrc.gov/docs/ML0609/ML060940293.pdf>.
- Statistics South Africa. 2005. *Natural resource accounts: Energy accounts for South Africa, 1995-2000*: Discussion document. Pretoria : Statistics South Africa.
- Stempniewicz, M.M., Winters, L. & Caspersson, S.A. 2012. Analysis of dust and fission products in a pebble bed NGNP. *Nuclear Engineering and Design* 251:433-442.
- Stoecker, W.F. and Jones, J.W. 1982. *Refrigeration and air conditioning*. Singapore : McGraw-Hill.
- Teravainen, T., Lehtonen, M., & Martiskainen, M. 2011. Climate change, energy security, and risk-debating nuclear new build in Finland, France and the UK. *Energy Policy* 39(6):3434-3442.
- Wong, H.Y. 1977. *Handbook of essential formulae and data on heat transfer for engineers*. New York, Longman.
- Wright, J.W.K, Wright, R.N. & Petti, D.A. 2010. Next Generation Nuclear Plant Steam Generator and Intermediate Heat Exchanger Materials Research and Development Plan. PLN-2804. Idaho National Laboratory.
- Zeng, Y., Shi, L. & Dong, Y. 2009. Thermohydraulic transient studies of the Chinese 200MWe HTR-PM for loss of forced cooling accidents. *Annals of Nuclear Energy* 36:742-751.
- Zhang, Z., Wu, Z., Wang, D., Xu., Y., Sun, Y., Li, F. & Dong, Y. 2009. Current status and technical description of Chinese 2x250 MWt HTR-PM demonstration plant. *Nuclear Engineering and design* 239:1212-1219.

APPENDIX A: STEADY-STATE CALCULATION OF THE HTMR

In the following sections calculations of the heat balances will be presented using the operating conditions provided in Table 4.1.

A.1 HELICAL COIL STEAM GENERATOR

In Chapter 5, simulation results of the HTMR are provided and compared to the corresponding HTR-PM results for validation in Chapter 6. As shown in Chapter 4, the once-through steam generator model is revealed to be quite complex due to the interconnection between thermodynamic properties of water for steam generation. For this reason, it was found necessary to use a relatively simple approach to provide a guideline for the modelling and simulation of this system assuming a full power steady-state operation.

A.1.1 Once-through helical coil steam generator design specifications

The helical coil steam generator used with the HTMR was designed based on NGNP values of RELAP5-3D specifications (Hoffer, et al., 2011). Assuming a steam generator with the same pipe length as specified in Table A.1 below and selecting the pipe diameter from Table A.2, the physical sizes and design characteristics of the HTMR steam generator were calculated for its specified thermal power.

TableA.1 NGNP design characteristics (Hoffer, et al., 2011)

Parameter	Given NGNP value *	Calculated value	RELAP5-3D value *
Heat load, MW _{th}	600	-	-
Primary inlet temperature, °C	750	-	757.37
Primary outlet temperature, °C	322	322	333.35
Primary mass flow rate, kg/s	250	270.17	270.17
Primary inlet pressure, MPa	7.0	-	7.22
Primary outlet pressure, MPa	6.976	-	6.982
Secondary inlet temperature, °C	200	-	205.35
Secondary outlet temperature, °C	540	540.04	540.54
Secondary mass flow rate, kg/s	216	245.31	232.0
Secondary inlet pressure, MPa	18.2	-	17.516
Secondary outlet pressure, MPa	17.2	-	17.203
Number of tubes	411	-	-
Single tube heated length, m	-	144	144
Heat transfer surface area, m ²	-	5022.51	5022.51
LMTD, °C	-	162.04	-
Overall heat transfer coefficient, J/m ² °C	-	737.25	-

* Hoffer *et al.* (2011)

Table A.2 NGNP operating conditions used to compute the overall heat transfer coefficient for the steam generator (Hoffer, et al., 2011)

Parameter	Symbol	Unit	Value
Heat load	\dot{Q}_{NGNP}	MW _{th}	600
Number of tubes	n_{NGNP}	-	441
Tube outer diameter	d	m	0.0318
Assumed single heated tube length	l_{NGNP}	m	144
Primary inlet temperature	$T_{\text{pin NGNP}}$	°C	750
Primary outlet temperature	$T_{\text{pout NGNP}}$	°C	322
Secondary inlet temperature	$T_{\text{sin NGNP}}$	°C	200
Secondary outlet temperature	$T_{\text{sout NGNP}}$	°C	540

A.1.2 Overall heat transfer coefficient of the HTMR (Steady state)

The number of pipes for the HTMR is obtained by assuming the same proportionality between the HTMR power and the NGNP power

$$n_p = \frac{n_{\text{NGNP}} \times \dot{Q}_{\text{HTMR}}}{\dot{Q}_{\text{NGNP}}} = \frac{441 \times 250}{600} = 184 \text{ pipes}$$

Combining equations 3.25, 3.26, 3.27 and 3.28, equation 3.29 is used to find the overall heat transfer coefficient of the steam generator. To do that, the heat transfer area A and the mean log temperature difference need to be evaluated in the following way.

The heat transfer area A is given by

$$A = n d \pi l = 184 \times 0.0318 \times \pi \times 144 = 2645.679 \text{ m}^2 \quad (\text{A.1})$$

while the HTMR mean log temperature difference for steady state regime can be approximated from using values of table 4.1 and equation 3.30 repeated as A.2 is given by

$$\Delta T_{\text{LMTD}} = \frac{(T_{\text{pin}} - T_{\text{sout}}) - (T_{\text{p1}} - T_{\text{s1}})}{\ln\left(\frac{T_{\text{pin}} - T_{\text{sout}}}{T_{\text{p1}} - T_{\text{s1}}}\right)} = \frac{(750 - 540) - (250 - 205)}{\ln\left(\frac{750 - 540}{250 - 205}\right)} = 107.11 \text{ }^\circ\text{C} \quad (\text{A.2})$$

The heat transfer rate can be found by

$$\dot{Q} = \dot{m} c_p (T_{\text{pin}} - T_{\text{pout}}) = 97.5 \times 5195 \times (750 - 250) = 253.256 \text{ MWth} \quad (\text{A.3})$$

where c_p , the specific heat of helium is 5195 J/kg K and the mass flow rate is found in table 6.1.

The overall heat transfer coefficient is now given by

$$U = \frac{\dot{Q}}{A \Delta T_{LMTD}} = \frac{253.256 \times 10^6}{2645.679 \times 107.11} = 893.7 \text{ W/m}^2\text{°C} \quad (\text{A.4})$$

The steam generator was divided in three sections. These sections were treated separately and the heat transfer equations of Chapter 3 where applied to the economiser, the evaporator and the superheater in turn. Figure A.1 (Figure 4.6 repeated) provides a schematic representation of a once-through steam generator.

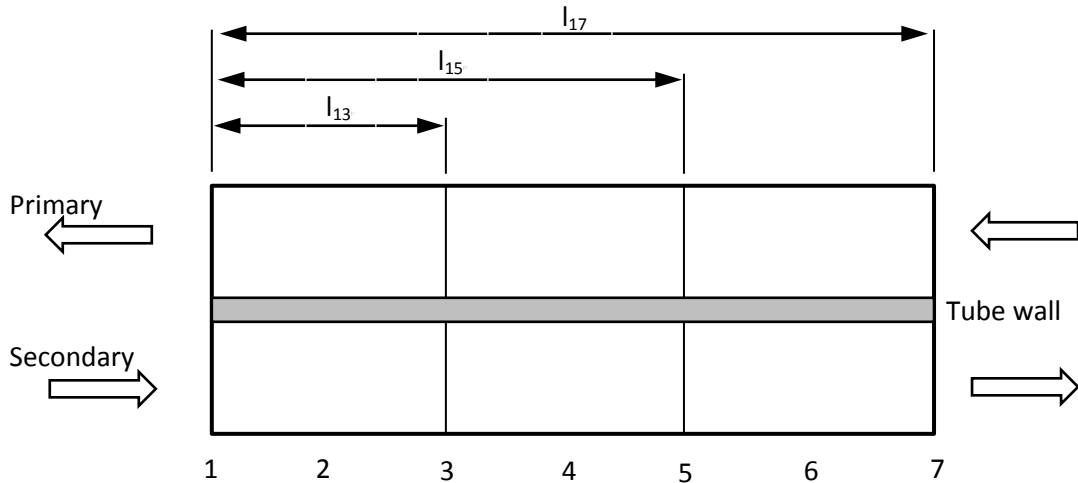


Figure A.1 Schematic model of a once-through steam generator

A.1.3 Superheater, economiser and evaporator lengths

a. Superheater

To evaluate the superheater pipe length equation A.5 (equation 3.51 repeated) was applied to the superheater. In equation A.5, \dot{m}_s , Δh , ΔT_{LMTD} and U are the steam mass flow rate, the change in enthalpy, the log mean temperature difference and the overall heat transfer coefficient respectively.

$$l = \dot{m}_s \frac{\Delta h}{\pi d U \Delta T_{LMTD}} \quad (\text{A.5})$$

To find the length of the superheater, the following assumptions were made:

- The required amount of heat to bring 97.5 kg/s of steam at about 13.5 MPa from the vapour saturation state to the desired outlet temperature will be used as heat rate, and this heat rate is obtained by multiplying the steam mass flow rate by the change in enthalpy between the vapour saturation state and the outlet temperature at the required pressure.

- The velocity of the primary fluid (helium) is assumed to be more-or-less constant throughout the steam generator and was given a reasonable velocity value of 17 m/s. Thus the coolant gas becomes the dominant parameter during the heat transfer process.

Superheater overall heat transfer coefficient U_{5-7}

Referring to Figure A.1, the superheater would be the section from points 5 to 7. The overall heat transfer coefficient is described by equation 3.44. Equation 3.44 applied to the superheater can also be simplified by multiplying both sides of the equation by the superheater length l_{5-7} and writing the overall heat transfer coefficient U_{5-7} as the subject of the formula, yielding the following:

$$U_{5-7} = \frac{h_h h_{s\ 5-7}}{h_{s\ 5-7} + h_h} \quad (\text{A.6})$$

To determine U_{5-7} in equation A.6, the steam heat transfer coefficient $h_{s\ 5-7}$ and the helium heat transfer coefficients were determined separately.

The heat transfer coefficient on the helium side can be determined using equation A.7 (equation 3.45 repeated) applied to the gas.

$$h_h = \frac{Nu_h k_h}{d} \quad (\text{A.7})$$

In equation A.7, the Nusselt number is obtained from equation A.8.

$$Nu_h = C_h Re_h^m \quad (\text{A.8a})$$

where Re_h is given by equation A.8b below:

$$Re_h = \frac{\rho_h v_h d}{\mu_h} = \frac{4.2 \times 17 \times 0.0318}{37.8 \times 10^{-6}} = 60\ 066.67 \quad (\text{A.8b})$$

Values for constant C_h and m for circular pipes are found in Table A.3 (Wong, 1977). Using A.8b, the Reynolds number Re_h was evaluated as 60 067. Constants C_h and m are selected depending on the Reynolds number range, which in this case gives to C_h and m as 0.0208 and 0.471 respectively.

Table A.3 Forced convective heat transfer for gas flow to cylinders (Wong, 1977)

Range of Re_h	C_h	m	Characteristic length
$10^{-4} - 4 \times 10^{-3}$	0.437	0.0895	d
$4 \times 10^{-3} - 9 \times 10^{-2}$	0.565	0.136	d
$9 \times 10^{-2} - 1$	0.800	0.280	d
1 – 35	0.795	0.384	d
35 – 5×10^3	0.583	0.471	d
$5 \times 10^3 - 5 \times 10^4$	0.148	0.633	d
$5 \times 10^4 - 5 \times 10^5$	0.0208	0.814	d

The calculated Reynolds number Re_h , C_h and m are used in equation A.8a to determine the helium Nusselt number Nu_h and thus the heat transfer coefficient can also be calculated.

$$Nu_h = 0.0208 \times 60066.67^{0.814} = 161.4$$

Combining equations A.7, A.8a and A.8b the helium heat transfer coefficient can be expressed by

$$h_h = C_h \frac{k_h}{d} \left(\frac{\rho_h d}{\mu_h} \right)^m v_h^m = 0.0208 \times \frac{0.273}{0.0318} \left(\frac{4.2 \times 0.0318}{37.8 \times 10^{-6}} \right)^{0.814} 17^{0.814}$$

$$= 1385.5 \text{ W/m}^2\text{C} \quad (\text{A.9})$$

At low mass flow rate and 20% load operation, the heat transfer coefficient can also be found using equation A.9. In equation A.9 the constants C_h and m are defined by the 20% load corresponding Reynolds number range calculated by equation A.8b.

$$Re_{h@20\%} = \frac{\rho_h v_{h@20\%} d}{\mu_h} = \frac{4.2 \times (17/5) \times 0.0318}{37.8 \times 10^{-6}} = 12\,013.33$$

Since the Re_h value is between 5×10^3 and 5×10^4 , C_h and m are 0.148 and 0.633 respectively. Therefore the heat transfer coefficient of the primary stream at 20% load operation can be calculated as:

$$h_{h@20\%} = C_h \frac{k_h}{d} \left(\frac{\rho_h d}{\mu_h} \right)^m v_{h@20\%}^m = 0.0208 \times \frac{0.273}{0.0318} \left(\frac{4.2 \times 0.0318}{37.8 \times 10^{-6}} \right)^{0.814} (17/5)^{0.814}$$

$$= 556.94 \text{ W/m}^2\text{C}$$

In equation A.9, v_h represents helium velocity in the steam generator, which is dependent on the mass flow rate. Therefore, the heat transfer coefficient of the primary

stream is reduced by about 60% when operating at 20% load. It can also be seen in equation A.9 that the heat transfer coefficient is directly linked to the velocity of the fluid. Helium heat conductivity, viscosity, Prandtl number, specific heat at constant pressure and density are approximated using values given in Table A.4.

Table A.4 Helium thermal properties at 0.1 MPa (Mills, 1995)

Temperature K	Heat conductivity W/m K	Density kg/m ³	Specific heat at constant pressure J/kg K	Dynamic viscosity kg/m s	Prandtl number
50	0.046	0.974	5200	6.46 x 10 ⁻⁶	0.73
100	0.072	0.487	5200	9.94 x 10 ⁻⁶	0.72
150	0.096	0.325	5200	13.0 x 10 ⁻⁶	0.70
200	0.116	0.244	5200	15.6 x 10 ⁻⁶	0.70
250	0.133	0.195	5200	17.9 x 10 ⁻⁶	0.70
300	0.149	0.1624	5200	20.1 x 10 ⁻⁶	0.70
400	0.178	0.1218	5200	24.4 x 10 ⁻⁶	0.71
500	0.205	0.0974	5200	28.2 x 10 ⁻⁶	0.72
600	0.229	0.0812	5200	31.7 x 10 ⁻⁶	0.72
800	0.273	0.0609	5200	37.8 x 10 ⁻⁶	0.72
1000	0.313	0.0487	5200	43.3 x 10 ⁻⁶	0.72

Steam heat transfer coefficient in the superheater is calculated using equation A.7 applied to the secondary stream of the superheater. In equation A.7, the steam Nusselt number (Nu) is given by equation 3.46 of repeated as equation A.10a. In equation A.10a, the steam Reynolds number Re_s , calculated in equation A.10c, is obtained using equation A.8b applied to the secondary stream of the superheater. The constants C, m and n are provided in Table 3.5 repeated as Table A.5. The velocity of the steam is calculated using equation A.10b and the Prandtl number using equation A.10c. Combining A.7, A.8b, A.10a, A.10b and A.10c, the heat transfer can be written as a function of the mass flow rate in equation A.10:

$$Nu_s = C Re_s^m Pr_s^n K \quad (A.10a)$$

$$v = \frac{4 \dot{m}}{\rho \pi d^2} \quad (A.10b)$$

$$Re_s = \frac{\rho_s v_s d}{\mu_s} \quad \text{and} \quad Pr_s = \frac{\mu_s c_{ps}}{k_s} \quad (A.10c)$$

$$\begin{aligned}
 h_{s\ 5-7} &= C K Pr_{s\ 6}^n \frac{k_{s\ 6}}{d} \left(\frac{4}{\pi d \mu_{s\ 6}} \right)^m \left(\frac{\dot{m}_s}{n_p} \right)^m \\
 &= 0.023 \times 1 \times \left(\frac{0.0926}{0.0318} \right) \times \left(\frac{4}{3.14 \times 0.0318 \times 2.6412 \times 10^{-5}} \right)^{0.8} \times \left(\frac{2.6412 \times 0.066}{0.0926} \right)^{0.4}
 \end{aligned}$$

$$x \left(\frac{97.5}{184} \right)^{0.8} = 4571.29 \text{ W/m}^2\text{°C} \quad (\text{A.10})$$

$Pr_{s,6}$ is calculated by applying equation A.10c to the superheater. The Prandtl number is calculated using average value $k_{s,6}$, $c_{ps,6}$ and $\mu_{s,6}$ calculated from data provided in Table A.5. $k_{s,6}$ is the average value between k_5 and k_7 , $c_{ps,6}$ is the average between c_{p5} and c_{p7} , and $\mu_{s,6}$ is the average value between μ_5 and μ_7 . Calculations in equation A.10 have shown that the steam heat transfer coefficient in the superheater is about 4571.29 $\text{W/m}^2\text{°C}$. Equation A.6 is then used to determine the superheater overall heat transfer coefficient U_{5-7} :

$$U_{5-7} = \frac{h_h h_{s,5-7}}{h_{s,5-7} + h_h} = \frac{1385.5 \times 4571.29}{4571.29 + 1385.5} = 1063.24 \text{ W/m}^2\text{°C}$$

The superheater overall heat transfer coefficient U_{5-7} is 1063.24 $\text{W/m}^2\text{°C}$, which is of the range helium heat transfer coefficient. This form as given in equation A.10 gives more flexibility for control process by varying the mass flow rate of helium in order to characterise the heat transfer process.

Table A.5 Nusselt number constants in equation A.10a as a function of Reynolds number for circular tube cross-section (Wong, 1977)

Operating conditions	C	m	n	K
Laminar flow short tube, Re < 2000, Gz > 10	1.86	$\frac{1}{3}$	$\frac{1}{3}$	$\left(\frac{d}{l}\right)^{\frac{1}{3}} \left(\frac{\mu}{\mu_w}\right)^{0.14}$
Laminar flow long tube, Re < 2000, Gz < 10	3.66	0	0	1
Turbulent flow of gases Re > 2000	0.023	0.8	0.4	1
Turbulent flow of highly viscous liquids, 0.6 < Pr < 100	0.027	0.8	0.33	$\left(\frac{\mu}{\mu_w}\right)^{0.14}$

Superheater log mean temperature difference $\Delta T_{LMTD\ 5-7}$

The log mean temperature difference across the superheater is obtained by applying equation 3.30 repeated as A.11 to the superheater as presented in Figure A.1. In equation A.11, T_{p5} was approximated from the energy balance equation across the superheater and T_{s5} can be read from Table A.6.

$$\Delta T_{\text{LMTD } 5-7} = \frac{(T_{p7} - T_{s7}) - (T_{p5} - T_{s5})}{\ln\left(\frac{T_{p7} - T_{s7}}{T_{p5} - T_{s5}}\right)} = \frac{(750 - 540) - (588 - 333.8)}{\ln\left(\frac{750 - 540}{588 - 333.8}\right)} = 231.7 \text{ } ^\circ\text{C} \quad (\text{A.11})$$

Superheater length l_{5-7}

The superheater length, measured as a single pipe length, is obtained using the pipe diameter specified in Table A.2, the superheater overall heat transfer coefficient and the log mean temperature difference in equation A.5 applied to the superheater.

$$l_{5-7} = \dot{m}_s \frac{\Delta h_{5-7}}{\pi d U_{5-7} \Delta T_{\text{LMTD } 5-7}} \quad (\text{A.12})$$

where the superheater change in steam enthalpy is given by the equation below (h_7 , h_5 read from Table A.6):

$$\Delta h_{5-7} = h_7 - h_5 = 3439.6 - 2650.8 = 842.8 \text{ kJ/kg} \quad (\text{A.13})$$

$$l_{5-7} = (97.5) \frac{842.8 \times 1000}{184 \times \pi \times 0.0318 \times 1063.24 \times 231.7} = 17.1 \text{ m}$$

Table A.6 Feedwater/Steam approximated thermodynamic proprieties of the helical coil steam generator using XSteam/Matlab

Parameter	Unit	Symbol	XSteam input parameters	Value
Temperature, T	°C	T_1	-	205
		T_3	P_3	339.5
		T_5	P_5	333.8
		T_7	-	540
Pressure, P	Bar	P_1	-	145
		P_3	-	145
		P_5	-	135
		P_7	-	135
Density, ρ	kg/m ³	ρ_1	T_1, P_1	867.73
		ρ_3	P_3	629.86
		ρ_5	P_5	82.53
		ρ_7	T_7, P_7	39.48
Specific heat at constant pressure, c_p	kJ/kg°C	c_{p1}	T_1, P_1	4.4519
		c_{p3}	P_3	7.5185
		c_{p5}	P_5	10.5445
		c_{p7}	T_7, P_7	2.6676
Thermal conductivity, k	W/m°C	k_1	T_1, P_1	0.6704
		k_3	P_3	0.4761
		k_5	P_5	0.1020
		k_7	T_7, P_7	0.0832
Viscosity, μ	Pa.s	μ_1	T_1, P_1	1.3378×10^{-4}
		μ_3	T_3-1, P_3	7.3535×10^{-5}
		μ_5	T_5+1, P_5	2.1967×10^{-5}
		μ_7	T_7, P_7	3.0857×10^{-5}
Specific enthalpy, h	kJ/kg	h_1	T_1, P_1	879.65
		h_3	P_3	1590.5
		h_5	P_5	2650.8
		h_7	T_7, P_7	3439.6

b. Economiser

The economiser length is determined using the same procedure used for the superheater except that the secondary stream in this case is the feedwater, which is thermodynamically described as compressed liquid water.

The economiser heat transfer coefficient is obtained by applying equation A.63 to the economiser represented by 1 to 3 in Figure A.1. The economiser overall heat transfer coefficient can be calculated using equation A.14; in this equation the velocity of the primary stream (helium) is assumed to be constant. The primary stream heat transfer coefficient is now calculated using the average temperature across the steam generator.

$$U_{1-3} = \frac{h_h h_{s1-3}}{h_{s1-3} + h_h} \quad (\text{A.14})$$

The value of h_{s1-3} in equation A.14 is calculated by equation A.15 given below. In equation A.15, the thermal properties of the water k_2 , c_{p2} and μ_2 are calculated using the average value between the economiser feedwater thermal properties k_1 , c_{p1} and μ_1 and the saturation state thermal properties k_3 , c_{p3} and μ_3 . To determine these values, the secondary stream inlet pressure of the steam generator was given a first guess value. This pressure was estimated assuming a pressure drop across the steam generator of about 1 MPa and this is based on a similar once-through steam generator estimated pressure drop (Hoffer, et al., 2011). This allowed one to guess the inlet pressure P_1 , the pressure at the end of the economiser P_3 and the pressure at the beginning of the superheater P_5 .

$$\begin{aligned} h_{s1-3} &= C K Pr_{s2}^n \frac{k_{s2}}{d} \left(\frac{4}{\pi d \mu_{s2}} \right)^m \left(\frac{\dot{m}_s}{n_p} \right)^m \\ &= 0.023 \times 1 \times \left(\frac{0.5733}{0.0318} \right) \times \left(\frac{4}{3.14 \times 0.0318 \times 1.037 \times 10^{-4}} \right)^{0.8} \times \left(\frac{1.037 \times 0.066}{0.5733} \right)^{0.4} \\ &\quad \times \left(\frac{97.5}{184} \right)^{0.8} = 7592.96 \text{ W/m}^2\text{C} \end{aligned} \quad (\text{A.15})$$

Considering 14.5 MPa as the guessed operating pressure value P_1 , the saturation temperature T_3 could be calculated and is given in Table A.5. The values of Pr_2 , k_2 , c_{p2} and μ_2 were then calculated since states 1 and 3 (see Figure A.1) are fully defined at this stage. This allowed the secondary heat transfer coefficient across the economiser h_{s1-3} to be calculated as being about 7592.96 W/m²C.

Substitution of h_{s1-3} and h_h values in equation A.14 gives

$$U_{1-3} = \frac{7592.96 \times 1385.5}{7592.96 + 1385.5} = 1171.7 \text{ W/m}^2\text{C}$$

The energy balance across the economiser shows the amount of heat required for heating 97.5 kg/s of feedwater, from 205°C at a guessed value of pressure of 14.5 MPa (Hoffer, et al., 2011) to a saturation state T_3 , as given in Table A.6. The change in enthalpy between the enthalpy of the feedwater at the economiser inlet h_1 and the enthalpy of the water at the end of the economiser h_3 represents the amount of heat required to bring one kilogram of feedwater to liquid saturation state. The enthalpies h_1 and h_3 are provided in Table A.6.

$$\dot{Q}_{1-3} = \dot{m}_s \Delta h_{1-3} = \dot{m}_s (h_3 - h_1) \quad (\text{A.16})$$

To determine the log mean temperature across the economiser, the primary inlet temperature to the economiser needs to be determined first. Since \dot{Q}_{1-3} is provided by helium, and the primary flow rate is known, the primary stream outlet enthalpy h_{p1} was evaluated as a function of temperature and its average operating pressure P_h by applying equation 3.22 to the primary stream outlet conditions. This enthalpy is calculated by equation A.17.

$$h_{p1}(p,T) = -129.8490 + 5.1944 T_{p1} + 0.0000 T_{p1}^2 + 3.2846 P_h - 0.0030 P_h^2 - 0.0017 P_h T_{p1} + 0.0000 T_{p1}^2 P_h + 0.0001 T_{p1} P_h^2 + 0.0000 P_h^2 T_{p1}^2 \quad (\text{A.17})$$

The primary inlet enthalpy to the economiser is obtained using the following:

$$h_{p3} = h_{p1} + \dot{Q}_{1-3} \quad (\text{A.18})$$

Thus the temperature T_{p3} could be calculated from equation 3.23 where T_{p3} is a function of h_{p3} and helium operating pressure P is given in Table 4.1. This temperature was evaluated to about 386 °C using equation 3.23 applied to the relevant position of the steam generator described by equation A.19 below.

$$T_{p3}(p,h) = 24.9981 - 0.6247 P_h + 0.0002 P_h^2 + 0.1925 h_{p3} - 0.0000 h_{p3}^2 - 0.0001 P_h h_{p3} + 0.0000 P_h^2 h_{p3} + 0.0000 P_h h_{p3}^2 + 0.0000 P_h^2 h_{p3}^2 \quad (\text{A.19})$$

The log mean temperature difference across the economiser is obtained by equation A.20

$$\Delta T_{m1-3} = \frac{(T_{p3} - T_{s3}) - (T_{p1} - T_{s1})}{\ln\left(\frac{T_{p3} - T_{s3}}{T_{p1} - T_{s1}}\right)} = \frac{(386 - 339.5) - (250 - 205)}{\ln\left(\frac{386 - 339.5}{250 - 205}\right)} = 48.5 \text{ °C} \quad (\text{A.20})$$

$$l_{1-3} = \dot{m}_s \frac{\Delta h_{1-3}}{\pi d U_{1-3} \Delta T_{m1-3}} \quad (\text{A.21})$$

where the economiser change in steam enthalpy is given by the equation A.22 (h_3, h_1 read from Table A.6):

$$\Delta h_{1-3} = h_3 - h_1 = 1590.5 - 879.65 = 710.85 \text{ kJ/kg} \quad (\text{A.22})$$

$$l_{1-3} = (97.5) \times \frac{710.85 \times 1000}{184 \times \pi \times 0.0318 \times 1171.7 \times 48.5} = 66.4 \text{ m}$$

c. Evaporator

The evaporator length is determined using the same approach as for the superheater and the economiser. The only difference is that the secondary stream in this case is assumed to be a homogenous mixture of steam and water. The thermodynamic properties of the fluid in this part of the steam generator are the averages between the saturation liquid state and the vapour saturation state.

The evaporator overall heat transfer coefficient U_{3-5} is obtained by applying equation A.6 to the evaporator represented by 3 to 5 in Figure A.1. The evaporator overall heat transfer coefficient is now calculated equation A.23

$$U_{3-5} = \frac{h_h h_{s\ 3-5}}{h_{s\ 3-5} + h_h} \quad (\text{A.23})$$

In equation A.23, $h_{s\ 3-5}$ is calculated by using equation A.24. The thermal properties of the homogenous mixture k_4 , c_{p4} and μ_4 are calculated using the average value between the liquid saturation state (economiser's end) thermal properties k_3 , c_{p3} and μ_3 and the vapour saturation state thermal properties k_5 , c_{p5} and μ_5 (superheater inlet conditions).

$$\begin{aligned} h_{s\ 3-5} &= C K Pr_{s\ 4}^n \frac{k_{s\ 4}}{d} \left(\frac{4}{\pi d \mu_{s\ 4}} \right)^m \left(\frac{\dot{m}_s}{n_p} \right)^m \\ &= 0.023 \times 1 \times \left(\frac{0.2891}{0.0318} \right) \times \left(\frac{4}{3.14 \times 0.0318 \times 4.7751 \times 10^{-5}} \right)^{0.8} \times \left(\frac{4.7751 \times 0.066}{0.2891} \right)^{0.4} \\ &\quad \times \left(\frac{97.5}{184} \right)^{0.8} = 10\ 236.98 \text{ W/m}^2\text{°C} \end{aligned} \quad (\text{A.24})$$

To determine the values in equation A.24, it was assumed that the entire pressure drop occurred during the phase change process. That is, the inlet pressure to the evaporator was assumed to be 14.5 MPa while the outlet pressure was assumed to be 13.5 MPa. These were recalculated to obtain better accuracy.

The thermodynamic properties of the homogenous mixture Pr_4 , k_4 , Cp_4 and μ_4 could now be calculated since states 3 and 5 are fully defined. This allowed determining the secondary heat transfer coefficient across the evaporator $h_{s\ 3-5}$ to about 10 236.98 W/m²°C.

Substitution of $h_{s\ 1-3}$ and h_h values in equation A.23 gives the following:

$$U_{3-5} = \frac{10236.976 \times 1385.5}{10236.976 + 1385.5} = 1\ 220.34 \text{ W/m}^2\text{°C}$$

The energy balance across the economiser shows that the amount of heat \dot{Q}_{3-5} required to evaporate 97.5 kg/s of water at 14.5 MPa is given by the change in enthalpy between the saturation states 3 and 5 as given in Table A.6

$$\dot{Q}_{3-5} = \dot{m}_s \Delta h_{3-5} = \dot{m}_s (h_5 - h_3) \quad (\text{A.25})$$

To determine the log mean temperature across the evaporator, the primary inlet temperatures to the superheater and outlet from the economiser are used together with those of the secondary stream. Therefore, the log mean temperature difference across the economiser is obtained by equation A.26.

$$\Delta T_{m\ 3-5} = \frac{(T_{p5} - T_{s5}) - (T_{p3} - T_{s3})}{\ln\left(\frac{T_{p5} - T_{s5}}{T_{p5} - T_{s3}}\right)} = \frac{(588 - 333.8) - (386 - 339.5)}{\ln\left(\frac{588 - 333.8}{386 - 339.5}\right)} = 122.3 \text{ }^\circ\text{C} \quad (\text{A.26})$$

The length of the evaporator is given by

$$l_{3-5} = \dot{m}_s \frac{\Delta h_{3-5}}{n \pi d U_{3-5} \Delta T_{m3-5}} \quad (\text{A.27})$$

where the economiser change in steam enthalpy is given by equation A.28 (h_3 , h_1 read from Table A.6).

$$\Delta h_{3-5} = h_5 - h_3 = 2650.8 - 1590.5 = 1\ 099.6 \text{ kJ/kg} \quad (\text{A.28})$$

$$l_{3-5} = (97.5) \frac{1099.6 \times 1000}{184 \times \pi \times 0.0318 \times 1220.34 \times 122.3} = 39.1 \text{ m}$$

Table A.7 Comparison between steady-state calculated values and simulated value of the steam generator

Parameter or symbol	Unit	Ideal value	Calculated or estimated value	Simulated value
T_{p7}	°C	750	-	764.4
T_{s7}	°C	540	-	534.3
T_{p5}	°C	-	588	614.8
T_{s5}	°C	-	333.8	333.8
T_{p3}	°C	-	386	409.7
T_{s3}	°C	-	339.5	339.5
T_{p1}	°C	250	-	272.2
T_{s1}	°C	205	205	205
U_{1-3}	W/m ² °C	-	1171.7	1217
U_{3-5}	W/m ² °C	-	1220.3	1203
U_{5-7}	W/m ² °C	-	1063.24	1092
$\Delta T_{m 1-3}$	°C	-	48.5	68.72
$\Delta T_{m 3-5}$	°C	-	122.3	152
$\Delta T_{m 5-7}$	°C	-	231.7	
l_{1-3}	m	-	66.4	45.3
l_{3-5}	m	-	39.1	30.9
l_{5-7}	m	-	17.1 (38.5)*	67.8

*The value (38.5) represents the part of pipe length left for the superheater after the economiser and evaporator.

Discrepancies are found in Table A.7 between the calculated and simulated results. These discrepancies are due to two main reasons. Firstly, the simulated outlet temperature is higher than the theoretical value by about 2%, introducing an initial deviation; secondly, the assumption of using the primary average temperature across the steam generator to determine the primary heat transfer coefficient introduces another inaccuracy adding to the main temperature deviation. For example, across the superheater, the average temperature calculated from ideal values should be 670 °C, 487 °C in the evaporator and 318 °C across the economiser instead of 500 °C used in the calculations as averaged value.

The initial deviation adds to slight error introduced by the primary heat transfer coefficient variation. The final error builds up to generate a final 20°C on the economiser log mean temperature difference which considerably impacts the estimation of the required pipe's length. The superheater length was determined in two ways. The first assumes the estimation of the required length. This value is calculated using the properties of the heat transfer process. The value in brackets represents the superheater length that is obtained by subtracting the evaporator and economiser lengths from the total pipe length.

A.2 Heat pipe heat exchanger

The heat pipe heat exchanger simulation results were also presented in Chapter 5. In this section, a guideline for steady-state calculations of main characteristics is provided. For these calculations, a full power operation is assumed.

A.2.1 Heat pipe design specifications

The heat pipe heat exchanger used for the HTMR is intended to provide superheated steam for a heat process that requires steam for coal conversion to liquid fuel (CTL). The steam thermodynamic conditions required for the CTL process are specified in Table A.9. The overall HTMR heat process is designed for $4 \times 60 \text{ MW}_{\text{th}}$. The calculations are based on a single heat pipe heat exchanger provided that similar results are expected for the last three since all four are identical. Other design characteristic can be found in Table A.9.

A.2.2 Heat pipe overall heat transfer coefficient

The heat pipe heat exchanger uses sodium as intermediate fluid for steam generation. Helium from the nuclear reactor flows inside primary stream pipes that go through the heat pipe. The high-temperature helium transfers heat to the liquid sodium. Sodium evaporates, the secondary stream pipes, in which flows the feedwater, pass through the heat pipe, sodium vapour condenses on the secondary stream pipes transferring heat to the feedwater, generating superheated steam.

Referring to Figure A.2, the heat pipe heat exchanger was approached from two perspectives. The boiling and condensation processes are analysed separately in this approach. The overall heat transfer coefficient of boiling and condensation are evaluated in the next sections.

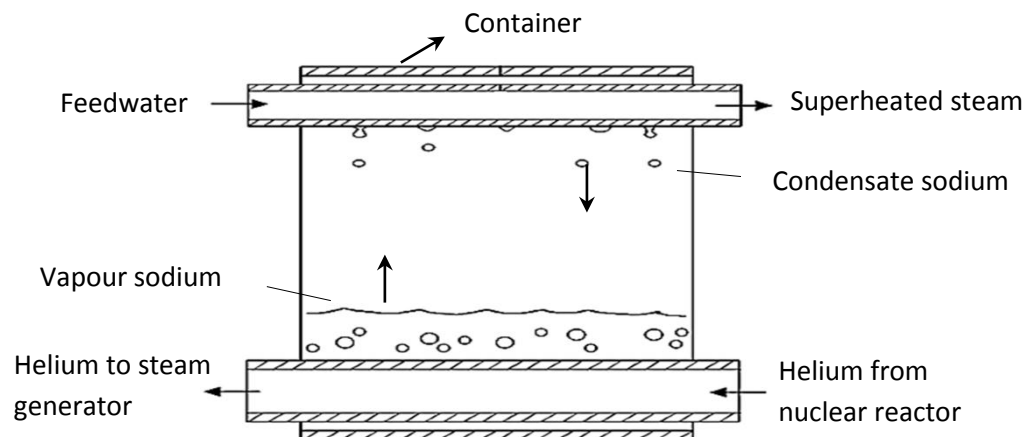


Figure A.2 Concept drawing of a heat pipe heat exchanger for steam generation layout (Dobson, et al., 2013)

a. Boiling heat transfer coefficient

The overall heat transfer coefficient can be obtained using equation A.29 applied to the sodium boiling process in the heat pipe heat exchanger. The average temperature between the inlet and the outlet of the primary stream to heat pipe heat exchanger is used to approximate the properties of helium for the steady-state calculation.

$$U_b = \frac{h_h h_b}{h_b + h_h} \quad (\text{A.29})$$

The heat transfer coefficient within the primary stream can be obtained using equation A.30, where helium properties are approximated using values from Table A.4, constants C, K, m and n are taken from Table A.5, and Table A.9 provides d_h and n_{hHP} .

$$\begin{aligned} h_h &= C K Pr_h^n \frac{k_h}{d_h} \left(\frac{4}{\pi d_h \mu_h} \right)^m \left(\frac{\dot{m}_h}{n_{hHP}} \right)^m \\ &= 0.023 \times 1 \times \left(\frac{0.313}{0.2} \right) \times \left(\frac{4}{3.14 \times 0.2 \times 43.3 \times 10^{-6}} \right)^{0.8} \times 0.72^{0.4} \times \left(\frac{97.5}{320} \right)^{0.8} \\ &= 166.1 \text{ W/m}^2\text{C} \end{aligned} \quad (\text{A.30})$$

The boiling heat coefficient is given in equation A.31 (Dobson, et al., 2013).

$$h_b = C_b \dot{Q}_b''^{0.7} Pr_b^{m_b} \quad (\text{A.31})$$

In equation A.31, constants $C_b = 13.7$ and $m_b = 0.22$ for $Pr_b < 0.001$, and for $Pr_b > 0.001$, $C_b = 6.9$ and $m_b = 0.12$ (Dobson, et al., 2013). The Prandtl number of the boiling process (Pr_b) is obtained using equation A.32. μ_{Na} , c_{plNa} and k_{lNa} are provided in Table A.8.

$$Pr_b = \frac{\mu_{lNa} c_{plNa}}{k_{lNa}} = \frac{2.018 \times 10^{-4} \times 1.25 \times 10^3}{61.25} = 0.00412 > 0.001 \quad (\text{A.32})$$

Knowing that the boiling heat flux \dot{Q}_b'' can be found using equation A.33, in which the boiling heat transfer area A_b is given by equation A.34, the boiling heat transfer coefficient can be determined using equation A.31.

$$\dot{Q}_b'' = \frac{\dot{Q}_{HP}}{A_b} \quad (\text{A.33})$$

$$A_b = n_{hHP} \pi d_h l_{HP} = 320 \times 3.14 \times 0.2 \times 18 = 3617.28 \text{ m}^2 \quad (\text{A.34})$$

The boiling heat transfer coefficient can then be determined:

$$h_b = 6.9 \times \left(\frac{60 \times 10^6}{3 \ 617.28} \right)^{0.7} \times 0.00412^{0.12} = 3209.78 \text{ W/m}^2\text{°C}$$

Thus the boiling overall heat transfer coefficient is calculated using equation A.29 giving the following,

$$U_b = \frac{h_h h_b}{h_b + h_h} = \frac{166.1 \times 3209.78}{166.1 + 3209.78} = 158 \text{ W/m}^2\text{°C}$$

The helium outlet temperature $T_{p \text{ out HP}}$ can also be approximated using the boiling overall heat transfer coefficient, the boiling heat transfer area, the heat pipe theoretical thermal power and the theoretical outlet temperature of the reactor in equation A.35.

$$T_{p \text{ out HP}} = T_{p \text{ out}} - \frac{\dot{Q}_{HP}}{A_b U_b} = 750 - \frac{60 \times 10^6}{3 \ 617.28 \times 158} = 645^\circ\text{C} \quad (\text{A.35})$$

Table A.8 Sodium thermal properties (Reay & Kew, 2006)

Temp. (°C)	Latent heat (kJ/kg)	Density (kg/m ³)		Viscosity (kg/ms)		Thermal conductivity (W/m°C)		Specific heat (kJ/kg°C)
		Liquid	Vapour	Liquid	Vapour	Liquid	Vapour	Vapour
500	4370	828.1	0.003	24×10^{-5}	18×10^{-6}	70.08	0.0343	90.4
600	4243	805.4	0.013	21×10^{-5}	19×10^{-6}	64.62	0.0406	90.4
700	4090	763.5	0.050	19×10^{-5}	20×10^{-6}	60.81	0.0455	90.4
800	3977	757.3	0.143	18×10^{-5}	22×10^{-6}	57.81	0.0492	90.4
900	3913	745.4	0.306	17×10^{-5}	23×10^{-6}	53.35	0.0522	90.4
1000	3827	725.4	0.667	16×10^{-5}	24×10^{-6}	49.08	0.0547	90.4

The thermal conductivity of vapour sodium values are approximated as given by Faghri (1995).

Table A.9 Heat pipe heat exchanger design characteristics and operating conditions

Parameter	Symbol	Unit	Value
Heat load	\dot{Q}_{HP}	MW _{th}	60
Number of tubes primary stream	n_{hHP}	-	320
Number of tubes secondary stream	n_{sHP}	-	15
Tube outer diameter primary	d_h	m	0.2
Tube outer diameter secondary	d_s	m	0.02
Assumed secondary tube length	l_{HP}	m	18
Assumed primary tube length	l_{HP}	m	18
Primary inlet temperature	$T_{pin HP}$	°C	750
Primary outlet temperature	$T_{pout HP}$	°C	650
Secondary inlet temperature	$T_{sin HP}$	°C	205
Secondary outlet temperature	$T_{sout HP}$	°C	430
Intermediate fluid temperature	$T_{sodium HP}$	°C	600

b. Condensation heat transfer coefficient

The overall heat transfer coefficient of condensation can be determined by equation A.36:

$$U_c = \frac{h_{sHP} h_c}{h_c + h_{sHP}} \quad (A.36)$$

In equation A.36, h_{sHP} and h_c are the steam heat transfer coefficient and the heat transfer coefficient of condensation of sodium vapour respectively.

The heat transfer coefficient of condensation can be evaluated using equation A.37 as suggested by Mills (1995).

$$h_c = 0.728 K \left[\frac{\rho_{lNa} (\rho_{lNa} - \rho_{vNa}) g h_{fgNa} k_{lNa}}{n_{sHP} \mu_{lNa} d_s (T_{satNa} - T_{sHP})} \right]^{1/4} \quad (A.37)$$

In equation A.37, K can be determined using equation A.37a. In equation A.37a, x represents for the quality of the sodium vapour. Assuming an average point, the quality x is 50%, therefore, K is calculated as 1.

$$K = \left[1 - \left(\frac{1-x}{x} \right) \left(\frac{\rho_{vNa}}{\rho_{lNa}} \right)^{2/3} \right]^{-3/4} = \left[1 - \left(\frac{1-0.5}{0.5} \right) \left(\frac{\rho_{vNa}}{\rho_{lNa}} \right)^{2/3} \right]^{-3/4} = 1 \quad (A.37a)$$

The steam generation due to condensation of sodium in the heat pipe can also be approached as per Figure A.1. Water is fed to the heat pipe at about 4.3 MPa for steam generation in a once-through process similar to that in a helical coil once-through steam generator.

The condensation heat transfer coefficient in the superheater can be determined using equation A.38. Equation A.38 is equivalent to equation A.37 applied to the superheater. The steam temperature considered in calculating the superheater's condensation heat transfer coefficient is the average temperature between the water vapour saturation temperature $T_{s5 \text{ HP}}$ and the heat pipe steam outlet temperature $T_{s7 \text{ HP}}$. These temperatures can be found in Table A.10

$$\begin{aligned}
 h_{c \text{ 5-7}} &= 0.728 \left[\frac{\rho_{l \text{ Na}} (\rho_{l \text{ Na}} - \rho_{v \text{ Na}}) g h_{fg \text{ Na}} k_{l \text{ Na}}^3}{n_{s \text{ HP}} \mu_{l \text{ Na}} d_s (T_{\text{sat Na}} - T_{s \text{ ave 5-7 HP}})} \right]^{\frac{1}{4}} \\
 &= 0.728 \times \left[\frac{801.8 \times (801.8 - 16.5 \times 10^{-3}) \times 9.81 \times 4 \ 243 \times 10^3 \times 61.25^3}{320 \times 2.018 \times 10^{-4} \times 0.0318 \times (600 - 340.2)} \right]^{\frac{1}{4}} \\
 &= 42 \ 414.9 \ \text{W/m}^2\text{°C}
 \end{aligned} \tag{A.38}$$

Equation A.39 allows the calculation of the evaporator's condensation heat transfer coefficient using the average temperature between the inlet $T_{s3 \text{ HP}}$ and the outlet steam temperature $T_{s5 \text{ HP}}$ to the heat pipe's evaporator provided in Table A.10.

$$\begin{aligned}
 h_{c \text{ 3-5}} &= 0.728 \left[\frac{\rho_{l \text{ Na}} (\rho_{l \text{ Na}} - \rho_{v \text{ Na}}) g h_{fg \text{ Na}} k_{l \text{ Na}}^3}{n_{s \text{ HP}} \mu_{l \text{ Na}} d_s (T_{\text{sat Na}} - T_{s \text{ ave 3-5 HP}})} \right]^{\frac{1}{4}} \\
 &= 0.728 \times \left[\frac{801.8 \times (801.8 - 16.5 \times 10^{-3}) \times 9.81 \times 4 \ 243 \times 10^3 \times 61.25^3}{320 \times 2.018 \times 10^{-4} \times 0.0318 \times (600 - 252.5)} \right]^{\frac{1}{4}} \\
 &= 39 \ 441.6 \ \text{W/m}^2\text{°C}
 \end{aligned} \tag{A.39}$$

A similar procedure is applied to the heat pipe economiser, using the average temperature between the feedwater inlet temperature $T_{s1 \text{ HP}}$ and the liquid saturation state temperature $T_{s3 \text{ HP}}$ provided in Table A.10. Equation A.40 calculated the heat pipe economiser's condensing heat transfer coefficient.

$$\begin{aligned}
 h_{c \text{ 1-3}} &= 0.728 \left[\frac{\rho_{l \text{ Na}} (\rho_{l \text{ Na}} - \rho_{v \text{ Na}}) g h_{fg \text{ Na}} k_{l \text{ Na}}^3}{n_{s \text{ HP}} \mu_{l \text{ Na}} d_s (T_{\text{sat Na}} - T_{s \text{ ave 1-3 HP}})} \right]^{\frac{1}{4}} \\
 &= 0.728 \times \left[\frac{801.8 \times (801.8 - 16.5 \times 10^{-3}) \times 9.81 \times 4 \ 243 \times 10^3 \times 61.25^3}{320 \times 2.018 \times 10^{-4} \times 0.0318 \times (600 - 229.8)} \right]^{\frac{1}{4}} \\
 &= 38 \ 823.4 \ \text{W/m}^2\text{°C}
 \end{aligned} \tag{A.40}$$

Table A.10 Feedwater/steam approximated thermodynamic proprieties of the heat pipe steam generator using XSteam/Matlab

Parameter	Unit	Symbol	XSteam input parameters	Value
Temperature, T	°C	T ₁	-	205
		T ₃	P ₃	254.68
		T ₅	P ₅	250.6
		T ₇	-	430
Pressure, P	Bar	P ₁	-	43
		P ₃	-	43
		P ₅	-	40
		P ₇	-	40
Density, ρ	kg/m ³	ρ ₁	T ₁ , P ₁	860.79
		ρ ₃	P ₃	791.84
		ρ ₅	P ₅	20.09
		ρ ₇	T ₇ , P ₇	12.92
Specific heat at constant pressure, c _p	kJ/kg°C	c _{p1}	T ₁ , P ₁	4.5042
		c _{p3}	P ₃	4.9167
		c _{p5}	P ₅	4.0217
		c _{p7}	T ₇ , P ₇	2.3251
Thermal conductivity, k	W/m°C	k ₁	T ₁ , P ₁	0.6623
		k ₃	P ₃	0.6122
		k ₅	P ₅	0.0513
		k ₇	T ₇ , P ₇	0.0616
Viscosity, μ	Pa.s	μ ₁	T ₁ , P ₁	1.3152 x 10 ⁻⁴
		μ ₃	T ₃ -1, P ₃	1.0447 x 10 ⁻⁴
		μ ₅	T ₅ +1, P ₅	1.7771 x 10 ⁻⁵
		μ ₇	T ₇ , P ₇	2.5674 x 10 ⁻⁵
Specific enthalpy, h	kJ/kg	h ₁	T ₁ , P ₁	875.97
		h ₃	P ₃	1.1086 x 10 ³
		h ₅	P ₅	2.8009 x 10 ³
		h ₇	T ₇ , P ₇	3.2847 x 10 ³

The secondary heat transfer coefficient in the heat pipe economiser can be obtained from equation A.15 adapted and rewrote as equation A.41. Table A.10 gives the water/steam properties across the heat pipe heat exchanger determined using XSteam/Matlab.

$$\begin{aligned}
 h_{s\ 1-3\ HP} &= C K Pr_{s\ 2HP}^n \frac{k_{s\ 2HP}}{d_s} \left(\frac{4}{\pi d \mu_{s\ 2HP}} \right)^m \left(\frac{\dot{m}_{sHP}}{n_{pHP}} \right)^m \\
 &= 0.023 \times 1 \times \left(\frac{0.6373}{0.02} \right) \times \left(\frac{4}{3.14 \times 0.0318 \times 1.18 \times 10^{-4}} \right)^{0.8} \times \left(\frac{1.18 \times 0.47105}{0.6373} \right)^{0.4}
 \end{aligned}$$

$$\times \left(\frac{25}{15}\right)^{0.8} = 40\,228 \text{ W/m}^2\text{°C} \quad (\text{A.41})$$

The feedwater mass flow rate used in equation A.41, steam mass flow rate across the heat pipe, can be found using equation A.42.

$$\dot{m}_{\text{sHP}} = \frac{\dot{Q}_{\text{HP}}}{h_{\text{s7 HP}} - h_{\text{s1 HP}}} = \frac{60 \times 10^6}{(3\,284.7 - 875.97) \times 10^3} = 25 \text{ kg/s} \quad (\text{A.42})$$

Equation A.15 applied to the superheater and the evaporator of the heat pipe gives equations A.43 and A.44 respectively. Equation A.43 calculates the secondary heat transfer coefficient in the heat pipe's superheater while equation A.44 gives the heat pipe evaporator's heat transfer coefficient.

$$\begin{aligned} h_{\text{s 5-7 HP}} &= C K Pr_{\text{s 6HP}}^n \frac{k_{\text{s 6HP}}}{d_s} \left(\frac{4}{\pi d \mu_{\text{s 6HP}}}\right)^m \left(\frac{\dot{m}_{\text{sHP}}}{n_{\text{pHP}}}\right)^m \\ &= 0.023 \times 1 \times \left(\frac{0.0564}{0.02}\right) \times \left(\frac{4}{3.14 \times 0.0318 \times 0.217 \times 10^{-4}}\right)^{0.8} \times \left(\frac{0.217 \times 0.3173}{0.0564}\right)^{0.4} \\ &\quad \times \left(\frac{25}{15}\right)^{0.8} = 15\,785 \text{ W/m}^2\text{°C} \end{aligned} \quad (\text{A.43})$$

$$\begin{aligned} h_{\text{s 3-5 HP}} &= C K Pr_{\text{s 4HP}}^n \frac{k_{\text{s 4HP}}}{d_s} \left(\frac{4}{\pi d \mu_{\text{s 4HP}}}\right)^m \left(\frac{\dot{m}_{\text{sHP}}}{n_{\text{pHP}}}\right)^m \\ &= 0.023 \times 1 \times \left(\frac{0.3317}{0.02}\right) \times \left(\frac{4}{3.14 \times 0.0318 \times 0.611 \times 10^{-4}}\right)^{0.8} \times \left(\frac{0.611 \times 0.44692}{0.3317}\right)^{0.4} \\ &\quad \times \left(\frac{25}{15}\right)^{0.8} = 45\,686 \text{ W/m}^2\text{°C} \end{aligned} \quad (\text{A.44})$$

Thus the overall heat transfer coefficient of condensation across the superheater, the evaporator and the economiser of the heat pipe heat exchanger can be found using equations A.45, A.46 and A.47 respectively.

$$U_{\text{c 5-7}} = \frac{h_{\text{s 5-7HP}} h_{\text{c 5-7}}}{h_{\text{c 5-7}} + h_{\text{sHP 5-7}}} = \frac{15\,785 \times 42\,414.9}{42\,414.9 + 15\,785} = 11\,504 \text{ W/m}^2\text{°C} \quad (\text{A.45})$$

$$U_{\text{c 3-5}} = \frac{h_{\text{s 3-5HP}} h_{\text{c 3-5}}}{h_{\text{c 3-5}} + h_{\text{sHP 3-5}}} = \frac{45\,686 \times 39\,441.6}{39\,441.6 + 45\,686} = 21\,167 \text{ W/m}^2\text{°C} \quad (\text{A.46})$$

$$U_{\text{c 1-3}} = \frac{h_{\text{s 1-3HP}} h_{\text{c 1-3}}}{h_{\text{c 1-3}} + h_{\text{sHP 1-3}}} = \frac{40\,228 \times 38\,823.4}{38\,823.4 + 40\,228} = 19\,757 \text{ W/m}^2\text{°C} \quad (\text{A.47})$$

A.2.3 Heat pipe economiser, evaporator and superheater lengths

The heat pipe heat economiser, evaporator and superheater lengths can be calculated using equations A.48, A.49 and A.50 respectively. These equations are obtained using equation A.5 separately applied to the three sections of the heat pipe. In equations A.48, A.49 and A.50, the log mean temperature differences for the three separate sections are calculated using equation A.51 across the economiser, A.52 across the evaporator and A.53 across the superheater.

$$l_{1-3 \text{ HP}} = \frac{\dot{m}_{\text{sHP}}}{n_{\text{sHP}}} \frac{\Delta h_{\text{s}1-3 \text{ HP}}}{\pi d_s U_{c \text{ 1-3}} \Delta T_{m \text{ 1-3 HP}}} = \frac{25 \times (1108.6 - 875.97) \times 10^3}{15 \times 3.14 \times 0.02 \times 19757 \times 369.6} = 0.85 \text{ m} \quad (\text{A.48})$$

$$l_{3-5 \text{ HP}} = \frac{\dot{m}_{\text{sHP}}}{n_{\text{sHP}}} \frac{\Delta h_{\text{s}3-5 \text{ HP}}}{\pi d_s U_{c \text{ 3-5}} \Delta T_{m \text{ 3-5 HP}}} = \frac{25 \times (2800.9 - 1108.6) \times 10^3}{15 \times 3.14 \times 0.02 \times 21167 \times 347.4} = 6.1 \text{ m} \quad (\text{A.49})$$

$$l_{5-7 \text{ HP}} = \frac{\dot{m}_{\text{sHP}}}{n_{\text{sHP}}} \frac{\Delta h_{\text{s}5-7 \text{ HP}}}{\pi d_s U_{c \text{ 5-7}} \Delta T_{m \text{ 5-7 HP}}} = \frac{25 \times (3284.7 - 2800.9) \times 10^3}{15 \times 3.14 \times 0.02 \times 11504 \times 249.1} = 4.5 \text{ m} \quad (\text{A.50})$$

$$\Delta T_{m \text{ 1-3 HP}} = \frac{(T_{\text{Na}} - T_{\text{s}3\text{HP}}) - (T_{\text{Na}} - T_{\text{s}1\text{HP}})}{\ln\left(\frac{T_{\text{Na}} - T_{\text{s}3\text{HP}}}{T_{\text{Na}} - T_{\text{s}1\text{HP}}}\right)} = \frac{(600 - 254.7) - (600 - 205)}{\ln\left(\frac{600 - 254.7}{600 - 205}\right)} = 369.6 \text{ }^\circ\text{C} \quad (\text{A.51})$$

$$\Delta T_{m \text{ 3-5 HP}} = \frac{(T_{\text{Na}} - T_{\text{s}5\text{HP}}) - (T_{\text{Na}} - T_{\text{s}3\text{HP}})}{\ln\left(\frac{T_{\text{Na}} - T_{\text{s}5\text{HP}}}{T_{\text{Na}} - T_{\text{s}3\text{HP}}}\right)} = \frac{(600 - 250.4) - (600 - 254.7)}{\ln\left(\frac{600 - 250.4}{600 - 254.7}\right)} = 347.4 \text{ }^\circ\text{C} \quad (\text{A.52})$$

$$\Delta T_{m \text{ 5-7 HP}} = \frac{(T_{\text{Na}} - T_{\text{s}7\text{HP}}) - (T_{\text{Na}} - T_{\text{s}5\text{HP}})}{\ln\left(\frac{T_{\text{Na}} - T_{\text{s}7\text{HP}}}{T_{\text{Na}} - T_{\text{s}5\text{HP}}}\right)} = \frac{(600 - 430) - (600 - 250.4)}{\ln\left(\frac{600 - 430}{600 - 250.4}\right)} = 249.1 \text{ }^\circ\text{C} \quad (\text{A.53})$$

Table A.6 Heat pipe heat exchanger steady-state calculated values for steam generation

Parameter or symbol	Unit	Ideal value	Calculated or estimated value
T_{p7}	°C	750	-
T_{s7}	°C	430	-
T_{Na}	°C	600	
T_{s5}	°C	-	250.36
T_{s3}	°C	-	254.68
T_{p1}	°C	650	-
T_{s1}	°C	205	-
U_{c1-3}	W/m ² °C	-	19 757
U_{c3-5}	W/m ² °C	-	21 167
U_{c5-7}	W/m ² °C	-	11 504
U_b	W/m ² °C	-	158
ΔT_{m1-3}	°C	-	369.6
ΔT_{m3-5}	°C	-	347.4
ΔT_{m5-7}	°C	-	249.1
l_{1-3}	m	-	0.85
l_{3-5}	m	-	6.1
l_{5-7}	m	-	4.5 (11.05)*

*The value (11.05) represents the available length for the superheater.

A.3 Nuclear reactor steady-state calculations

The HTMR's design is similar to that the HTR-PM. In the next paragraphs, the reactor's main characteristics are calculated on a full power steady-state operation to highlight the procedure used in the simulation.

a. Reactor power

The reactor is assumed to be initially operating at 20% load. The power is then increased to full power. The increase is operated by increasing the control rods reactivity from an initial value of 0.0053 to 0 within 16 minutes. Since the full power is set to 250 MW, equation A.54 will be used to find the neutrons lifetime l and the reactor period T .

$$P = P_{20} e^{\frac{\rho_{20}}{l} t} = (50 \times 10^6) \times e^{\frac{0.0053}{l} \times 16 \times 60} = 250 \times 10^6 \text{ MW} \quad (\text{A.54})$$

Solving equation A.54 (King, 1964) for the neutron's lifetime, it was found that the neutrons lifetime for this operation is about 3.16 seconds while the reactor period is 596.2 seconds. This period is obtained using equation A.55 below.

$$T = \frac{l}{\rho} = \frac{3.16}{0.0053} = 596.2 \text{ seconds} \quad (\text{A.55})$$

b. Helium outlet temperature

The reactor power is transferred to the coolant gas (helium) which will increase the temperature while flowing through the reactor. The energy balance equation relative to the heat transfer is given in equation A.3 applied to the reactor, yielding equation A.56.

$$\dot{Q} = \dot{m} c_p (T_{\text{pout}} - T_{\text{pin}}) = 97.5 \times 5195 \times (T_{\text{pout}} - 250) = 250 \text{ MWth} \quad (\text{A.56})$$

The outlet temperature is obtained from equation A.56. It is found that the outlet temperature of the coolant gas T_{pout} is about 743.5 °C.

c. Reactor heat transfer coefficient

To evaluate the heat transfer coefficient across the reactor core, the reactor core is assumed to be using a nuclear fuel element bed of 39% porosity. The specific area of flow in the reactor core is given by equation A.57 (Mills, 1995). The reactor bed is made of fuel elements of diameter d_p equals 0.06 m.

$$a = \frac{6}{d_p} (1 - \varepsilon) = \frac{6}{0.06} \times (1 - 0.39) = 61 \text{ m}^{-1} \quad (\text{A.57})$$

The characteristic velocity and length are obtained from equations A.58 and A.59 respectively.

$$V_c = \frac{\dot{m}}{\rho \varepsilon A_c} = \frac{97.5 \times 4}{4.2 \times 0.39 \times 3.14 \times 3^2} = 8.425 \text{ m/s} \quad (\text{A.58})$$

$$L = \left(\frac{\varepsilon}{1 - \varepsilon} \right) d_p = \left(\frac{0.39}{1 - 0.39} \right) \times 0.06 = 0.0384 \text{ m} \quad (\text{A.59})$$

The density of helium can be read from the chart of Figure A.3 or else equation A.60 can be used to evaluate the density of helium as a function of its temperature and pressure. In equation A.60 (Zeng, et al., 2009), the pressure is considered in atmosphere (atm) and the temperature in Kelvin (K).

$$\begin{aligned} \rho &= 48.14 \frac{\text{P}}{\text{T}} \left(1 + 0.4446 \frac{\text{P}}{\text{T}^{1.2}} \right)^{-1} = 48.14 \frac{70}{(500+273)} \left[1 + 0.4446 \frac{70}{(500+273)^{1.2}} \right]^{-1} \\ &= 4.2 \text{ kg/m}^3 \end{aligned} \quad (\text{A.60})$$

The Reynolds number is calculated using equation A.61.

$$\text{Re}_c = \frac{\rho v d}{\mu} = \frac{4.2 \times 8.425 \times 0.0384}{31.7 \times 10^{-6}} = 42 \ 863.85 \quad (\text{A.61})$$

The Nusselt number used to find the heat transfer coefficient across the reactor's pebble-bed is obtained using equation A.62, while the heat transfer coefficient is obtained using equation A.63.

$$\begin{aligned} \text{Nu} &= 1.27 \frac{\text{Pr}^{1/3}}{\varepsilon^{1.18}} \text{Re}^{0.36} + 0.033 \frac{\text{Pr}^{1/2}}{\varepsilon^{1.07}} \text{Re}^{0.86} \\ &= 1.27 \times \frac{0.72^{1/3}}{0.39^{1.18}} \times 42\,863.85^{0.36} + 0.033 \times \frac{0.72^{1/2}}{0.39^{1.07}} \times 42\,863.85^{0.86} = 899.35 \end{aligned} \quad (\text{A.62})$$

$$h_c = \frac{\text{Nu}_c k}{L} = \frac{899.35 \times 0.273}{0.0384} = 6393.82 \text{ W/m}^2\text{C} \quad (\text{A.63})$$

Before entering the reactor core, helium is preheated while cooling down the reflector of the reactor. During this process helium flows upwards in 30 channels uniformly distributed across the annulus reflector. The diameter of the channels is obtained from equation A.64. To derive equation A.64, the same velocity (same cross-section) of the gas through the annulus's coaxial pipe that lets helium into the reactor was assumed.

$$d_{\text{ch}} = \sqrt{\frac{D_{\text{in}}^2 - D_{\text{co}}^2}{n_{\text{ch}}}} = \sqrt{\frac{1.565^2 - 1.030^2}{30}} = 0.215 \text{ m} \quad (\text{A.64})$$

The heat transfer coefficient of the coolant gas across the reflector side, calculated in equation A.65, is similar to the heat transfer coefficient of a flow through a cylindrical pipe of diameter d_{ch} .

$$\begin{aligned} h_r &= C K \text{Pr}_r^n \frac{k_r}{d_{\text{ch}}} \left(\frac{4}{\pi d_{\text{ch}} \mu_r} \right)^m \left(\frac{\dot{m}_h}{n_{\text{ch}}} \right)^m \\ &= 0.023 \times 1 \times \left(\frac{0.205}{0.215} \right) \times \left(\frac{4}{3.14 \times 0.215 \times 28.2 \times 10^{-6}} \right)^{0.8} \times 0.72^{0.4} \times \left(\frac{97.5}{30} \right)^{0.8} \\ &= 894.2 \text{ W/m}^2\text{C} \end{aligned} \quad (\text{A.65})$$

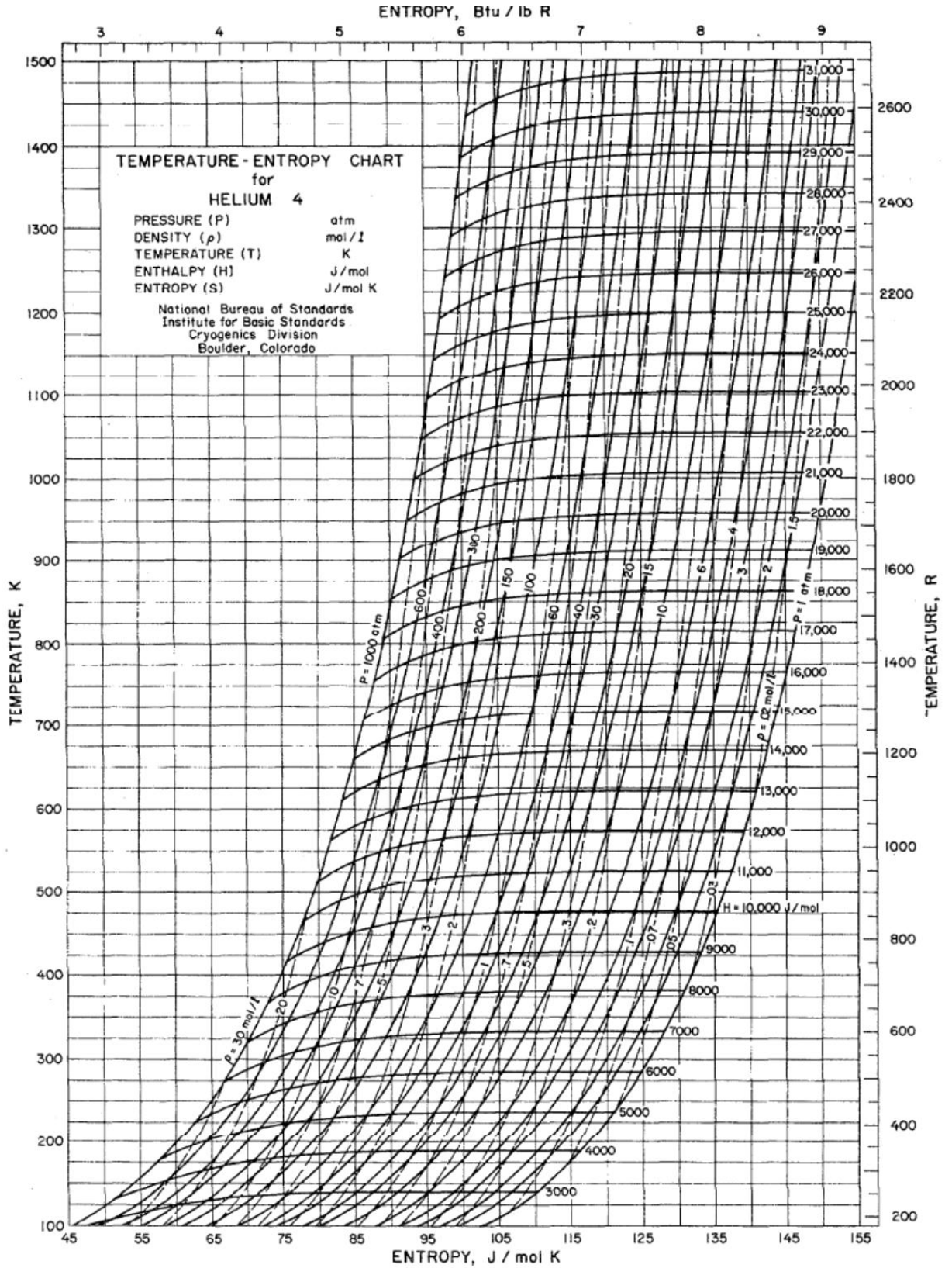


Figure A.3 Helium thermodynamic properties (Barron, 1985)

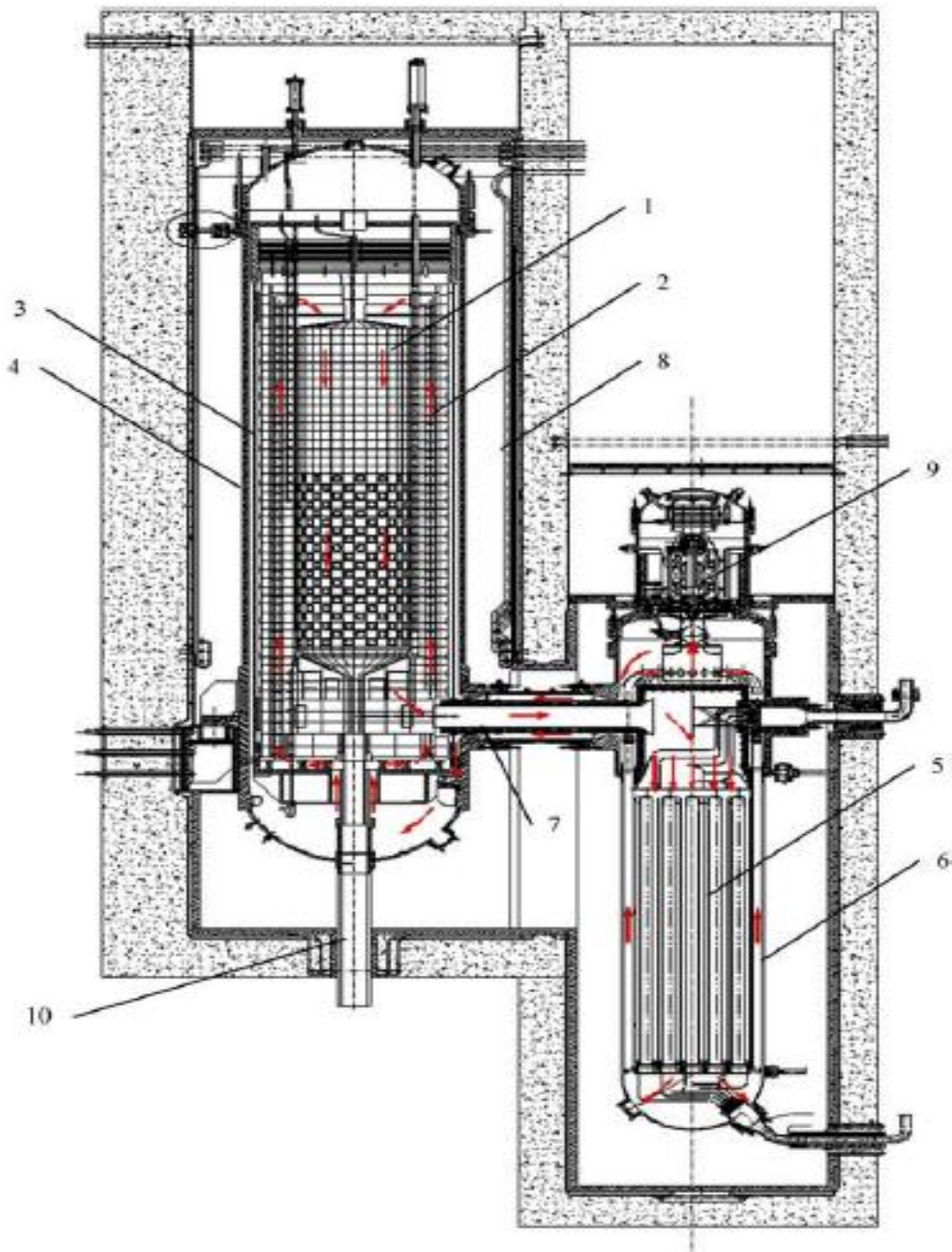


Figure A.4 Cross section of helium loop of the HTR-PM (Zeng, et al., 2009)

In Figure A.4, note: 1 Core of the reactor; 2 Reflector side and carbon thermal shield; 3 Core barrel; 4 Reactor pressure vessel; 5 Steam generator; 6 Steam generator vessel; 7 Coaxial gas duct; 8 Water-cooling panel; 9 Blower; 10 Fuel discharge tube (Zeng, et al., 2009).

A simplified coolant gas flow pattern through the nuclear reactor is provided in figure A.5. It can be seen that cold helium from the steam generator is directly supplied to the reactor where it accesses from the bottom, lower plenum, then flows upward through channels provided in the annulus reflector side referred to as riser. The reflector is cooled by the rising coolant gas. The coolant gas from the riser is then collected in the upper header which is approached as a mixing chamber. From the upper header the coolant gas will access to the reactor core made up of a pebble-bed. A coaxial pipe for coolant gas inlet/outlet to the reactor is used. The hot gas from the reactor flows in the inner tube while the cold gas from the steam generator flows in the annulus.

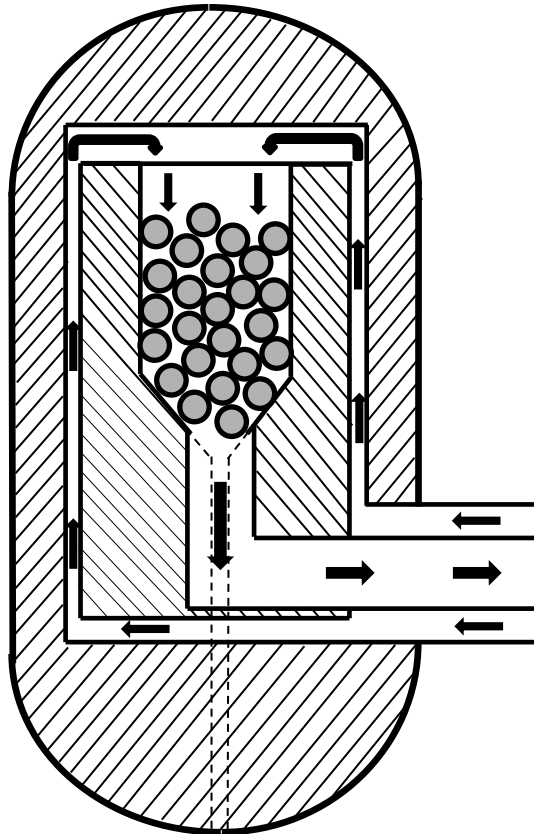


Figure A.5 Schematic nuclear reactor coolant flow path

APPENDIX B: HTMR SIMULATION M-FILE IN MATLAB FOR STEADY STATE

Power unit and Nuclear reactor

```

Cm =23.9 % Inconel 617 thermal conductivity in W/mC %
Tin = 205;
Tout = 540;
P = 250e6;
Ps7 = 135;
mdot = 97.5
mdotprim = 97.5
N=441;
P1= 600e6;
n = ceil(N*P/P1)
d=0.0318;
l17= 144;
Aht = pi*d*l17*n
Cppave = 5195
%check Overall heat transfer coefficient%
Tpin = 750;
Tpout = 250;
Thave = (Tpin-Tpout)/2
Thave = (Tpin+Tpout)/2
Tcave = (Tout+Tin)/2
Uoverall = P/(Aht*(Thave-Tcave))
thickness = 0.0035/2;
di = d-2*thickness;
ro = d/2;
ri = di/2;
A = n*pi*di*di/4;
Ap = A/n
rhos3 = XSteam('rhoL_p',Ps7)
v3 = 1/rhos3
rhos1 = XSteam('rho_pT',Ps7,Tin)
rhoaveco = (rhos1+rhos3)/2
Veco = mdot/(A*rhoaveco)
rhos7 = XSteam('rho_pT',Ps7,Tout)
rhos5 = XSteam('rhoV_p',Ps7)
v5 = 1/rhos5
rhoavesup = (rhos5+rhos7)/2
Vsup = mdot/(A*rhoavesup)
mys1 = XSteam('my_pT',Ps7,Tin)
T3 = XSteam('Tsat_p',Ps7)
T5 = XSteam('Tsat_p',Ps7)
mys5 = XSteam('my_pT',Ps7,T5+1)
mys3 = XSteam('my_pT',Ps7,T3-1)

```

```

mys7 = XSteam('my_pT',Ps7,Tout)
mys2 = (mys1+mys3)/2
mys4 = (mys5+mys3)/2
mys6 = (mys5+mys7)/2
Re2 = rhoaveeco*di*Veco/mys2
Re2 = rhoaveeco*di*Veco/mys4
rho4 =(rhos3+rhos5)/2
V4 = mdot/(rho4*A)
Re4 = rho4*V4*di/mys4
Re6 = rhoavesup*di*Vsup/mys6
k1 = XSteam('tc_pT',Ps7,Tin)
k3 = XSteam('tcL_p',Ps7)
k5 = XSteam('tcV_p',Ps7)
k7 = XSteam('tc_pT',Ps7,Tout)
k6 = (k7+k5)/2
k4 = (k3+k5)/2
k2 = (k3+k1)/2
Cp1 = XSteam('Cp_pT',Ps7,Tin)
Cp7 = XSteam('Cp_pT',Ps7,Tout)
Cp3 = XSteam('CpL_p',Ps7)
Cp5 = XSteam('CpV_p',Ps7)
Cp6 = (Cp7+Cp5)/2
Cp4 = (Cp3+Cp5)/2
Cp2 = (Cp1+Cp3)/2
Pr2 = 1e3*mys2*Cp2/k2
Pr4 = 1e3*mys4*Cp4/k4
Pr6 = 1e3*mys6*Cp6/k6
C2 = 0.023;
C6 = 0.023;
C4 = 0.023;
C2 = 0.027;
m2 = 0.8;
m4 = 0.8;
m6 = 0.8;
n2 = 0.33;
n4 = 0.4;
n6 = 0.4;
Nu2 = C2*(Re2).^m2*(Pr2).^n2
Nu4 = C4*(Re4).^m4*(Pr4).^n4
Nu6 = C6*(Re6).^m6*(Pr6).^n6
K1 = C6*(Pr6).^n6
K2 = (4/(pi*d*mys6)).^m6
K3 = K1*K2
K1ev = C4*(Pr4).^n4
K2ev = (4/(pi*d*mys4)).^m4
K3ev = K1ev*K2ev
K1ec = C2*(Pr2).^n2

```

```

K2ec = (4/(pi*d*mys2)).^m2
K3ec = K1ec*K2ec
h2 = Nu2*k2/di
h6 = Nu6*k6/di
kw4 = 43;
Nu4 = 0.087*(Re4)^0.6*(Pr2)^(1/6)*(rhoaveco/rhoavesup)^0.2*(kw4/k2)^0.09
k4 = (k3+k5)/2
h4 = Nu4*k4/di
U = (1/h2 + 1/h4 + 1/h6)^-1
% Superheater %
Enthalpy7 = XSteam('h_pT',Ps7,Tout)
Enthalpy5 = XSteam('hV_p',Ps7)
Enthalpy3 = XSteam('hL_p',Ps7)
Enthalpy1 = XSteam('h_pT',Ps7,Tin)
Qdot6est = mdot*(Enthalpy7 - Enthalpy5)
Qdot4est = mdot*(Enthalpy5 - Enthalpy3)
Qdot2est = mdot*(Enthalpy3 - Enthalpy1)
Qest = Qdot2est + Qdot4est + Qdot6est
hp7 = 3783.546;
hp1 = 1188.268;
hp5 = hp7 - Qdot6est/mdot
hp3 = hp5 - Qdot4est/mdot
hp1c = hp3 - Qdot2est/mdot
M = [1 29.31 859.0761 3.063 9.381969 89.77653 2631.350094 274.9855114
8059.825339
1 30.99 960.3801 9.114 83.064996 282.44286 8752.904231 2574.184226
79773.96916
1 30.59 935.7481 1.006 1.012036 30.77354 941.3625886 30.95818124
947.0107641
1 548.6 300961.96 3.063 9.381969 1680.3618 921846.4835 5146.948193
2823615.779
1 556.2 309358.44 9.114 83.064996 5069.2068 2819492.822 46200.75078
25696857.58
1 549.7 302170.09 1.006 1.012036 552.9982 303983.1105 556.3161892
305807.0092
1 954.7 911452.09 1.006 1.012036 960.4282 916920.8025 966.1907692
922422.3274
1 953.6 909352.96 3.063 9.381969 2920.8768 2785348.116 8946.645638
8531521.281
1 953.3 908780.89 9.114 83.064996 8688.3762 8282629.031 79185.86069
75487880.99
];
Mh = [1 32.3 1043.29 3.063 9.381969 98.9349 3195.59727 303.0375987
9788.114438
1 60.5 3660.25 9.114 83.064996 551.397 33359.5185 5025.432258 304038.6516
1 32.3 1043.29 1.006 1.012036 32.4938 1049.54974 32.6887628 1055.847038

```


1 2727.8 7440892.84 3.063 9.381969 8355.2514 22791454.77 25592.13504
 69810225.96
 1 2784.3 7752326.49 9.114 83.064996 25376.1102 70654703.63 231277.8684
 643946968.9
 1 2727.8 7440892.84 1.006 1.012036 2744.1668 7485538.197 2760.631801
 7530451.426
 1 4830.6 23334696.36 1.006 1.012036 4859.5836 23474704.54 4888.741102
 23615552.77
 1 4830.6 23334696.36 3.063 9.381969 14796.1278 71474174.95 45320.53945
 218925397.9
 1 4844.8 23472087.04 9.114 83.064996 44155.5072 213924601.3 402433.2926
 1949708816

];

T=[29.31;30.99;30.59;548.6;556.2;549.7;954.7;953.6;953.3];

C = Mh\T % C is the coefficient matrix %

Ca = C(1,1); Cb = C(2,1); Cc = C(3,1); Cd = C(4,1); Ce = C(5,1); Cf = C(6,1); Cg = C(7,1); Ch = C(8,1); Ci = C(9,1);

P7 = 7

P5 = P7 % to be corrected %

P3 = P5 % to be corrected %

P1 = P3 % to be corrected %

Tp7 = Ca + Cb*hp7 + Cc*hp7^2 + Cd*P7 + Ce*P7^2 + Cf*hp7*P7 + Cg*hp7^2*P7 +
 Ch*hp7*P7^2 + Ci*hp7^2*P7^2 %Refrigeration and Air conditioning %

Tp5 = Ca + Cb*hp5 + Cc*hp5^2 + Cd*P5 + Ce*P5^2 + Cf*hp5*P5 + Cg*hp5^2*P5 +
 Ch*hp5*P5^2 + Ci*hp5^2*P5^2 %Refrigeration and Air conditioning %

Tp3 = Ca + Cb*hp3 + Cc*hp3^2 + Cd*P3 + Ce*P3^2 + Cf*hp3*P3 + Cg*hp3^2*P3 +
 Ch*hp3*P3^2 + Ci*hp3^2*P3^2 %Refrigeration and Air conditioning %

Tp1 = Ca + Cb*hp1 + Cc*hp1^2 + Cd*P1 + Ce*P1^2 + Cf*hp1*P1 + Cg*hp1^2*P1 +
 Ch*hp1*P1^2 + Ci*hp1^2*P1^2 %Refrigeration and Air conditioning %

DeltaTm57 = ((Tp7-Tout)-(Tp5-T5))/log((Tp7-Tout)/(Tp5-T5))

U57I57 = Qdot6est/(DeltaTm57*pi*d)

DeltaTm35 = ((Tp5-T5)-(Tp3-T3))/log((Tp5-T5)/(Tp3-T3))

U35I35 = Qdot4est/(DeltaTm35*pi*d)

DeltaTm13 = ((Tp3-T3)-(Tp1-Tin))/log((Tp3-T3)/(Tp1-Tin))

U13I13 = Qdot2est/(DeltaTm13*pi*d)

B = h4/U35I35;

D = h2/U13I13;

C = h6/U57I57;

Smat = [-D*h4 B*h2;C*h2+D*h4 C*h2]

Ansmat = [h2-h4;144*C*h2-h2+h6]

L15 = Smat\Ansmat

I13 = L15(1,1)

I35 = L15(2,1)

I57 = I17 - I13 -I35

hh = h6/(C*I57-1)

Aht2 = pi*d*I13;

Aht4 = pi*d*I35;

```

Aht6 = pi*d*I57;
theta = 3.18*pi/180; % Pipes angle in radians%
g = 9.81; % Gravity %
% Pressure drops calculations %
% Superheater %
mdotp = mdot/n
Cf6 = 0.079*Re6^(-0.25) %friction coefficient factor%
kexit = 1;
kbend = 0.6;
F6 = kexit + kbend + 4*Cf6*I57/di
deltaPf57 = I57*F6*(mdotp^2)/(rhoavesup*Ap) % Friction pressure drop %
deltaPg57 = rhoavesup*g*sin(theta)*I57 % Pressure drop due to gravity %
deltaPm57 = I57*(rhos7-rhos5)*(mdotp/rhoavesup)^2 % Momentum pressure drop %
Ps5 = Ps7 + 1e-5*(deltaPf57 + deltaPg57 + deltaPm57)
% Evaporator %
Cf4 = 0.079*Re4^(-0.25) %friction coefficient factor%
F4 = kbend + 4*Cf4*I35/di
deltaPf35 = I35*F4*(mdotp^2)/(rho4*Ap) % Friction pressure drop %
deltaPg35 = rho4*g*sin(theta)*I35 % Pressure drop due to gravity %
deltaPm35 = I35*(rhos5-rhos3)*(mdotp/rho4)^2 % Momentum pressure drop %
Ps3 = Ps5 + 1e-5*(deltaPf35 + deltaPg35 + deltaPm35)
% Economizer %
kinlet = 0.5;
Cf2 = 0.079*Re2^(-0.25) %friction coefficient factor%
F2 = kinlet + kbend + 4*Cf2*I13/di
deltaPf13 = I13*F2*(mdotp^2)/Ap % Friction pressure drop %
deltaPg13 = rhoaveeco*g*sin(theta)*I13 % Pressure drop due to gravity %
deltaPm13 = I13*(rhos3-rhos1)*(mdotp/rhoaveeco)^2 % Momentum pressure drop %
Ps1 = Ps3 + 1e-5*(deltaPf13 + deltaPg13 + deltaPm13)
sin(theta)
hfgs = Enthalpy5-Enthalpy3
u1 = XSteam('u_pT',Ps1,Tin)
u3 = XSteam('u_pT',Ps3,T3)
u5 = XSteam('u_pT',Ps5,T5)
Q17 = Qdot2est+Qdot4est+Qdot6est
Qp17 = mdotprim*Cpvave*(Tp7 - Tp1)
UA57 = ((1/(2*pi*I57)*((1/(ro*hh))+1/(ri*h2))+log(ro/ri)/Cm))))^-1
Tsteam = Tp7 - Qdot6est/UA57
UA1 = ((1/(2*pi*I57)*((1/(ri*h6))+log(ro/ri)/Cm))))^-1
Tm7 = Tsteam + Qdot6est/UA57
UA13 = ((1/(2*pi*I13)*((1/(ri*h2))+log(ro/ri)/Cm))))^-1
Tm1 = Tin + Qdot2est/UA13
Tm3 = T3 + Qdot2est/UA13
Tm2 = (Tm1+Tm3)/2
Tm4 = Tm3
Tm5 = Tm4
Tm6 = (Tm5+Tm7)/2

```

U35 = U35I35/I35
 U57 = UA57/(I57*pi*d)

% NUCLEAR REACTOR %

%Simulation of the Chinese HTR-PM 2X250 MWth Using SI units%

% Input Nuclear reactor%

rhoex = [-.0053:0.0053/960:0];
 Tpinn = [230:0.01:270];
 Gpinn = [17.87:79/960:97.53];
 Tpin = 250 % Helium inlet temperature%
 Ppin = 7e6 %Inlet helium pressure in Pascals%
 Gpin = 97.53 %helium mass flow rate inlet%
 rhorod1 = [-0.0053:0.00053/(16*60):0]; % Control rod reactivity %
 rhorod = 0
 Gsin = 97.53 % Secondary steam generator flow rate inlet %
 Tsin = 205 % Secondary steam generator inlet temperature%
 Psout = 13.5e6 % Secondary steam generator outlet pressure Pascals%

%Independante variables%

t=length(rhorod) %Time%
 Tcin = 250 % Designed inlet core temperature %
 Tcout = 750 %Designed outlet core Temperature %
 Tcore = (Tcin+Tcout)/2

%Helium: Pressure range, 0.1Mpa<P<10MPa; and temperature 293K<T<1773K%
 %Conversion Units 1 bar = 0.1 MPa = 1e5 N/m2 %

Hc = 11 %Active core height%
 Dc = 3 %Active core diameter%
 epsilon = 0.39 %porosity of pebble%
 Drpv = 6 %Outer diameter reactor pressure vessel%
 Drpvi = 5.7 %Inner diameter of the reactor pressure vessel%
 Df = 0.06 %Fuel diameter%
 a = 6*(1-epsilon)/Df %Specific surface area%
 Dh = epsilon/a % Hydraulic diameter %
 nf = 420000 %Number of fuel elements in the reactor%
 Vf = 4/3*pi*(Df*100/2)^3 % Volume of the fuel in cm3 %
 np = 30 %Number of cooling helium pipes in the reflector%
 Dcent = 0.75 %Diameter of the central tube of the coaxial duct%
 Dcoaxin = 1.565 %Inner diameter of the annular channel of the coaxial duct%
 Dcoaxout = 1.030 %Outer diameter of the annular channel of the coaxial duct%
 dp = sqrt((Dcoaxin^2 - Dcoaxout^2)/np) %helium pipes diameter of the riser%

$l_r = d_p$ %Characteristic length in the riser%
 $H_p = 11$ %Active height of the helium pipes in the riser TO BE CHECKED%
 $d_{wcp} = 8.4$ %Inside diameter of the water cooling pannel%
 $h_{wcp} = 14.5$ %Active height of the water cooling pannel%
 $n_{pw} = 72$ %Number of water cooling pipes in helice%
 $Prated = 250e6$; %Rated power%
 $A_c = \pi * \text{square}(D_c) / 4$ %Core cross section Area%
 $n_{rod} = 8$ %number of control rods %
 $T_{c0} = 841$ % steady state core temperature C%
 $T_{r0} = 271.21$ %TO BE CHECKED steady state reflector temperature%
 $t_1 = 55.7$ % Half-life time in sec precursor 1%
 $t_2 = 22.7$ % Half-life time in sec precursor 2%
 $t_3 = 6.22$ % Half-life time in sec precursor 3%
 $t_4 = 2.30$ % Half-life time in sec precursor 4%
 $t_5 = 0.61$ % Half-life time in sec precursor 5%
 $t_6 = 0.23$ % Half-life time in sec precursor 6%
 $BETA = 0.1$ %leakage ratio %
 $\beta_1 = 0.024$ % Delayed Neutrons fraction precursor 1%
 $\beta_2 = 0.160$ % Delayed Neutrons fraction precursor 2%
 $\beta_3 = 0.143$ % Delayed Neutrons fraction precursor 3%
 $\beta_4 = 0.288$ % Delayed Neutrons fraction precursor 4%
 $\beta_5 = 0.084$ % Delayed Neutrons fraction precursor 5%
 $\beta_6 = 0.030$ % Delayed Neutrons fraction precursor 6%
 $C_p = 5195$ %Average specific heat of helium J/kgK against 5189 RELAP5 Steam generator%
 $C_v = 3117$ %Average constant-volume specific heat capacity value J/kgK%
 $\text{caplambda} = 0.0011$ %neutron generation time in secondes%
 $\beta_{2} = 0.01$ %leakage through the discharge fuel from the lower plenum%
 $\beta_{tag} = 0.04$ %leakage through graphite components%
 $\beta_{arod} = 0.01$ %leakage through the control rods%
 $\chi_3 = 0.015$ % Pressure loss coefficient <http://www.aquatext.com/tables/coe-rough.htm>%
 $\chi_5 = \chi_3$
 $\alpha_f = -4.36e-05$ % temperature coefficient Reactivity of the moderator in dk/k/C%
 $\alpha_m = -0.94e-05$ % temperature coefficient Reactivity of the fuel in dk/k/C%
 $\alpha_r = 1.49e-05$ % temperature coefficient Reactivity of the reflector in dk/k/C%

% COMPUTE %

$P_c = P_{pin}$ %Inlet pressure in the core%
 $G_1 = G_{pin}$ % ASSUMING CONSTANT DENSITY IN THE LOWER PLENUM %
 $G_{23} = G_1 * (1 - \beta_2)$ % lower header flow rate and same in the riser%
 $G_{26} = G_1 * \beta_2$ %By pass to outer header of the reactor%
 $G_c = G_1 * (1 - \beta_2 - \beta_{tag} - \beta_{arod})$ %Helium Mass flow rate in the core%
 $P_1 = P_{pin}$
 $P_2 = P_1$
 $T_1 = T_{pin}$

$T2 = T1$
 $\rho_{h2} = 48.18 \cdot (P2/T2) \cdot (1 + 0.4446 \cdot (P2/T2)^{1.2})^{-1}$ %helium density in the lower header%
 $P3 = P2 - \chi_{h3} \cdot G23^2 / \rho_{h2}$
 $P4 = P3$

$\lambda_{h1} = 0.693/t1$ % Decay constant of the precursor 1%
 $\lambda_{h2} = 0.693/t2$ % Decay constant of the precursor 2%
 $\lambda_{h3} = 0.693/t3$ % Decay constant of the precursor 3%
 $\lambda_{h4} = 0.693/t4$ % Decay constant of the precursor 4%
 $\lambda_{h5} = 0.693/t5$ % Decay constant of the precursor 5%
 $\lambda_{h6} = 0.693/t6$ % Decay constant of the precursor 6%
 $\beta = \beta_{h1} + \beta_{h2} + \beta_{h3} + \beta_{h4} + \beta_{h5} + \beta_{h6}$
 $C1 = \beta_{h1}/\beta$ % Concentration precursor 1%
 $C2 = \beta_{h2}/\beta$ % Concentration precursor 2%
 $C3 = \beta_{h3}/\beta$ % Concentration precursor 3%
 $C4 = \beta_{h4}/\beta$ % Concentration precursor 4%
 $C5 = \beta_{h5}/\beta$ % Concentration precursor 5%
 $C6 = \beta_{h6}/\beta$ % Concentration precursor 6%
 $d5 = \epsilon \cdot Dc$ %equivalent diameter%

$\text{SumprodIC} =$
 $\lambda_{h1} \cdot C1 + \lambda_{h2} \cdot C2 + \lambda_{h3} \cdot C3 + \lambda_{h4} \cdot C4 + \lambda_{h5} \cdot C5 + \lambda_{h6} \cdot C6$
 $\rho_{hc} = 48.18 \cdot (Pc/Tcore) \cdot (1 + 0.4446 \cdot (Pc/Tcore)^{1.2})^{-1}$ %helium density in the core%
 $l_c = Df \cdot \epsilon / (1 - \epsilon)$ %Characteristic length core %
 $V_c = G23 / (\rho_{hc} \cdot A_c \cdot \epsilon)$ %Characteristic Velocity%

$A_f = 4 \cdot \pi \cdot (Df/2)^2$ % surface area of a single fuel ball%
 $A_{contact} = n_f \cdot 4 \cdot \pi \cdot (Df/2)^2$ %contact area helium-pebbles%
 $A = \pi \cdot d5^2 \cdot 1/4$ %equivalent area in the core%
 $\eta_{r3} = 3.674e-07 \cdot Tr0^{0.7}$ %Kinectic viscosity in the riser%
 $\eta_{c5} = 3.674e-07 \cdot Tcore^{0.7}$ %Kinectic viscosity in the core%
 $Re5 = l_c \cdot V_c / \eta_{c5}$ %Renold number in the downcomer%
 $\Psi = 320 / (Re5 / (1 - \epsilon)) + 6 / ((Re5 / (1 - \epsilon))^{0.1})$
 $\Delta Pc = \Psi \cdot ((1 - \epsilon) / \epsilon^3) \cdot (1 / Dc) \cdot (0.5 / \rho_{hc}) \cdot \text{square}(Gc / (\epsilon \cdot A_c)) \cdot Hc$
 $P5 = P4 - \Delta Pc$
 $\lambda_{dah} = 2.682e-03 \cdot (1 + 1.123e-03) \cdot Tcore^{(0.71 \cdot (1 - (2e-04 \cdot P4 \cdot 1e-5)))}$ %heat conductivity W/mK in the core%
 $\lambda_{dahr} = 2.682e-03 \cdot (1 + 1.123e-03) \cdot Tr0^{(0.71 \cdot (1 - (2e-04 \cdot P2 \cdot 1e-5)))}$ %heat conductivity W/mK in the riser%
 $A_{c3} = \pi \cdot \text{square}(dp) / 4$ %cross section of the riser%
 $Re3 = (G23 / (n_p \cdot A_{c3})) \cdot dp / \eta_{r3}$ %Renold number in the riser%
 $\rho_{h3} = 48.14 \cdot P_{pin} / Tr0 \cdot 1 / (1 + 0.4446 \cdot (P_{pin} / Tr0)^{1.2})$ %helium density in the riser%
 $diff3 = \lambda_{dahr} / (C_p \cdot \rho_{h3})$ %Diffusivity of the riser%
 $Pr3 = \eta_{r3} \cdot \rho_{h2} / \lambda_{dahr}$ %Prandtl Number in the riser%

%helium density in the core%

$\text{diff5} = \lambda_{\text{dah}} / (\text{Cp} * \text{rho}_c)$ %Diffusivity of the core%
 $\text{Pr5} = \eta_5 * \text{C}_{\text{ppave}} / \lambda_{\text{dah}}$ %Prandtl Number in the core%
 $\text{Nu5} = 1.27 * (\text{Pr5}^{1/3}) * (\text{Re5}^{0.36}) / \epsilon^{1.18} + 0.033 * (\text{Pr5}^{1/2}) * (\text{Re5}^{0.86}) / \epsilon^{1.07}$ %Nusselt number in the downcomer%
 $\text{Nu3} = 0.094 * \text{Re3}^{0.72} * \text{Pr3}^{0.33}$ %Nusselt number in the riser%
 $\alpha_3 = \text{Nu3} * \lambda_{\text{dah}} / l_r$ %heat transfer coefficient of the riser%
 $\alpha_5 = \text{Nu5} * \lambda_{\text{dah}} / l_c$ %heat transfer coefficient of the core%
 $A_3 = n_p * \pi * d_p * H_p$ %riser heat transfer area %
 $V_3 = n_p * H_p * \pi * d_p^2 / 4$ %Volume of the riser%
 $V_5 = \pi * H_c * D_c^2 / 4$ % Volume downcomer reactor %
 $A_5 = 4 * \pi * n_f * (D_f/2)^2 + \pi * D_c * H_c$ %heat transfer area in the reactor%
 $A_{cr} = \pi * D_c * H_c$ %Heat transfer area from core to reflector%
 $V_r = \pi * H_p * D_{rpv}^2 / 4 - (V_5 + n_p * \pi / 4 * H_p * (d_p)^2)$ % Volume of the reflector %
 $f_3 = 4 * 0.078 * \text{Re3}^{-0.25}$ %friction factor of the riser%
 $f_5 = 4 * 0.078 * \text{Re5}^{-0.25}$ %friction factor in the core%

$V_1 = 0.5 * 4/3 * \pi * (D_{rpv}/2)^3$
 $G_3 = G_{23}$
 $G_4 = G_{23}$
 $P_6 = P_5$
 $\rho_5 = \rho_c$ %helium density in the core%
 $\rho_6 = 48.18 * (P_6 / T_{\text{cout}}) * (1 + 0.4446 * (P_6 / T_{\text{cout}})^{1.2})^{-1}$ %helium density in the outlet
header%
 $V_6 = \rho_3 * V_3 / \rho_6$
 $G_5 = G_c$
 $T_3 = T_2$
 $T_4 = T_3$
 $G_6 = G_1$
 $\alpha_1 = \alpha_3$ %Assumed for same flow%
 $K_1 = -\alpha_1 * T_{c0} - \alpha_{phar} * T_{r0} - \beta$
 $n_{\text{Bar}} = (-\beta / \text{cap} \lambda_{\text{delta}}) \sum \text{prod} I C$ % Steady state neutron's density at full power %
 $\alpha_{\text{phacr}} = 17.5$
 $C_r = 1793$ % Specific heat of graphite rfr to heat transfer book Dobson%
 $C_c = C_r$
 $\text{XXX} = 2.5$ % Thermo conductivity %
 $\rho_{\text{hor}} = 1394.8$ % Density graphite rfr to heat transfer book Dobson %
 $\rho_{\text{hog}} = \rho_{\text{hor}}$ % Density graphite rfr to heat transfer book Dobson %
 $\rho_{\text{ho1}} = 48.18 * (P_1 / T_1) * (1 + 0.4446 * (P_1 / T_1)^{1.2})^{-1}$ %helium density in the lower
plenum%
 $t = 960$
 $l = 0.1$ % Average lifetime%
 $k = 1.38e-16$ % Plank constant %
 $n_m = 1.66e-24$ % neutron mass %
 $v_n = 100 * \sqrt{(8 * k * (T_{\text{core}} + 273.15)) / (\pi * n_m)}$ % Neutron average velocity %
 $\gamma = 0.089$ % Enrichment %
 $\rho_{\text{hoU}} = 19.1$ % Uranium density %

Na = 6.022e23 % Avogadro number %
MmU = 235.0429 % Uranium molar mass %
NU235= (gamma*rhoU*Na)/MmU % Number of uranium atoms per cm %
SigmaU235 = 582e-24
Sigmaf = SigmaU235*NU235 % Macroscopic cross section %
gammaf = 200*1.6e-13 % Conversion factor in Wsec/fission %
nbar = Prated/(Vf*vf*vn*gammaf*Sigmaf) % Steady state neutron density at full power %

Cogeneration unit

$C_m = 23.9$ % Inconel 617 thermal conductivity in W/mC %

$T_{in} = 205$;

$T_{inhp} = 205$;

$T_{out} = 540$;

$T_{outhp} = 430$;

$P = 250e6$;

$P_{hp} = 60e6$;

$P_{s7} = 135$;

$P_{s7hp} = 40$;

$\dot{m} = 72.5$;

$\dot{m}_{ohp} = 25$;

$\dot{m}_{otprim} = 97.5$;

$N = 441$;

$P_1 = 600e6$;

$n = \text{ceil}(N * P / P_1)$

$N_{hp} = 320$

$d = 0.0318$;

$l_{17} = 144$;

$l_{17hp} = 18$;

$A_{ht} = \pi * d * l_{17} * n$

$A_{hthp} = \pi * d * l_{17hp} * N_{hp}$

$C_{ppave} = 5195$

%check Overall heat transfer coefficient%

$T_{pin} = 750$;

$T_{pout} = 250$;

$T_{have} = (T_{pin} - T_{pout}) / 2$

$T_{have} = (T_{pin} + T_{pout}) / 2$

$T_{cave} = (T_{out} + T_{in}) / 2$

$U_{overall} = P / (A_{ht} * (T_{have} - T_{cave}))$

thickness = 0.0035/2;

$d_i = d - 2 * \text{thickness}$;

$r_o = d / 2$;

$r_i = d_i / 2$;

$A = n * \pi * d_i * d_i / 4$;

$A_{hp} = N_{hp} * \pi * d_i * d_i / 4$;

$A_p = A / n$

$A_{php} = A_{hp} / N_{hp}$

$\rho_{s3} = \text{XSteam}('rhoL_p', P_{s7})$

$\rho_{s3hp} = \text{XSteam}('rhoL_p', P_{s7hp})$

$v_3 = 1 / \rho_{s3}$

$v_{3hp} = 1 / \rho_{s3hp}$

$\rho_{s1} = \text{XSteam}('rho_pT', P_{s7}, T_{in})$

$\rho_{s1hp} = \text{XSteam}('rho_pT', P_{s7hp}, T_{inhp})$

$\rho_{oaveco} = (\rho_{s1} + \rho_{s3}) / 2$

$\rho_{oavecohp} = (\rho_{s1hp} + \rho_{s3hp}) / 2$


```

Veco = mdot/(A*rhoaveeco)
Vecohp = mdothp/(Ahp*rhoaveeco)
rhos7 = XSteam('rho_pT',Ps7,Tout)
rhos7hp = XSteam('rho_pT',Ps7hp,Touthp)
rhos5 = XSteam('rhoV_p',Ps7)
rhos5hp = XSteam('rhoV_p',Ps7hp)
v5 = 1/rhos5
v5hp = 1/rhos5hp
rhoavesup = (rhos5+rhos7)/2
rhoavesuphp = (rhos5hp+rhos7hp)/2
Vsup = mdot/(A*rhoavesup)
Vsuphp = mdothp/(Ahp*rhoavesuphp)
mys1 = XSteam('my_pT',Ps7,Tin)
mys1hp = XSteam('my_pT',Ps7hp,Tinhp)
T3 = XSteam('Tsat_p',Ps7)
T3hp = XSteam('Tsat_p',Ps7hp)
T5 = XSteam('Tsat_p',Ps7)
T5hp = XSteam('Tsat_p',Ps7hp)
mys5 = XSteam('my_pT',Ps7,T5+1)
mys5hp = XSteam('my_pT',Ps7hp,T5hp+1)
mys3 = XSteam('my_pT',Ps7,T3-1)
mys3hp = XSteam('my_pT',Ps7hp,T3hp-1)
mys7 = XSteam('my_pT',Ps7,Tout)
mys7hp = XSteam('my_pT',Ps7hp,Touthp)
mys2 = (mys1+mys3)/2
mys2hp = (mys1hp+mys3hp)/2
mys4 = (mys5+mys3)/2
mys4hp = (mys5hp+mys3hp)/2
mys6 = (mys5+mys7)/2
mys6hp = (mys5hp+mys7hp)/2
Re2 = rhoaveeco*di*Veco/mys2
Re2hp = rhoaveeco*di*Vecohp/mys2hp
rho4 = (rhos3+rhos5)/2
rho4hp = (rhos3hp+rhos5hp)/2
V4 = mdot/(rho4*A)
V4hp = mdothp/(rho4hp*Ahp)
Re4 = rho4*V4*di/mys4
Re4hp = rho4hp*V4hp*di/mys4hp
Re6 = rhoavesup*di*Vsup/mys6
Re6hp = rhoavesuphp*di*Vsuphp/mys6hp
k1 = XSteam('tc_pT',Ps7,Tin)
k1hp = XSteam('tc_pT',Ps7hp,Tinhp)
k3 = XSteam('tcL_p',Ps7)
k3hp = XSteam('tcL_p',Ps7hp)
k5 = XSteam('tcV_p',Ps7)
k5hp = XSteam('tcV_p',Ps7hp)
k7 = XSteam('tc_pT',Ps7,Tout)

```

```

k7hp = XSteam('tc_pT',Ps7hp,Touthp)
k6 = (k7+k5)/2
k6hp = (k7hp+k5hp)/2
k4 = (k3+k5)/2
k4hp = (k3hp+k5hp)/2
k2hp = (k3hp+k1hp)/2
k2 = (k3+k1)/2
Cp1 = XSteam('Cp_pT',Ps7,Tin)
Cp1hp = XSteam('Cp_pT',Ps7hp,Tinhp)
Cp7 = XSteam('Cp_pT',Ps7,Tout)
Cp7hp = XSteam('Cp_pT',Ps7hp,Touthp)
Cp3 = XSteam('CpL_p',Ps7)
Cp3hp = XSteam('CpL_p',Ps7hp)
Cp5 = XSteam('CpV_p',Ps7)
Cp5hp = XSteam('CpV_p',Ps7hp)
Cp6 = (Cp7+Cp5)/2
Cp6hp = (Cp7hp+Cp5hp)/2
Cp4 = (Cp3+Cp5)/2
Cp4hp = (Cp3hp+Cp5hp)/2
Cp2 = (Cp1+Cp3)/2
Cp2hp = (Cp1hp+Cp3hp)/2
Pr2 = 1e3*mys2*Cp2/k2
Pr2hp = 1e3*mys2hp*Cp2hp/k2hp
Pr4 = 1e3*mys4*Cp4/k4
Pr4hp = 1e3*mys4hp*Cp4hp/k4hp
Pr6 = 1e3*mys6*Cp6/k6
Pr6hp = 1e3*mys6hp*Cp6hp/k6hp
C2 = 0.023;
C6 = 0.023;
C4 = 0.023;
C2 = 0.027;
m2 = 0.8;
m4 = 0.8;
m6 = 0.8;
n2 = 0.33;
n4 = 0.4;
n6 = 0.4;
Nu2 = C2*(Re2).^m2*(Pr2).^n2
Nu2hp = C2*(Re2hp).^m2*(Pr2hp).^n2
Nu4 = C4*(Re4).^m4*(Pr4).^n4
Nu4hp = C4*(Re4hp).^m4*(Pr4hp).^n4
Nu6 = C6*(Re6).^m6*(Pr6).^n6
Nu6hp = C6*(Re6hp).^m6*(Pr6hp).^n6
K1 = C6*(Pr6).^n6
K1hp = C6*(Pr6hp).^n6
K2 = (4/(pi*d*mys6)).^m6
K2hp = (4/(pi*d*mys6hp)).^m6

```

```

K3 = K1*K2
K3hp = K1hp*K2hp
K1ev = C4*(Pr4).^n4
K1evhp = C4*(Pr4hp).^n4
K2ev = (4/(pi*d*mys4)).^m4
K2evhp = (4/(pi*d*mys4hp)).^m4
K3ev = K1ev*K2ev
K3evhp = K1evhp*K2evhp
K1ec = C2*(Pr2).^n2
K1echp = C2*(Pr2hp).^n2
K2ec = (4/(pi*d*mys2)).^m2
K2echp = (4/(pi*d*mys2hp)).^m2
K3ec = K1ec*K2ec
K3echp = K1echp*K2echp
h2 = Nu2*k2/di
h2hp = Nu2hp*k2hp/di
h6 = Nu6*k6/di
h6hp = Nu6hp*k6hp/di
kw4 = 43;
Nu4 = 0.087*(Re4)^0.6*(Pr2)^(1/6)*(rhoaveco/rhoavesup)^0.2*(kw4/k2)^0.09
Nu4hp =
0.087*(Re4hp)^0.6*(Pr2hp)^(1/6)*(rhoavecohp/rhoavesuphp)^0.2*(kw4/k2hp)^0.09
k4 = (k3+k5)/2
k4hp = (k3hp+k5hp)/2
h4 = Nu4*k4/di
h4hp = Nu4hp*k4hp/di
U = (1/h2 + 1/h4 + 1/h6)^-1
Uhp = (1/h2hp + 1/h4hp + 1/h6hp)^-1
% Superheater %

Enthalpy7 = XSteam('h_pT',Ps7,Tout)
Enthalpy7hp = XSteam('h_pT',Ps7hp,Touthp)
Enthalpy5 = XSteam('hV_p',Ps7)
Enthalpy5hp = XSteam('hV_p',Ps7hp)
Enthalpy3 = XSteam('hL_p',Ps7)
Enthalpy3hp = XSteam('hL_p',Ps7hp)
Enthalpy1 = XSteam('h_pT',Ps7,Tin)
Enthalpy1hp = XSteam('h_pT',Ps7hp,Tinhp)
Qdot6est = mdot*(Enthalpy7 - Enthalpy5)
Qdot6esthp = mdothp*(Enthalpy7hp - Enthalpy5hp)
Qdot4est = mdot*(Enthalpy5 - Enthalpy3)
Qdot4esthp = mdothp*(Enthalpy5hp - Enthalpy3hp)
Qdot2est = mdot*(Enthalpy3 - Enthalpy1)
Qdot2esthp = mdothp*(Enthalpy3hp - Enthalpy1hp)
Qest = Qdot2est + Qdot4est + Qdot6est
Qesthp = Qdot2esthp + Qdot4esthp + Qdot6esthp
hp7 = 3783.546;

```

$hp7hp = hp7$
 $hp1 = 1188.268;$
 $hp1hp = 3168.161;$
 $hp5 = hp7 - Qdot6est/mdot$
 $hp5hp = hp7hp - Qdot6esthp/mdothp$
 $hp3 = hp5 - Qdot4est/mdot$
 $hp3hp = hp5hp - Qdot4esthp/mdothp$
 $hp1c = hp3 - Qdot2est/mdot$
 $hp1chp = hp3hp - Qdot2esthp/mdothp$

$M = [1 \ 29.31 \ 859.0761 \ 3.063 \ 9.381969 \ 89.77653 \ 2631.350094 \ 274.9855114$
 8059.825339
 $1 \ 30.99 \ 960.3801 \ 9.114 \ 83.064996 \ 282.44286 \ 8752.904231 \ 2574.184226$
 79773.96916
 $1 \ 30.59 \ 935.7481 \ 1.006 \ 1.012036 \ 30.77354 \ 941.3625886 \ 30.95818124$
 947.0107641
 $1 \ 548.6 \ 300961.96 \ 3.063 \ 9.381969 \ 1680.3618 \ 921846.4835 \ 5146.948193$
 2823615.779
 $1 \ 556.2 \ 309358.44 \ 9.114 \ 83.064996 \ 5069.2068 \ 2819492.822 \ 46200.75078$
 25696857.58
 $1 \ 549.7 \ 302170.09 \ 1.006 \ 1.012036 \ 552.9982 \ 303983.1105 \ 556.3161892$
 305807.0092
 $1 \ 954.7 \ 911452.09 \ 1.006 \ 1.012036 \ 960.4282 \ 916920.8025 \ 966.1907692$
 922422.3274
 $1 \ 953.6 \ 909352.96 \ 3.063 \ 9.381969 \ 2920.8768 \ 2785348.116 \ 8946.645638$
 8531521.281
 $1 \ 953.3 \ 908780.89 \ 9.114 \ 83.064996 \ 8688.3762 \ 8282629.031 \ 79185.86069$
 75487880.99
 $];$

$Mh = [1 \ 32.3 \ 1043.29 \ 3.063 \ 9.381969 \ 98.9349 \ 3195.59727 \ 303.0375987$
 9788.114438
 $1 \ 60.5 \ 3660.25 \ 9.114 \ 83.064996 \ 551.397 \ 33359.5185 \ 5025.432258 \ 304038.6516$
 $1 \ 32.3 \ 1043.29 \ 1.006 \ 1.012036 \ 32.4938 \ 1049.54974 \ 32.6887628 \ 1055.847038$
 $1 \ 2727.8 \ 7440892.84 \ 3.063 \ 9.381969 \ 8355.2514 \ 22791454.77 \ 25592.13504$
 69810225.96
 $1 \ 2784.3 \ 7752326.49 \ 9.114 \ 83.064996 \ 25376.1102 \ 70654703.63 \ 231277.8684$
 643946968.9
 $1 \ 2727.8 \ 7440892.84 \ 1.006 \ 1.012036 \ 2744.1668 \ 7485538.197 \ 2760.631801$
 7530451.426
 $1 \ 4830.6 \ 23334696.36 \ 1.006 \ 1.012036 \ 4859.5836 \ 23474704.54 \ 4888.741102$
 23615552.77
 $1 \ 4830.6 \ 23334696.36 \ 3.063 \ 9.381969 \ 14796.1278 \ 71474174.95 \ 45320.53945$
 218925397.9
 $1 \ 4844.8 \ 23472087.04 \ 9.114 \ 83.064996 \ 44155.5072 \ 213924601.3 \ 402433.2926$
 1949708816
 $];$

```

T = [29.31;30.99;30.59;548.6;556.2;549.7;954.7;953.6;953.3];
C = Mh\T % C is the coefficient matrix %
Ca = C(1,1); Cb = C(2,1); Cc = C(3,1); Cd = C(4,1); Ce = C(5,1); Cf = C(6,1); Cg = C(7,1); Ch =
C(8,1); Ci = C(9,1);
P7 = 7
P5 = P7 % to be corrected %
P3 = P5 % to be corrected %
P1 = P3 % to be corrected %
Tp7 = Ca + Cb*hp7 + Cc*hp7^2 + Cd*P7 + Ce*P7^2 + Cf*hp7*P7 + Cg*hp7^2*P7 +
Ch*hp7*P7^2 + Ci*hp7^2*P7^2 %Refrigeration and Air conditioning %
Tp7hp = Ca + Cb*hp7hp + Cc*hp7hp^2 + Cd*P7 + Ce*P7^2 + Cf*hp7hp*P7 +
Cg*hp7hp^2*P7 + Ch*hp7hp*P7^2 + Ci*hp7hp^2*P7^2
Tp5 = Ca + Cb*hp5 + Cc*hp5^2 + Cd*P5 + Ce*P5^2 + Cf*hp5*P5 + Cg*hp5^2*P5 +
Ch*hp5*P5^2 + Ci*hp5^2*P5^2 %Refrigeration and Air conditioning %
Tp5hp = Ca + Cb*hp5hp + Cc*hp5hp^2 + Cd*P5 + Ce*P5^2 + Cf*hp5hp*P5 +
Cg*hp5hp^2*P5 + Ch*hp5hp*P5^2 + Ci*hp5hp^2*P5^2
Tp3 = Ca + Cb*hp3 + Cc*hp3^2 + Cd*P3 + Ce*P3^2 + Cf*hp3*P3 + Cg*hp3^2*P3 +
Ch*hp3*P3^2 + Ci*hp3^2*P3^2 %Refrigeration and Air conditioning %
Tp3hp = Ca + Cb*hp3hp + Cc*hp3hp^2 + Cd*P3 + Ce*P3^2 + Cf*hp3hp*P3 +
Cg*hp3hp^2*P3 + Ch*hp3hp*P3^2 + Ci*hp3hp^2*P3^2
Tp1 = Ca + Cb*hp1 + Cc*hp1^2 + Cd*P1 + Ce*P1^2 + Cf*hp1*P1 + Cg*hp1^2*P1 +
Ch*hp1*P1^2 + Ci*hp1^2*P1^2 %Refrigeration and Air conditioning %
Tp1hp = Ca + Cb*hp1hp + Cc*hp1hp^2 + Cd*P1 + Ce*P1^2 + Cf*hp1hp*P1 +
Cg*hp1hp^2*P1 + Ch*hp1hp*P1^2 + Ci*hp1hp^2*P1^2
DeltaTm57 = ((Tp7-Tout)-(Tp5-T5))/log((Tp7-Tout)/(Tp5-T5))
DeltaTm57hp = ((Tp7hp-Touthp)-(Tp5hp-T5hp))/log((Tp7hp-Touthp)/(Tp5hp-T5hp))
U57I57 = Qdot6est/(DeltaTm57*pi*d)
U57I57hp = Qdot6esthp/(DeltaTm57hp*pi*d)
DeltaTm35 = ((Tp5-T5)-(Tp3-T3))/log((Tp5-T5)/(Tp3-T3))
DeltaTm35hp = ((Tp5hp-T5hp)-(Tp3hp-T3hp))/log((Tp5hp-T5hp)/(Tp3hp-T3hp))
U35I35 = Qdot4est/(DeltaTm35*pi*d)
U35I35hp = Qdot4esthp/(DeltaTm35hp*pi*d)
DeltaTm13 = ((Tp3-T3)-(Tp1-Tin))/log((Tp3-T3)/(Tp1-Tin))
DeltaTm13hp = ((Tp3hp-T3hp)-(Tp1hp-Tinhp))/log((Tp3hp-T3hp)/(Tp1hp-Tinhp))
U13I13 = Qdot2est/(DeltaTm13*pi*d)
U13I13hp = Qdot2esthp/(DeltaTm13hp*pi*d)
B = h4/U35I35;
Bhp = h4hp/U35I35hp;
D = h2/U13I13;
Dhp = h2hp/U13I13hp;
C = h6/U57I57;
Chp = h6hp/U57I57hp;
Smat = [-D*h4 B*h2;C*h2+D*h4 C*h2]
Smathp = [-Dhp*h4hp Bhp*h2hp;Chp*h2hp+Dhp*h4hp Chp*h2hp]
Ansmat = [h2-h4;144*C*h2-h2+h6]
Ansmathp = [h2hp-h4hp;18*Chp*h2hp-h2hp+h6hp]

```

```

L15 = Smat\Ansmat
L15hp = Smathp\Ansmathp
l13 = L15(1,1)
l13hp = L15hp(1,1)
l35 = L15(2,1)
l35hp = L15hp(2,1)
l57 = l17 - l13 -l35
l57hp = l17hp - l13hp -l35hp
hh = h6/(C*I57-1)
hhhp = h6hp/(Chp*I57hp-1)
Aht2 = pi*d*I13;
Aht2hp = pi*d*I13hp;
Aht4 = pi*d*I35;
Aht4hp = pi*d*I35hp;
Aht6 = pi*d*I57;
Aht6hp = pi*d*I57hp;
theta = 3.18*pi/180; % Pipes angle in radians%
thetahp = 0;
g = 9.81; % Gravity %
% Pressure drops calculations %
% Superheater %
mdotp = mdot/n
mdotphp = mdothp/Nhp
Cf6 = 0.079*Re6^(-0.25) %friction coefficient factor%
Cf6hp = 0.079*Re6hp^(-0.25)
kexit = 1;
kbend = 0.6;
F6 = kexit + kbend + 4*Cf6*I57/di
F6hp = kexit + kbend + 4*Cf6hp*I57hp/di
deltaPf57 = I57*F6*(mdotp^2)/(rhoavesup*Ap) % Friction pressure drop %
deltaPf57hp = I57hp*F6hp*(mdotphp^2)/(rhoavesuphp*Aphp)
deltaPg57 = rhoavesup*g*sin(theta)*I57 % Pressure drop due to gravity %
deltaPg57hp = rhoavesuphp*g*sin(thetahp)*I57hp
deltaPm57 = I57*(rhos7-rhos5)*(mdotp/rhoavesup)^2 % Momentum pressure drop %
deltaPm57hp = I57hp*(rhos7hp-rhos5hp)*(mdotphp/rhoavesuphp)^2
Ps5 = Ps7 + 1e-5*(deltaPf57 + deltaPg57 + deltaPm57)
Ps5hp = Ps7hp + 1e-5*(deltaPf57hp + deltaPg57hp + deltaPm57hp)

% Evaporator %

Cf4 = 0.079*Re4^(-0.25) %friction coefficient factor%
Cf4hp = 0.079*Re4hp^(-0.25)
F4 = kbend + 4*Cf4*I35/di
F4hp = kbend + 4*Cf4hp*I35hp/di
deltaPf35 = I35*F4*(mdotp^2)/(rho4*Ap) % Friction pressure drop %
deltaPf35hp = I35hp*F4hp*(mdotphp^2)/(rho4hp*Aphp)
deltaPg35 = rho4*g*sin(theta)*I35 % Pressure drop due to gravity %

```

```

deltaPg35hp = rho4hp*g*sin(thetahp)*l35hp
deltaPm35 = l35*(rhos5-rhos3)*(mdotp/rho4)^2 % Momentum pressure drop %
deltaPm35hp = l35hp*(rhos5hp-rhos3hp)*(mdotphp/rho4hp)^2
Ps3 = Ps5 + 1e-5*(deltaPf35 + deltaPg35 + deltaPm35)
Ps3hp = Ps5hp + 1e-5*(deltaPf35hp + deltaPg35hp + deltaPm35hp)

% Economizer %

kinlet = 0.5;
Cf2 = 0.079*Re2^(-0.25) %friction coefficient factor%
Cf2hp = 0.079*Re2hp^(-0.25)
F2 = kinlet + kbend + 4*Cf2*l13/di
F2hp = kinlet + kbend + 4*Cf2hp*l13hp/di
deltaPf13 = l13*F2*(mdotp^2)/Ap % Friction pressure drop %
deltaPf13hp = l13hp*F2hp*(mdotphp^2)/Aphp
deltaPg13 = rhoaveeco*g*sin(theta)*l13 % Pressure drop due to gravity %
deltaPg13hp = rhoaveecohp*g*sin(thetahp)*l13hp
deltaPm13 = l13*(rhos3-rhos1)*(mdotp/rhoaveeco)^2 % Momentum pressure drop %
deltaPm13hp = l13hp*(rhos3hp-rhos1hp)*(mdotphp/rhoaveecohp)^2
Ps1 = Ps3 + 1e-5*(deltaPf13 + deltaPg13 + deltaPm13)
Ps1hp = Ps3hp + 1e-5*(deltaPf13hp + deltaPg13hp + deltaPm13hp)
hfgs = Enthalpy5-Enthalpy3
hfgshp = Enthalpy5hp-Enthalpy3hp
u1 = XSteam('u_pT',Ps1,Tin)
u1hp = XSteam('u_pT',Ps1hp,Tinhp)
u3 = XSteam('u_pT',Ps3,T3)
u3hp = XSteam('u_pT',Ps3hp,T3hp)
u5 = XSteam('u_pT',Ps5,T5)
u5hp = XSteam('u_pT',Ps5hp,T5hp)
Q17 = Qdot2est+Qdot4est+Qdot6est
Q17hp = Qdot2esthp+Qdot4esthp+Qdot6esthp
Qp17 = mdotprim*Cpave*(Tp7 - Tp1)
Qp17hp = mdotprim*Cpave*(Tp7hp - Tp1hp)
UA57 = ((1/(2*pi*I57)*((1/(ro*hh))+1/(ri*h2))+log(ro/ri)/Cm)))^-1
UA57hp = ((1/(2*pi*I57hp)*((1/(ro*hhhp))+1/(ri*h2hp))+log(ro/ri)/Cm)))^-1
Tsteam = Tp7 - Qdot6est/UA57
Tsteamhp = Tp7hp - Qdot6esthp/UA57hp
UA1 = ((1/(2*pi*I57)*((1/(ri*h6))+log(ro/ri)/Cm)))^-1
UA1hp = ((1/(2*pi*I57hp)*((1/(ri*h6hp))+log(ro/ri)/Cm)))^-1
Tm7 = Tsteam + Qdot6est/UA57
Tm7hp = Tsteamhp + Qdot6esthp/UA57hp
UA13 = ((1/(2*pi*I13)*((1/(ri*h2))+log(ro/ri)/Cm)))^-1
UA13hp = ((1/(2*pi*I13hp)*((1/(ri*h2hp))+log(ro/ri)/Cm)))^-1
Tm1 = Tin + Qdot2est/UA13
Tm1hp = Tinhp + Qdot2esthp/UA13hp
Tm3 = T3 + Qdot2est/UA13
Tm3hp = T3hp + Qdot2esthp/UA13hp

```

$$T_{m2} = (T_{m1} + T_{m3})/2$$

$$T_{m2hp} = (T_{m1hp} + T_{m3hp})/2$$

$$T_{m4} = T_{m3}$$

$$T_{m4hp} = T_{m3hp}$$

$$T_{m5} = T_{m4}$$

$$T_{m5hp} = T_{m4hp}$$

$$T_{m6} = (T_{m5} + T_{m7})/2$$

$$T_{m6hp} = (T_{m5hp} + T_{m7hp})/2$$

$$U_{35} = U_{35l35}/l_{35}$$

$$U_{35hp} = U_{35l35hp}/l_{35hp}$$

$$U_{57} = UA_{57}/(l_{57} \cdot \pi \cdot d)$$

$$U_{57hp} = UA_{57hp}/(l_{57hp} \cdot \pi \cdot d)$$